WMRC Reports
Waste Management and Research Center

Development of an Activated Carbon Fiber Cloth Adsorption/ Regeneration System to Recover and Reuse Toxic Volatile Organic Compounds

Mehrdad Lordgooei,
Kelly R. Carmichael,
Mark J. Rood,
Susan Larson

University of Illinois

RR-E81
April 1999
Electronic Version

About WMRC's Electronic Publications:

This document was originally published in a traditional format.

It has been transferred to an electronic format to allow faster and broader access to important information and data.

While the Center makes every effort to maintain a level of quality during the transfer from print to digital format, it is possible that minor formatting and typographical inconsistencies will still exist in this document.

Additionally, due to the constraints of the electronic format chosen, page numbering will vary slightly from the original document.

The original, printed version of this document may still be available.

Please contact WMRC for more information:

WMRC
One E. Hazelwood Drive
Champaign, IL 61820
217-333-8940 (phone)

www.wmrc.uiuc.edu

WMRC is a division of the Illinois Department of Natural Resources

RR-81

Development of an Activated Carbon Fiber Cloth Adsorption/Regeneration System to Recover and Reuse Toxic Volatile Organic Compounds

Mehrdad Lordgooei
Kelly R. Carmichael
Mark J. Rood[a]
Susan Larson[b]

Environmental Engineering & Science Program,
Department of Civil & Environmental Engineering,
University of Illinois at Urbana-Champaign

a. Principle Investigator and corresponding author
b. Co-Principle Investigator

Final Report
April 1999

Submitted to the
Illinois Waste Management and Research Center
One E. Hazelwood Drive
Champaign, IL 61820
www.wmrc.uiuc.edu

Printed by the Authority of the State of Illinois
99/100

This report is part of WMRC's Research Report Series. Mention of trade names or commercial products does not constitute endorsement or recommendation for use.

TABLE OF CONTENTS

APPENDIX

List of Figures

List of Tables

ABSTRACT

Many anthropogenic chemicals released into the atmosphere are toxic and can cause adverse effects on human health. Under the 1990 Clean Air Act Amendment (CAAA), the United States Environmental Protection Agency (USEPA established Maximum Achievable Control Technology (MACT) standards to reduce emissions of industrial toxic materials. These regulations have encouraged the development of new technologies to capture and recover toxic chemical vapors from industrial gas streams. In this research, a new activated carbon fiber cloth (ACFC) adsorber coupled with an electrothermal regenerator and a cryogenic condenser was designed and developed to efficiently capture and recover toxic volatile organic compounds (TVOCs) from simulated industrial gas streams. The system was characterized for adsorption by ACFC, electrothermal desorption, and cryogenic condensation to recover acetone and methyl ethyl ketone (MEK). Acetone was listed as a TVOC at the initiation of this project, has large emissions to the atmosphere, and is a good surrogate for other TVOCs. Results for research pertaining to acetone are also reported have. Results for research pertaining to acetone are also reported here. ACFC demonstrated good performance characteristics due to its high adsorption capacity, faster adsorption and desorption rates, zero ash content, and desirable electrical conductivity for an efficient electrothermal regeneration. The adsorption throughput ratios (TPRs) averaged from 65% to 86% for an effective bed length of 18 cm, a packing density of 94 mg/g and ACFC content of 27 g and 19 g. During electrothermal regeneration, supersaturated effluent vapor was produced in a very short time and low consumption energy (e.g. 63% by volume acetone was generated in 5.4 min with a consumption energy of 1 KJ/g-acetone/g-carbon) while heat loss to the carrier gas stream was not appreciable. Generating a concentrated vapor during a short time period by electrothermal regeneration reduces the size and operating cost of the cryogenic condenser. Cryogenic treatment of the effluent gas stream condensed TVOCs to concentrations to meet MACT standards. The Net Present Value analysis of the entire system including the adsorption, desorption and condensation processes indicated good prospects for economical recovery of the TVOCs. Sensitivity analysis showed the effect of component cost on the total break-even price of recovered acetone. Reducing the adsorption cycle time reduced the total cost and made the total cost less sensitive to changes in ACFC price. Experimental evaluation of the system and preliminary economic analysis provide encouraging results for developing a pilot-scale system for further analysis.

1. INTRODUCTION

Toxic volatile organic compound (TVOC) abatement has gained recent attention due to a better understanding of the effects of releasing these compounds into the environment. Both the magnitude and hazards of emissions of toxic compounds have led to public health concern and recent government regulations to reduce emissions.

Approximately $19.4 billion will be spent by current sources of releases to meet requirements of Title I and Title III of the 1990 Clean Air Act Amendments (McIlvaine et al., 1992). Of the $19.4 billion direct expenditures for air pollution control, equipment cost is estimated to account for $6.5 billion (McIlvaine et al., 1992). The development of new control equipment is at least in part necessitated by the requirements to remove TVOCs from point source emissions. Because of the size of this investment, there is interest in developing new, efficient means of TVOC control.

In this research, a novel activated carbon fiber cloth (ACFC) adsorption system is designed, developed and characterized for possible use as a method for point source reduction of TVOCs. In the developed system, adsorption by ACFC is followed by electrothermal regeneration resulting in formation of a concentrated organic vapor which is cryogenically condensed from the gas phase. Electrothermal desorption allows for optimizing the desorption time and the concentration profile of the desorbed TVOC to allow minimal use of cryogen. A bench-scale cryogenic condenser is used to assess the fundamental performance of condensing TVOCs at low temperature.

Liquid nitrogen (LN_2) is used as the cryogen. LN_2 can reduce TVOC emissions to parts per billion (ppbv) concentrations due to its high cooling capacity and low temperature. One advantage of the LN_2 system compared to other refrigeration systems is the multiple use of LN_2. The cooling capacity of LN_2 is used to condense TVOCs. Then the evaporated N_2 can be used for other process needs such as inerting and safety blanketing. Another advantage of LN_2 refrigeration over conventional mechanical condensation systems is the absence of moving parts such as compressors. However, LN_2 consumption rates are high for typical industrial effluent concentrations. The effluent TVOC concentrations are typically <1% by volume due to the limitations caused by their lower explosion limits. Ideal LN_2 consumption (minimum mass of LN_2 required per unit mass of TVOC condensed in an isolated thermodynamic system) is proportional to the inverse of the TVOC concentration (Figure 1.1). Results for acetone are reported here too although it is not currently on TVOC.

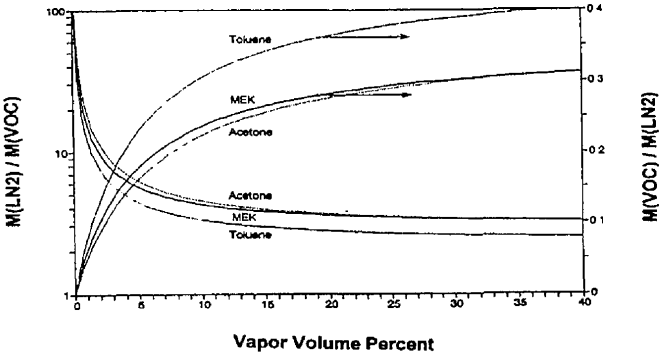

Figure 1.1 Ideal LN_2 consumption and amount of TVOC recovery as a function of the TVOC concentration

If TVOC concentration can be increased, then LN_2 consumption can be decreased. This is due to the fact that some portion of the cooling capacity transfers to the non-condensable carrier gas. Therefore, ACFC adsorption technology is used to pre-concentrate the effluent TVOCs for efficient vapor recovery.

Toxic Releases into the Environment

The United States Environmental Protection Agency (USEPA) began compiling a database of toxic releases into the environment in all 50 states and U.S. jurisdictions in 1987. Facilities manufacturing or processing 11,340 kg/yr of toxic materials and/or 4,500 kg/yr of other use toxic materials (e.g., solvents, cleaning materials, etc.) are required to report to the USEPA their toxic releases into the environment. The 1991 Toxic Release Inventory (TRI) included 302 individual toxic chemicals and 20 categories of chemical compounds. Selection of compounds were first compiled by USEPA from lists established by the states of Maryland and New Jersey for state reporting. These compounds have been identified as posing a risk to human health or the environment. The list of 302 toxic chemicals is under continual public, USEPA and U.S. Congressional review for modification. Toxic releases were divided into six different release pathways, the largest of which was direct emissions to the atmosphere. Table 1.1 lists those emission pathways for both the United States and the State of Illinois. Illinois ranked sixth overall in toxic releases into the environment. Emissions to the atmosphere in Illinois accounted for 4.3×10^7 kg of the total 1.1×10^9 kg emitted in the United States (USEPA[b], 1993).

Table 1.1 Magnitude and pathway of toxic releases into the environment in the United States and the State of Illinois in 1989 (USEPA Toxic Release Inventory, 1991).

	United States	Illinois
Total Releases and Transfers (kg)	2.59×10^9	1.13×10^8
Air (%)	42.54	38.15
Surface Water (%)	3.31	6.76
Land (%)	7.79	4.21
Underground (%)	20.70	4.32
Public Sewage (%)	9.66	23.60
Off-Site (%)	16.00	22.95

From the list of toxic emissions, USEPA has identified 188 hazardous air pollutants (HAPS; listed in Appendix A) for federal regulation (USEPA, 1990). Many of these HAPs are TVOCs. In general, USEPA categorizes volatile organic compounds (VOCs) as low, moderate and high volatility based on the compounds vapor pressure at 293 K (Table 1.2). Atmospheric emissions of TVOCs appearing on the USEPAs list of 188 HAPs totaled 4.5×10^8 kg in 1991 (USEPA[a], 1993).

Table 1.2 USEPA VOC categories based on vapor pressure (USEPA Control Technology Guideline Series, 1991).

VOC Category	Vapor Pressure at 293 K (MPa)
Low Volatility	< 0.01
Moderate Volatility	0.01 to 0.02
High Volatility	> 0.02

Atmospheric releases of the top eight emitted TVOCs account for approximately 95% of the TVOC total emissions HAPS (Figure 1.2). Methanol, toluene, trichloroethane, xylene and methyl ethyl ketone constituted the largest TVOC emissions to the atmosphere in 1991 (USEPA[a], 1993). In general, emissions of VOCs to the atmosphere have declined from 1987 to 1991 by approximately 5% per year (USEPA[a], 1993). This is in large part due to government regulation of VOC emissions (McIlvaine et al., 1992).

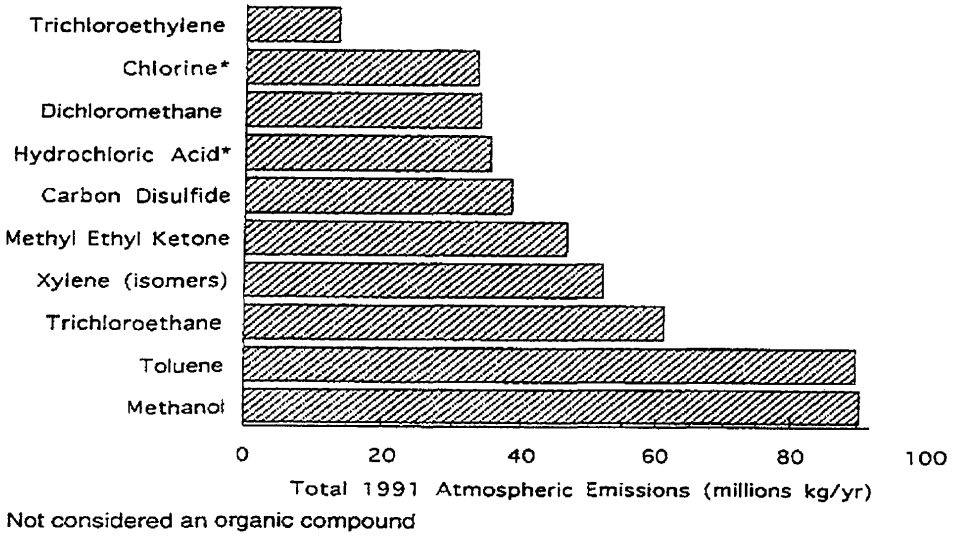

Figure 1.2 Top ten HAPs emitted to the atmosphere in the U.S. in 1991, all of which are considered TVOCs except chlorine and hydrochloric acid (USEPA[a], 1993).

Point Source Emission Trends

Atmospheric emissions from point sources can come from a variety of locations within a facility. These emission points include process vents, process vent leaks, transfer operations, storage vessels, waste water treatment and equipment leaks (USEPA[a], 1991). Typically, atmospheric emission inventories at a specific site must include releases from all of these categories and any other pathways that may exist (Ruhl, 1993).

Industrial toxic emissions to the atmosphere are attributed to a number of source types within the United States. Approximately 31% of the total toxic emissions to the atmosphere were emitted from the chemical industry (Figure 1.3). The chemical manufacturing industry emits as much as 150 of the 188 HAPS to the atmosphere (USEPA[a], 1993). Under the USEPA proposed Hazardous Organic National Emissions Standards for Hazardous Air Pollutants (HON) rule, 370 chemical manufacturing facilities and 1,050 chemical manufacturing processes will be required to reduce the TVOC emissions from 5.6×10^8 kg emitted in 1989 to 1.1×10^8 kg by 1998 (USEPA[a], 1993).

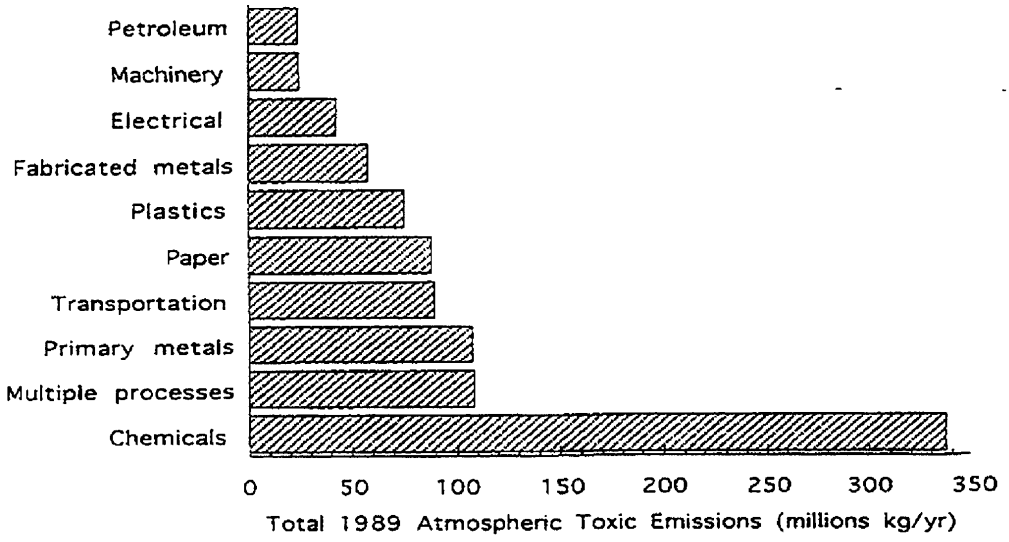

Figure 1. 3 The top ten industries emitting of HAPs in the U.S. during 1989 (USEPA[b], 1993)

Effects of TVOCs on Human Health

Selection of many of the 189 HAPS listed in Section 112 of the 1990 CAAA was based on the compound's potential to cause increased mortality or serious illness. For example, many of these air toxics are known to be human carcinogens (USEPA[a], 1993). Exposure is also known or suspected to cause many other noncancerous effects (Table 1.3), including poisoning and immunological, neurological, reproductive, developmental, mutagenic and respiratory problems (Burge and Hodgson, 1988). Risk assessment of exposure to air toxics is difficult for cancereous effects and much more difficult for non-cancerous effects due to the many different possible means of exposure pathways (USEPA[a], 1993). USEPA is required under the 1990 CAAA to evaluate residual risk remaining after the implementation of technology-based standards.

Table 1.3 TVOC and acetone sources, pathways, exposure and human health effects (National Institute for Occupational Safety and Health Guide to Chemical Hazards, 1990).

TVOC	Sources	Pathways	Exposure Limits[1] (ppmv)	IDLH[1,2] (ppmv)	Effects
Acetone	Common solvent	Inhalation, ingestion	750	20,000	Irritate eyes, nose & throat, headache; dizziness
Toluene	Oil refinement, paint and plastic solvent	Inhalation, Ingestion, skin/eye contact	100	2,000	Fatigue, damage to nervous system, nausea, death
MEK	Solvent, synthetic rubber production, adhesives	Inhalation, skin absorption	200	3,000	Numbness, respiratory irritant, nausea, headache, smog precursor
Benzene	Solvent, chemical manufacturing	Inhalation, ingestion, skin/eye contact	1	3,000	Damage to nervous system, nausea, death
Xylenes	Catalytic reformat of petroleum	Inhalation, ingestion, skin/eye contact	100	1,000	Lung damage, nausea, reduced coordination

[1] Occupational Safety and Health Administration established standard
[2] IDLH = immediately dangerous to life or health concentration

Many TVOCs are also known to be tropospheric ozone precursors. Ozone can cause eye, nose, throat and respiratory problems in humans, especially in urban areas (Tolley et al., 1993). This is in part the reason for the mandated reduction of VOCs under Title I in ozone non-attainment areas (USEPA, 1990).

Federal TVOC Regulations

Between 1970 and 1990, the USEPA regulated only eight HAPs (arsenic, asbestos, benzene, beryllium, mercury, radio nuclides, radon-222 and vinyl chloride) under the National Emission Standards for Hazardous Air Pollutants (NESHAPS). During this time, however, the 1977 Clean Air Act Amendments were further changed, and these new amendments were signed into law in 1990. As a result of this 1990 legislation, USEPA is required to establish technology-based guidelines (e.g., RACT and MACT explained below) for the reduction of TVOC emissions to the atmosphere from point sources (USEPA, 1990). Specifically, control-based reduction of VOCs falls under Title I and Title III of the 1990 CAAA. Effectively, VOC emissions in ozone non-attainment areas are governed by Title I, and TVOCs are governed by Title I and Title III.

Under Title I of the 1990 CAAA, USEPA is required to establish reasonable achievable control technology (RACT) standards for point source VOC emissions in ozone-related non-attainment areas. State environmental regulatory agencies are responsible for establishing implementation of RACT standards. RACT is defined as the lowest emission limitation that a particular source is capable of meeting by the application of control technology that is reasonably available considering technological and economic feasibility (USEPA[c], 1991). A compilation of

information was developed for state use in determining state specific RACT implementation. For example, the USEPA developed an information base on VOC emissions of 17 categories of industries (USEPA[a], 1993), control technology techniques and cost of implementation of various control technologies (USEPA[c], 1991) have been developed by USEPA.

Title III of the 1990 CAAA requires USEPA to establish maximum achievable control technology (MACT) standards for point source emissions of HAPs. MACT standards are based on the best demonstrated control technology and/or practices and is not dependent on the cost of the technology. These standards apply to all major sources with the potential to emit at least 10 tons per year of any one of the HAPs or at least 25 tons per year of any combination of HAPs. All area sources are also subject to MACT standards. HAP emission standards for point sources based on MACT must be promulgated by November 15, 2000. Furthermore, sources regulated under Title III must meet permit requirements within three years of promulgation. (USEPA[c], 1991)

The USEPA has classified 17 primary categories of industrial sources emitting HAPS (USEPA, 1990) as given in Table 1.4.

Table 1.4 Primary categories of industrial sources emitting HAPs. (USEPA, 1990)

Fuel combustion	Agriculture chemicals production
Non-ferrous metals processing	Fibers production processes
Ferrous metal processing	Polymers and resins production
Mineral products processing	Production of organic chemicals
Petroleum and natural gas production	Miscellaneous processes (e.g., dry
Petroleum and natural gas refining	cleaning)
Liquid distribution	Food and agricultural processes
Surface coating processes	Pharmaceutical production processes
Waste treatment and disposal	Area sources

These sources fall under new regulations that are the most comprehensive to date for TVOC emission reductions (American Consulting Engineers Council, 1994). McIlvaine (1992) reports that gas phase reductions of air toxics will amount to approximately 70% of the current emission levels. It is likely that new technologies will need to be developed to reach these reduction levels in a cost effective manner. A projected 74% increase in demand for incineration and adsorption systems will result from current facilities attempting to meet the 1990 CAAA VOC and HAP requirements (McIlvaine, 1992).

Point Source Reduction of TVOC Emissions

Point source TVOC emission reduction is generally accomplished by: 1) process modification, 2) feed stream modification, 3) source shutdown and/or 4) utilization of ancillary control devices. While process modification is generally the most economical method of reducing TVOC emissions, further reduction of these emissions below what can be obtained through modification usually requires the addition of control devices along the waste stream (Ruddy and Carroll, 1993).

The seven most widely used control devices that remove VOCs from gas streams are: 1) thermal incinerators, 2) catalytic incinerators, 3) flares, 4) boilers/process heaters, 5) carbon adsorbers, 6) absorbers and 7) condensers (USEPA[c], 1991). These control devices are described below. Selection of an appropriate technology is dependent on the process gas stream

characteristics, capital and annual costs and the desired removal efficiency (Table 1.5). Further considerations for TVOC control device selection include: 1) recycling potential, 2) variability of loading, 3) average loading, 4) diversity of TVOCs in the gas stream, 5) lower and upper explosion limits of the TVOCs present in the gas stream, 6) gas stream temperature, 8) fouling problems, 9) locating the control device and 10) required maintenance of the control device (Ruddy and Carroll, 1993).

Thermal oxidation systems include thermal and catalytic incinerators, flares and boiler processes. Thermal incineration systems oxidize the VOCs in the gas stream at temperatures typically between 950 K and 1250 K (Ruddy and Carroll, 1993), producing mostly CO_2 and water vapor. The required temperature is dependent on the composition of the gas stream and the desired removal efficiency. Catalytic incinerators are essentially thermal incinerators with a catalyst present to reduce the operating temperature of the reactor. Typical operating temperatures for catalytic incinerators are 650 K to 750 K.

Table 1.5 Control devices commercially available for VOC removal from effluent gas streams (Ruddy and Carroll, 1993).

Control Device	VOC Content (ppmv)	Flow Rate (scfm)	Capital Cost 1993 ($/cfm)	Annual Cost 1993 ($/cfm)	Removal Efficiency	Advantages	Disadvantages
Thermal Incinerator	100-2000[2]	1000 to 500,000	10 to 450	15 to 150	95-99+%	Up to 95% energy recovery	Halogenated compounds may require additional control
Catalytic Incinerator	100-2000[2]	1000 to 100,000	20 to 250	10 to 90	90-95%	Up to 70% energy recovery	Catalyst poisoning
Flare[1]		<2,000,000			>98% Steam-assisted	VOC destruction of variable emission conditions	Low heating value VOC requires auxiliary fuel
Boiler[1]		Steady			>98%	Supplement fuel	Variations may affect process
Carbon Adsorber	20-5000[2]	100 to 60,000	15 to 120	10 to 35	90-98%	Vapor recovery, pre-concentrator	High RH may lower capacity, pore fouling
Absorber	500-5000	2000 to 100,000	15 to 70	25 to 120	95-98%	Vapor recovery	Scale build-up, liquid waste
Condenser	>5000	100 to 20,000	10 to 80	20 to 120	50-90%	Vapor recovery	Scale build-up, liquid waste

[1] Source: USEPA[b], 1991
[2] <25% of lower explosion limit
RH = relative humidity

Flares directly combust the VOC present in the gas stream using an open flame, typically with a secondary fuel such as natural gas (USEPA[b], 1991). This type of VOC abatement technology is often used for gas streams in which the VOC cannot economically be recovered and when process stream characteristics are highly variable. Flares are also used as a safety mechanism in conjunction with other control devices (e.g., a sudden increase in gas flow rate that overloads another control device can be sent to the flare).

The use of boilers to remove TVOCs from gas streams is site specific (USEPA[b], 1991). TVOC destruction is achieved with an on-site boiler that is used for other processes within the facility.

Adsorption systems capture TVOCs at the adsorbents' internal and external surface areas. Activated carbon is the most widely used adsorbent for VOC removal (USEPA[b], 1991; Noll et al. 1992). Typically the adsorbent is regenerated either thermally at an elevated temperature (typically with steam) or under a vacuum.

Absorbers transfer VOCs from gas streams to a relatively non-volatile liquid (USEPA[b], 1991). Absorption rates are typically dependent on the VOC concentration gradient between the gas phase and liquid phase, the physical properties of the gas/liquid system (e.g., diffusivity, viscosity and density) and the operating conditions of the absorber (e.g., temperature and flow rate). Absorption is typically enhanced by lower operating temperatures, achieving large concentration gradients between the gas and liquid phase and allowing greater interfacial surface area.

Condensers can be used to remove VOCs from gas streams by lowering the temperature of the stream below the saturation temperature of the VOC. The gaseous VOC will change phase from a gas to a liquid at the saturation temperature and concentration, and thus the contaminant would be removed from the gas stream. Recovery of VOCs by condensation should be considered when a relatively pure condensate with a monetary value greater than $0.66/kg can be recovered (Dyer and Muhlholland, 1994).

The applicability of these technologies to a specific gas stream is dependent on the type of VOCs in the gas stream (Table 1.6). Thermal incinerators, catalytic incinerators and condensers can be applied to the widest range of VOC categories.

Table 1.6 Applicability of VOC control technologies to specific VOC categories (Moretti and Mukhopadhyay, 1993).

Technology	VOC Category[1]
Thermal Incinerator	AHC, HHC, A, K
Catalytic Incinerator	AHC, HHC, A, K
Flare	AHC, A, K
Boiler	AHC, A, K
Carbon Adsorber	AHC, HHC, A
Absorber	A, K
Condenser	AHC, HHC, A, K

[1] AHC = aliphatic and aromatic hydrocarbons
HHC = halogenated hydrocarbons
A = alcohols, glycols, ethers, epoxides and phenols
K = ketones and aldehydes

This manuscript reports on the development of an ACFC adsorption system that has been integrated with electrothermal desorption and LN_2 cryogenic condensation to reduce the TVOC emission levels to the MACT standards and provide for reuse of the TVOCs that are recovered. In the adsorber, TVOCs are selectively separated from the influent gas stream by the attraction force fields generated from micropore walls in the ACFC fibers. ACFC adsorption is followed by electrothermal regeneration, using nitrogen as the carrier gas, resulting in formation of a nonexplosive concentrated organic vapor. Then the concentrated TVOC is efficiently condensed using LN_2 as the required refrigerant. ACFCs higher adsorption capacity and faster adsorption

and desorption rates along with higher energy transfer through electrothermal desorption allows for optimizing the desorption time and TVOC concentration profile to allow minimal use of LN_2. LN_2 can reduce TVOC emission concentrations to ppbv levels due to its low temperature and high latent heat of vaporization. This system can enable TVOC sources to meet air quality control regulations while providing a high quality liquid TVOC product for reuse.

2. RESEARCH OBJECTIVES

The objectives of this project are to: 1) design and construct an ACFC adsorption system utilizing electrothermal regeneration and cryogenic vapor recovery, 2) conduct experimental measurements of removal efficiencies and breakthrough times for select TVOCs and acetone with the fixed bed of ACFC, 3) cryogenically recover the concentrated vapor and analyze purity of the condensate, 4) evaluate the experimental results with existing models for adsorption and condensation, and 5) describe new or larger-scale applications of the developed laboratory system. Acetone was listed as a TVOC at the initiation of this project, has large emissions to the atmosphere, and is a good surrogate for other TVOCs. Results for research pertaining to acetone are also reported here. Our research activities to meet these objectives are discussed in the next three main sections.

3. DESIGN AND DEVELOPMENT OF THE SYSTEM

A flow diagram of the ACFC adsorption/electrothermal regeneration/LN_2 condensation system for TVOC recovery is given in Figure 3.1. The system can utilize one or more fixed-beds. The system can be classified as an electrothermal-swing adsorption (ETSA) process. The industrial TVOC effluent passes through an ACFC fixed-bed where ACFC separates the TVOC by adsorption. The bed exhaust (cleaned gas) is then recycled for other process needs or vented to the atmosphere. After breakthrough of TVOC from the fixed bed, the untreated TVOC stream can be directed to the second bed for a continuous process operation while the exhausted bed is switched to a regeneration step. During the regeneration process an order of magnitude lower flow rate pure N_2 gas is passed through the adsorption bed and electrical power is supplied to the ACFC. Electrothermal energy regenerates the ACFC and provides a N_2 gas stream containing a concentrated desorbed TVOC.

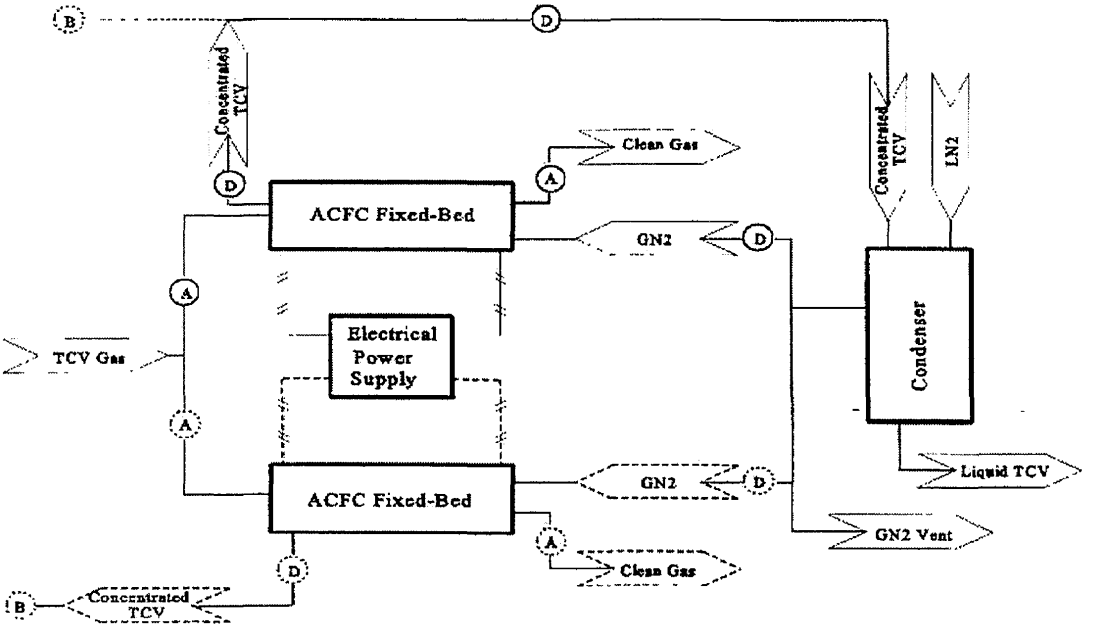

Figure 3.1 Flow diagram of the ACFC adsorption/electrothermal regeneration/cryogenic recovery system. Letters A and D denote adsorption and desorption streams.

TVOC concentration in the N_2 carrier gas is controlled by the amount of electrical power supplied and the flow rate and temperature of the carrier gas. The concentrated vapor stream is then directed to a LN_2 cryogenic condenser where the TVOC is condensed and separated from the noncondensible carrier gas. The cold nitrogen gas from the condenser exhaust can be used to cool the adsorber after the desorption step, and then it can be used for other process needs.

Adsorption

Physical adsorption is a process in which attraction force fields at the solid surfaces pull molecules or ions from the gas phase and bind them reversibly to the surface. The strength of adsorption forces depend on the nature and state of the solid and of the individual gas molecules. The difference in strength of interaction between a solid surface and different gas molecules is the basis of adsorption separation. Intimate binding by physical adsorption is most pronounced in a monomolecular layer at the solid surface, although the adsorption layer can persist to three or four molecular layers at some locations of the surface (Ruthven, 1984). The thickness of the adsorption layer depends on the strength of the local force field, the nature of the adsorbate, and the gas phase concentration of adsorbate. In general, the amount of adsorbate that can be attracted by an adsorbent is a function of available surface area and the strength of the force fields at the surface. Therefore, increasing the surface area in combination with increasing the attraction force fields increases the adsorption capacity. One way to increase the force fields is by generating small pores in the adsorbent materials. The overlap of the force fields from the opposite pore walls strongly enhances the adsorption in the micropores. Another significance of small pores is that condensable vapors can be liquefied in sufficiently narrow pores at a pressure

lower than the saturation pressure of the vapors. This mechanism of binding vapors in pores is called capillary condensation.

The requirement for an adequate adsorptive capacity restricts the choice of adsorbents for practical separation processes to microporous materials with pore diameters ranging from a few Angstroms to a few tens of an Angstrom (Ruthven, 1984). Discovery of naturally microporous adsorbents, such as zeolite, and development of the new adsorbents, such as activated carbon and silica gel, provided the opportunity to efficiently utilize adsorption phenomena in industrial separation processes. Some industrial separation processes that have successfully utilized physical adsorption phenomenon are mentioned in Table 3.1.

Industrial adsorption systems are classified either by their method of regeneration or by their type and configuration of adsorber. By regeneration method, they are either thermal-swing adsorber (TSA), pressure-swing adsorber (PSA), purge-swing, and elution systems. Classified by the type of adsorber, they are either fluidized-beds, moving-beds, or fixed-beds. Fluidized beds are mainly used when waste hot gas is available for use during regeneration. In fluidized beds, the adsorbent is contacted counter-currently with the gas stream on perforated trays in relatively shallow beds. The gas uniformly distributes over the bottom cross section of the bed. Due to momentum transfer, the bed expands and the solid particles move freely and circulate through two adsorption and desorption sections. In moving-beds, both adsorbent and gas mixture move through the adsorber in a continuous manner. The adsorbent is moved from an adsorption chamber to a regeneration chamber. Numerous moving-bed adsorbers have been designed and built, but relatively few are in large-scale use (Vermeulen, 1975). Combination of fluidized-bed adsorption and moving-bed desorption has also been used. However, both fluidized-and-moving beds are unpopular for their complexity of design, attrition of adsorbent particles that can lead to excessive adsorbent losses, and operation difficulties.

Table 3.1 Industrial gas adsorption separation processes (Keller, 1983).

Process	Gas Mixture	Adsorbent
Gas Bulk Separation	Acetone/Vent streams	Activated Carbon
	Acethylene/Vent streams	Activated Carbon
	Normal Paraffins/Iso-paraffins, Aromatics	Zeolite
	N_2/O_2	Zeolite, CMS *
	CO, CH_4, CO_2, N_2, Ar, NH_3, H_2	Activated Carbon
Gas Purification	Organics/Vent streams	Activated Carbon
	Odors/Air	Activated Carbon
	H_2O/Olefin-containing cracked glass	Silica, Alumina
	Natural gas, Air, Synthesis Gas, etc.	Zeolite
	CO_2/C_2H_4, Natural Gas, Hydrogen, LPG	Zeolite
	NO_x/N_2	Zeolite
	SO_2/Vent streams	Zeolite
	Hg/Chlor-alkali cell gas effluent	Zeolite

* CMS: carbon molecular sieve

Unlike moving-and-fluidized beds, fixed-bed systems are very simple in design and operation, having relatively few moving parts. In the fixed-beds, the gas mixture passes through a stationary bed of adsorbent material. Figure 3.2 shows a schematic illustration of a typical fixed-bed and the method of flow distribution through it.

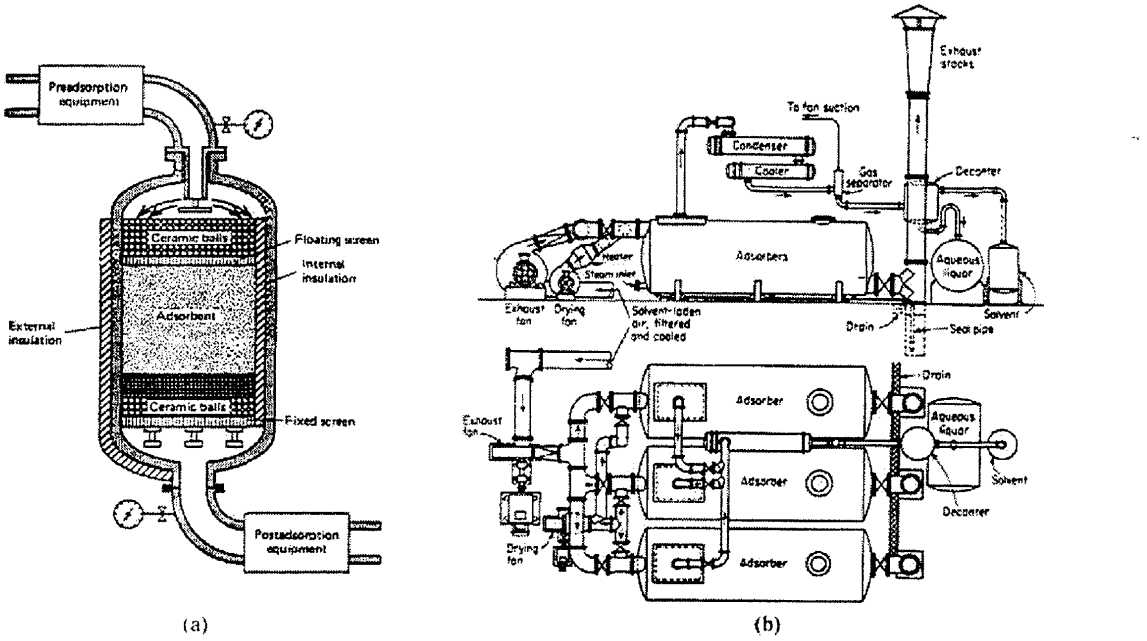

Figure 3.2 Schematic illustration of (a) a typical fixed-bed and (b) a fixed-bed adsorber system (Treybal, 1980)

The most common problem of conventional fixed-beds is channeling. In channeling, some of the adsorbate passes through open channels in the bed without coming into contact with adsorbent. This can happen, for example, with bed leakage. Even small leaks produce channeling in the bed. Channeling reduces the adsorption efficiency rapidly and severely.

Usually a typical processing system uses more than one fixed-bed adsorber. The gas mixture passes through some of the fixed-beds while the others are being regenerated. A typical TSA fixed-bed adsorption system for solvent vapor recovery that consists of three adsorbers in parallel is also shown in Figure 3.2. One bed will undergo adsorption, one regeneration and one will cool after it is regenerated. The number of adsorbers are selected based on optimization of overall process operation and cost benefits. However, the most common processing scheme is a pair of adsorbers alternating between the adsorption step and the regeneration step. In situations where the effluent stream is discharged intermittently, it is possible to use one fixed-bed. However, in general, one fixed-bed provides interrupted flow while multiple beds can ensure continuous flow for the vapor recovery unit.

As an adsorbate laden gas stream passes through a fixed-bed, it is selectively adsorbed. This causes a concentration change at the solid phase and in the gas phase. At the beginning, the highest mass transfer takes place at the locations where the fluid first contacts the adsorbent. Thus the gas concentration drops exponentially from the inlet to the end of the bed. As time passes, the adsorbent at the bed inlet becomes saturated and the mass transfer zone (MTZ) moves from the inlet toward the end of the bed. By definition, the MTZ refers to the region in which the

adsorbate gas concentration changes from 95% to 5% of its inlet value. This is the region where most of the mass transfer takes place. With respect to time, a S-shaped concentration profile develops for the MTZ which travels down the bed. The sharpness of the MTZ primarily depends on the adsorption capacity and shape of the equilibrium isotherms, the parameters that affect transport processes in the bed (such as velocity, size of adsorbent particles, packing density and diffusion resistances) and secondary effects from transport processes within the adsorbent particles. In order to utilize the adsorbent efficiently and reduce the amount of energy during regeneration, the MTZ should be narrow.

The concentration of contaminant at the outlet of the adsorber is negligible from the beginning of the process to the time that the MTZ reaches the outlet. From then on, the concentration level at the outlet rises until it reaches the inlet concentration value. A plot of the outlet concentration with respect to time is called the breakthrough curve (BTC). The break point or breakthrough time is often used to refer to the time at which the outlet concentration reaches a specific permissible value. For this project, this value is taken to be 5% of the inlet concentration. After the break point, the concentration at the bed outlet rises rapidly to about 50% and then it approaches 100% more slowly. The breakthrough curve takes a S-shaped form for a favorable isotherm with the symmetric point at the 50% concentration level. For a symmetric concentration profile, it can be shown that the adsorbed amount from the start to the completion of breakthrough is equal to the amount of adsorbate that has been passed through the bed until the time of 50% outlet concentration. Furthermore, this amount would be very close to the value adsorbed if the entire bed was at equilibrium with gas inlet concentration in a quiescent condition. Due to this property, the time of 50% concentration level is called stoichiometric time. In the hypothetical situation of a bed outlet concentration suddenly jumping from the zero value to the inlet value, stoichiometric time would designate the breakthrough time, and it could be estimated by the following relation

$$t_s = \frac{(M_a)(W_c)}{(U_s C_i A)} \tag{3.1}$$

where M_a = total mass of adsorbent, (g)
W_c = working capacity of bed = $(W_e - W_o)$, (cm^3/g)
W_e = equilibrium capacity, (cm^3/g)
W_o = initial retained capacity, (cm^3/g)
U_s = superficial gas velocity, (cm/s)
C_i = inlet gas concentration, (cm^3/cm^3)
A = bed intersection area, (cm^2)

In realistic situations, breakpoint time t_b is shorter than t_s, recognizing that the breakthrough curve will not be a step function due to mass transfer limitations. Given a set break point concentration, the shorter the time interval between t_b and t_s, the sharper the breakthrough curve and the higher the bed capacity would be at breakpoint. The shape and sharpness of the breakthrough curve for a given adsorbent depend on the type of equilibrium isotherm, the mass and heat transfer rates, and hydrodynamic factors such as mixing and contact time.

Target TVOC Adsorbates

Based on an economic and engineering study on VOC control technologies (Dyer and Mulholland, 1994), if the VOCs have a value greater than $0.66/kg, then carbon adsorption and vapor recovery is a profitable process. Regardless of price, if the effluent gas flow rate is greater than 28 m^3/min and TVOC concentrations are greater than 500 ppmv, the most cost effective ancillary control technology is carbon adsorption (Dyer and Mulholland, 1994).

Another criteria for selection of carbon adsorption for TVOC recovery is based on the adsorbate retentivity. Adsorption affinity of activated carbons increases as a function of molecular weight of TVOCs. However, the higher the molecular weight, the less volatile the TVOC would be. Both the low volatility and high adsorption affinity increase the retentivity of these compounds and makes their desorption process more difficult.

Considering the above criteria, examples of industrial TVOC emissions that may be recovered efficiently by carbon adsorption technology are listed in Table 3.2.

Table 3.2 Industrial TVOC emissions that may be recovered efficiently by ACFC sorption..

Dichloro methane	Benzene	Propylene oxide
Methyl ethyl ketone (MEK)	Hexane	Methylene chloride
Ethanol	Heptane	Perchloro ethylene
Methanol	Cyclohexane	Phosgene
Isopropyl alcohol	Xylene	1,1,1-trichloroethane
Normal butanol	Tetrachloro ethylene	Dichlorodifluoromethane
Ethylene oxide	Phenol	Trichlorotrifluoro ethane
Gasoline	Styrene	Chloroform
Tetrahydrofuran	Toluene	Carbon tetrachloride
Vinyl chloride	Natural gas	Methyl-tert-butyl-ether (MTBE)
Ethyl acetate	Tetrahydrofuran	Ethyl-tert-butyl-ether (ETBE)
Vinyl acetate		

Suitable Adsorbents

The most commonly used materials for gas separation and purification are activated carbon, silica gel, activated alumina, carbon molecular sieves, and zeolite (crystalline aluminosilicate). Table 3.3 lists some of commercial adsorbents that are used in gas separation and purification processes. From the variety of adsorbents, activated carbon is the most suitable material for separation of TVOCs from industrial gas streams. Carbon selectively adsorbs organic compounds (especially non-polar ones) unlike most inorganic adsorbents. Furthermore, the inorganic adsorbents lack another attractive feature of activated carbons, that is their availability in various pore structures as indicated by total pore volume and pore size distribution. For a given TVOC concentration, the carbon adsorbent that will provide a high adsorption capacity has a high percentage of total surface area and pore volume distributed in optimal pore size ranges.

Table 3.3 Commercial adsorbents that are commonly used in gas separation and purification. (Noll, 1991)

Adsorbent	Shape	Average Pore radius (Å)	Surface Area (m^2/g)	Commercial name
Activated Aluminas	Granular	35-45	235	Alcoa F-1
	Spherical Beads	40-50	400	Alcoa H-151
Alumino-Silicates	Cylindrical Pellet	3-5	600	Siliporite
	Spherical Beads	3-5	700	NK10-30
	Powder	3-6	700	NK10AP-NK20AP
Magnesia Silica Gel	Granular	30	300	Florisil
Fullers Earth	Granular	40	130-250	Cecacite
Silica Gel	Granular	20-40	650-900	Cecagel
Activated Carbon	Granular	20	600-1,000	Cochranex
	Granular & Powder	18-20	800-1,500	Pittsburgh
	Granular	5-20	1,300-1,400	Supersorbon
	Powder	8-30	1,000-1,500	Carboraffin
	Granular	30-40	500-1,600	Norit
	Granular	20-38	500-700	Darco
	Granular	5-15	1,300-1,500	Contarbon
	Spherical	32	800-1,100	Union Carbide

Pore size distribution can drastically affect the adsorption characteristics of the adsorbent. The International Union of Pure and Applied Chemistry (IUPAC) classifies pores into three categories based on their diameter, d, as follows: micropores have $d < 20$ Å, mesopores have 20 Å $< d <$ 500 Å, and macropores have 500 Å $< d$. Micropores are further broken down into ultramicropores with $d < 7$ Å and supermicropores with 7 Å $< d <$ 20 Å (Kaviany, 1994; Gregg and Sing, 1982). These divisions are mainly based on the different types of forces which control adsorption behavior in different size ranges. For example, adsorption in ultramicropores is generally restricted to a monolayer. In the supermicropores, the superposition of pore wall force fields enhances the physical adsorption by formation of multilayer adsorption and pore filling. The upper limit of 20 Å for the micropore classification is introduced because of the disappearance of the adsorption-desorption hysteresis loop at this pore size. This hysteresis is caused by capillary condensation at relative pressures of approximately 0.3-0.4, depending on the nature of the adsorbent and adsorbate (Bhandarkar et al., 1992). For gas purification processes at TVOC concentrations < 10 ppmv, ultramicropores generally provide a higher adsorption capacity. For TVOC concentration > 10 ppmv, pores with diameters in the range of supermicropores and transitional range are preferred. These larger pores are preferred because the adsorbent will have a higher total specific pore volume and the pores are filled at the concentration levels greater then 10 ppmv.

Regeneration

At the end of the adsorption process, when the working capacity of an adsorber is exhausted, it has to be regenerated. The conventional regeneration methods for this task are classified as: 1) thermal swing desorption, 2) pressure swing desorption, 3) elution desorption, and 4) inert purging desorption.

In a thermal swing system, desorption takes place by raising the bed temperature. The bed temperature is raised by passing a hot inert gas through the adsorber or heating the bed by internal or external heating elements. If hot inert gas is used, it is commonly generated from combustion of fuel. In a pressure swing system, desorption takes place by providing a suitable pressure differential between the adsorption and desorption processes. If, for example, the adsorption pressure is atmospheric, vacuum is applied to regenerate the bed. The vacuum pressure is usually generated by refrigeration. In elution desorption, the adsorbate is replaced by an eluate that has more affinity for adsorption. In inert purging desorption, an inert gas is sent through the adsorber and desorption takes place under a mass transfer controlling condition.

Combinations of these methods are also used. One example is thermal swing desorption using saturated low pressure steam. In this process, steam in direct contact with the adsorbent is condensed and replaces the adsorbate molecules in the pores by adsorption or capillary condensation. This elution of water vapor is an exothermic process that provides additional heating. The combination of these three effects provides a higher desorption rate than those of the thermal swing methods that use an inert hot gas.

Each of these systems have their own advantages and disadvantages. In direct steam regeneration, working capacity is reduced due to water vapor adsorption, capillary condensation and carbon oxidation. This reduction in working capacity is called heel. The requirement for drying after steam regeneration is another disadvantage of steam regeneration. Furthermore steam regeneration can contribute to polymerization reactions on the surface of carbon adsorbents and cause a smoldering fire. This type of reaction is usually caused by the breakdown of ketones on the carbon surface in the presence of steam, air or transitional metals (McInnes, 1995). This mostly happens for higher molecular weight VOCs that require higher steam temperature for desorption. Other disadvantages of steam regeneration are requirements of a post distillation process for separation of the liquid adsorbates from water.

An advantage of a pressure swing or vacuum regeneration is that it cools down the bed instead of heating it up. Disadvantages of vacuum regeneration are requirement of complicated equipment and stronger mechanical design to prevent material collapsing under vacuum.

In this project, electrothermal desorption is used to regenerate the adsorption capacity of adsorbent. Electrothermal desorption is a relatively new method of regeneration that is not yet fully utilized in adsorption systems. In the electrothermal regeneration process, an electric current is passed through the carbon adsorbent. Electrical work due to phonon and defect scattering (Donnet and Bansal, 1990) in activated carbon is directly transformed to thermal energy in the adsorbent and the adsorbed TVOC. By the continuous flow of electric current, the thermal energy of the adsorbed molecules increases to a level that overcomes the surface bonding energy, and the TVOC desorbs from the ACFC. Since electrical work is transformed to desorption energy directly, the carrier gas temperature can be substantially lower than the ACFC temperature.

During electrothermal desorption, the temperature gradient along the radius of adsorbent is negative (or zero, depending on the Biot number) as opposed to conventional thermal desorption methods where the temperature gradient along the adsorbent radius is positive. This

negative gradient causes positive contributions to the rate of desorption from heat transfer, the Soret effect and pore effusion. In contrast, these mass transfer contributions are negative for conventional thermal desorption methods. Therefore, electrothermal regeneration should have higher energy efficiency compared to conventional thermal regeneration methods. Another advantage of electrothermal desorption is that the energy transfer rate can be very high and can be controlled easily. This enables a careful control of desorption time and a regenerated TVOC concentration profile for a better cryogenic recovery.

Condensation

Condensation can be used to remove unwanted vapors from gas streams. These constituents can often times be re-used after distillation or can be handled more easily as a liquid for ultimate disposal (Ruhl, 1993). Recovery of vapors is dependent on the type of condensation system selected. Various condenser designs and refrigerants are available for implementation (USEPA[b], 1991).

Condensation Principles

Two general methods of condensation are to increase system pressure or to reduce system temperature (USEPA[c], 1991). Reduction of the gas stream temperature to remove VOCs is more common than direct gas compression (Wilbur, 1985). Condensation by temperature reduction occurs when the temperature of a gas stream is lowered below the saturation concentration temperature of one or more of the vapors in the gas mixture. Further condensation of the vapors will occur as the temperature is reduced. The amount condensed and the gas phase concentration is dependent on the vapors saturation concentrations at the given temperature.

The dependence of the vapor concentration on temperature can be examined using the semi-empirical Wagner equation, given as (Reid et al., 1977):

$$\ln \frac{P_{VP}}{P_C} = \left(\frac{(VP_A)x + (VP_B)x^{1.5} + (VP_C)x^3 + (VP_D)x^6}{(1-x)} \right) \qquad (3.2)$$

where $x = 1 - \frac{T}{T_C}$

P_{VP} = Vapor Pressure (bar)
P_c = Critical Pressure (bar)
T_c = Critical Temperature (K)
T = Temperature (K)
VP_A, VP_B, VP_C, & VP_D = Experimental Constants

Using reported experimental values (Table 3.1), the saturation vapor concentration as a function of temperature is evaluated in Figure 3.3 for three commonly emitted TVOCs: acetone, toluene and MEK.

Table 3.4 Experimental constants for use in the Wagner equation (Reid et al., 1977).

	Acetone	Toluene	MEK
Pc (bar)	47.0	41.0	42.1
Tc (K)	508.1	591.8	536.8
VP_A	-7.45514	-7.28607	-7.71476
VP_B	1.20200	1.38091	1.71061
VP_C	-2.43926	-2.83433	-3.68770
VP_D	-3.35590	-2.79168	-0.75169

Dependence of acetone's and toluene's saturation vapor concentrations on temperature that were observed from the experiments (Figure 3.3; Vargaftik, 1975) are consistent with the

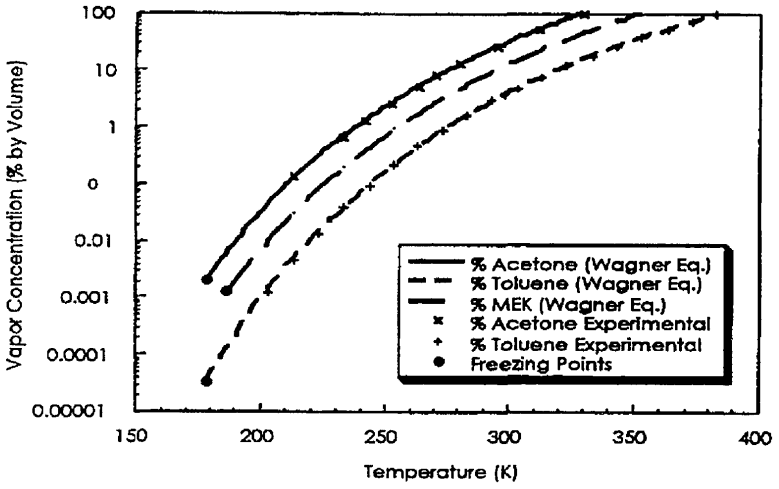

Figure 3.3 Modeled and experimental saturation vapor concentrations, experimental data from Vargaftik (1975).

calculated vapor pressures from the Wagner equation (Table 3.4.) At equilibrium, the concentration of vapor at a given temperature can be determined from eq. (3.2). Also, by knowing the initial concentration of vapor and the final temperature (thus equilibrium saturation concentration), the amount of vapor condensed can be determined assuming equilibrium conditions at the condenser outlet.

Heat Exchange Condenser Principles

Heat exchange condensers operate on the principle of lowering the temperature of a gas stream containing a condensable gas to a temperature corresponding to a saturation vapor concentration below the entering saturation vapor concentration. The equilibrium saturation vapor concentration is dependent on the temperature of the condenser gas stream. Lowering the temperature of the condenser will result in lower effluent vapor concentrations as discussed above (Figure 3.3). The temperature of the vapor laden gas stream is dependent on the transfer of heat from the refrigerant to the vapor.

Two general types of heat exchange condensers are commercially available, direct contact and indirect contact (Buonicore and Davis, 1992). The heat exchange condensation process can also be enhanced by compressing the gas stream in tandem with temperature reduction (USEPA[b,c], 1991). Gas stream compression for VOC condensation is not as widely utilized either individually or combined with direct and indirect contact methods (Buonicore and Davis, 1992).

Direct contact condensers mix the refrigerant with the process gas stream. Heat is more efficiently exchanged due to the intimate contact between the refrigerant and VOC. Direct contact condensation is typically simpler, less expensive to install and requires less auxiliary equipment (Buonicore and Davis, 1992). However, the refrigerant is mixed with the process stream. This may prevent refrigerant recycling and/or cause contamination of the refrigerant.

Indirect contact condensers utilize a physical barrier across which only heat is exchanged between the refrigerant and the process gas stream. Heat exchange is therefore less efficient in indirect methods. Keeping the refrigerant separate from the process gas stream allows for refrigerant re-use. This is beneficial if the refrigerant undergoes a cyclic mechanical refrigeration process. Indirect contact condensers typically cost more and are more complicated to design and operate (Buonicore and Davis, 1992). Because of the indirect contactors advantages, however, it is the most common type of condenser in air pollution control applications (USEPA[b], 1991).

Commercially Available Condenser/Heat Exchanger Designs

VOC recovery using condensation in industrial applications is typically conducted using a four step process (Dunn and El-Halwagi, 1994): 1) dehumidification, 2) heat integration, 3) VOC condensation in a condenser, and 4) distillation to separate VOCs (Figure 3.4). Dehumidification removes water vapor from the gas stream, via condensation, typically by reducing gas temperature to 274 K. This is necessary if TVOC condensation is conducted at temperatures below 273 K to prevent fouling in the condenser from frozen water vapor. The system designed for this research uses LN_2 as a refrigerant and a carbon adsorber pre-concentrator. The vaporized LN_2 emitted from the condenser can be recycled to the inlet of the carbon adsorber. The TVOC is thus desorbed in a pure N_2 carrier gas, and minimal water vapor is present. This reduces the dehumidification load before TVOC condensation.

Heat integration exchanges heat between the entering TVOC laden gas stream and the exit gas stream. This process lowers the gas stream temperature entering the condenser and therefore reduces the amount of refrigerant required. The vast majority of condensation will occur in the condenser. The refrigerant is injected in either a direct or indirect contactor to cool the condenser to the desired temperature and thus the desired TVOC outlet concentration. Distillation of the condensate can be used to separate the TVOCs for re-use. The selection of a distillation process is dependent on the composition of the condensate and the desired degree of TVOC separation (USEPA[b], 1991).

A wide variety of heat exchange condenser designs are available for VOC condensation (Jacobs and Nadig, 1987; Wilbur, 1985; Perry and Green, 1984; Kern, 1950). The solid curtain condenser and the jet condenser are two common direct contact condenser designs that utilize a liquid refrigerant (Jacobs and Nadig, 1987). Most designs incorporate a falling refrigerant with the VOC laden gas stream flowing up the condenser counter-current to the refrigerant (Figure 3.5).

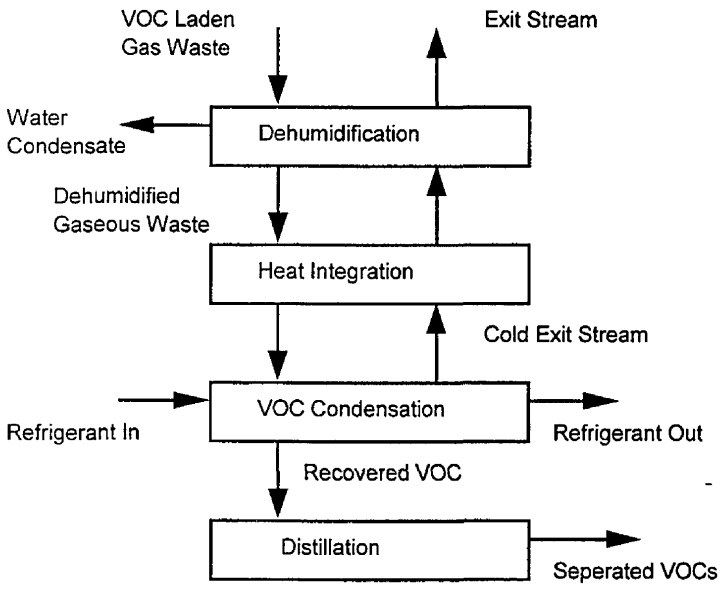

Figure 3.4 Schematic of a typical industrial VOC condensation process

A common type of indirect contact condenser is the shell-and-tube design (Wilbur, 1985).

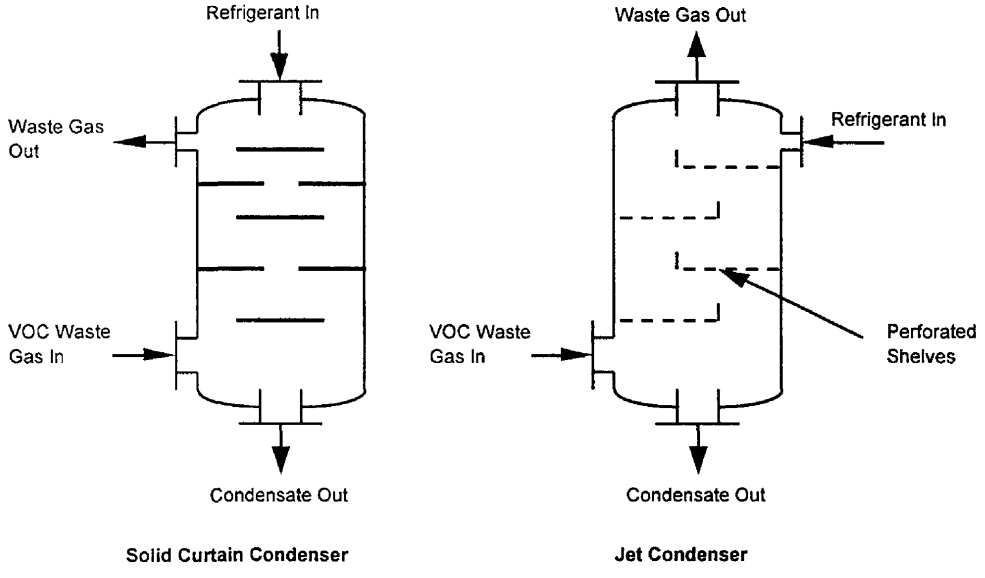

Figure 3.5 Solid curtain and jet heat exchange direct contact condenser designs (Jacobs and Nadig, 1987)

A common type of indirect-contact condenser is the shell-and-tube design (Wilbur, 1985). Condenser-surface areas from under 1 m^2 to 30,000 m^2 are available. Construction specifications for shell-and-tube designs can be obtained from the Tubular Exchangers Manufacturers Association (TEMA) Standards (TEMA, 1978). A multitude of design variations exist for these designs depending on the specific application criteria (e.g. minimize pressure drop, maximize surface area or maximize residence time). A simple 1-2 exchanger has one shell pass and two tube passes (Figure 3.6).

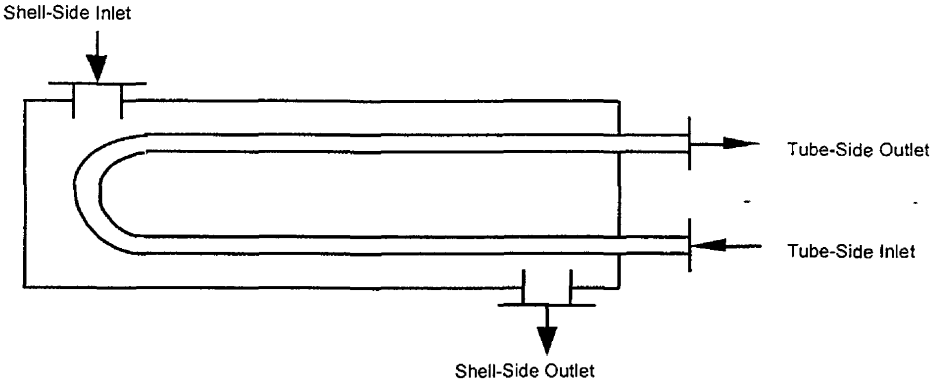

Figure 3.6 1-2 exchanger for indirect contact heat exchange (Kern, 1950)

The selection of tube-side or shell-side refrigerant flow is dependent on the variables that are to be optimized. As a general rule, selection can be based on balancing the residence times of the flows as to maximize the heat transfer times (Kern, 1950). Other considerations include condensation surface area differences between the shell and tube, heat loss to the outer shell wall, condenser cleaning and extraction of the condensate (Wilbur, 1985). Selection of flow direction is also important in optimizing condenser performance (Perry and Green, 1984). Typical flow patterns include co-current, countercurrent, reversed, cross-flow and mixed flow orientations. When faced with the choice between co-current and countercurrent flow selection for condensation, there is a thermal disadvantage in selecting a co-current flow (Kern, 1950). The minimum attainable VOC temperature (for a condenser of infinite surface area) is the outlet temperature of the refrigerant. In countercurrent flow the VOC can attain temperatures closer to the inlet refrigerant temperature (Figure 3.7). For other flow selections, Perry and Green (1984) provide detailed design parameters to determine flow selection.

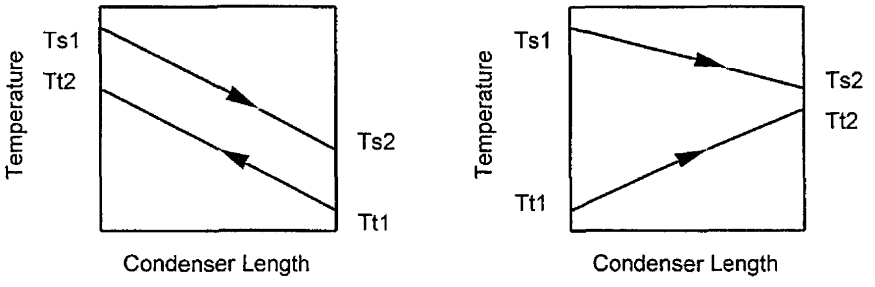

Figure 3.7 Representative temperature profiles for (a) contercurrent and (b) cocurrent flows in a heat exchanger with the refrigerant in the shell. s = shell, t = tube, 1 = flow entrance and 2 = flow exit

Refrigerants

Another condensation design criteria is the selection of an appropriate refrigerant. Refrigerant selection can be based on achievable temperature range, thermodynamic properties, cost, ease of use, handling and required auxiliary equipment (Dunn and El-Halwagi, 1994; USEPA[b], 1991; Wilbur, 1985; Perry and Green, 1984). The VOC removal efficiency and thus VOC recovery is based on the condenser temperature as outlined in section 3. Lower condenser temperatures will result in greater removal efficiencies and more product recovery. Temperature is often the primary refrigerant selection criteria for this reason (USEPA[b], 1991).

Selection of a refrigerant based on the desired outlet concentration is dependent on the refrigerant temperature range achievable. By knowing the desired effluent concentration of the vapor, the required condenser temperature can be determined from the Wagner equation. A refrigerant is selected that can achieve this temperature (Table 3.5).

A common refrigerant used in pollutant removal condensers is water (Wilbur, 1985). Water is inexpensive and easy to handle. However, because the condenser temperature is limited by the refrigerant temperature, cooling water results in low mass removal efficiencies for many TVOCs (Table 3.6). Mass removal efficiencies were determined for a 10% volume concentration TVOC stream to the equilibrium saturation vapor concentration. For applications where the process stream needs to be cooled below ambient temperatures, the use of cooling water typically requires auxiliary equipment to chill the water prior to use.

Table 3.5 Refrigerant selection based on temperature.

Required Condensation Temperature (K)	Refrigerant	Required Temperature of Refrigerant [2] (K)
289 - 300 [1]	Water	280 - 291 [3]
280 - 289 [1]	Chilled water	273 - 280
239 - 280 [1]	Brine solutions (e.g. ethylene glycol)	230 - 271
> 77	LN_2	77

[1] Source: USEPA[b] (1991)
[2] Source: USEPA[b] (1991) based on an assumed 9 K increase in refrigerant temperature during delivery to the condenser
[3] Dependent on climate

Table 3.6 Theoretical removal efficiencies for three refrigerants, Acetone and two TVOCs with a 10% by volume inlet gas stream.

Refrigerant	Operating Temperature (K)	Acetone		Methyl Ethyl Ketone		Toluene	
		Saturation [1] Vapor Concentration (ppmv)	Removal (%)	Saturation [1] Vapor Concentration (ppmv)	Removal (%)	Saturation [1] Vapor Concentration (ppmv)	Removal (%)
Water	278	102,000	0	40,000	60	5,500	94
60% Ethylene Glycol + H_20	240	15,000	85	3,800	96	420	99+
LN_2	200	300	99+	70	99+	2	99+

[1] determined from the Wagner equation (Reid et al., 1977)

Ethylene glycol and water mixtures are also commonly used refrigerants (ASHRAE, 1983). Lower operating temperatures can be achieved with this mixture than for pure water, thereby lowering the effluent TVOC concentration and recovering more condensate (Table 3.6). Ethylene glycol water mixtures are exclusively used with indirect contact condensers to prevent ethylene glycol losses to the effluent gas stream (ASHRAE, 1983). Auxiliary equipment is needed to cool the mixture to temperatures below ambient temperature.

Using LN_2 as a refrigerant can provide a wide range of condenser temperatures by controlling the LN_2 flow rate delivered to the condenser. The ability to lower condenser temperature near the freezing point of TVOCs results in theoretical removal efficiencies as high as 99+% (Table 3.6). Furthermore, because LN_2 undergoes a phase change in the condenser, both the enthalpy of vaporization and sensible heat provide cooling capacity. The use of LN_2 as a refrigerant generally requires a vacuum jacketed storage vessel and well insulated or vacuum jacketed delivery lines. However, auxiliary cooling equipment is not necessary, as the refrigerant is available in liquid form from commercial sources. LN_2 can be used in direct or indirect contactors. After the LN_2 passes through the condenser, the gaseous N_2 refrigerant can be used as a blanket gas in process streams or as a purge stream during desorption. Using the gaseous N_2 refrigerant as a purge stream during the adsorber desorption cycle helps reduce moisture levels, normally present in air purge streams, that may foul the condenser and helps prevent explosive hazards.

Below 273 K, condenser fouling may occur from frozen water vapor. In high humidity process streams, two condensers can be used in series. The first condenser can operate at temperatures above the freezing point of water to remove water vapor from the stream. The second condenser can then be operated at temperatures below the freezing point of water to achieve greater removal efficiencies of the organic and reduce condenser fouling from frozen water vapor. The use of LN_2 can maintain low condenser temperatures and eliminates the need for a dehumidification process. Condensation is a recoverable type of control technology that provides a method to recover TVOCs for re-use. The amount of condensate recovered is dependent on the temperature of the condenser. Lower condenser temperatures result in higher removal efficiencies and more recovered TVOC. The Wagner equation provides a method to determine the TVOC equilibrium saturation concentration dependence on temperature. A variety of condenser designs and refrigerants are available for implementation for condensation of

VOCs. The selection of an appropriate condensation system is dependent on many factors including the inlet gas characteristics and the desired outlet TVOC concentrations.

Design of the Laboratory-Scale ACFC System

Design steps of the laboratory-scale adsorption/regeneration/recovery system were identifying TVOC target adsorbates and concentration levels in typical effluent streams of full-scale facilities and selection of suitable adsorbent materials, adsorber type, regeneration method, condensation method, mechanical design of adsorber and condenser, and instrumentation design of the process. Development steps of the system were: fabrication of the adsorber and condenser, development of the gas generation unit, and assembly of the units and integration with analytical and measurement instruments.

The bench-scale ACFC adsorption-cryogenic vapor recovery system is presented in Figure 3.8. The system is composed of the units for sample gas generation, the ACFC fixed bed, cryogenic recovery, and analytical measurement. The calibrated gas stream passes through the fixed bed of ACFC, where the organic material is separated from the carrier gas by adsorption. The exhaust gas from the fixed-bed is analyzed continuously for the vapor concentration to make sure that breakthrough has not occurred. Then the vapor free carrier gas is vented under an exhaust hood.

Breakthrough for this project is defined as the condition when the concentration of the organic contaminant in the effluent reaches 5% of the influent concentration. After breakthrough of TVOC from the fixed bed, pure N_2 gas is passed through the adsorption bed and electrical power is supplied to the ACFC. Electrothermal energy regenerates the adsorption capacity of the ACFC and provides a N_2 gas stream containing concentrated desorbed TVOC. The TVOC concentration in the N_2 carrier gas is controlled by the supplied electrical power and the flow rate of the carrier gas. The concentrated vapor stream is then directed to the custom-designed shell-and-tube cryogenic condenser where the TVOC is condensed on the condensers internal cold surfaces. The condensed TVOC is transferred from the bottom of the condenser into an Erlenmeyer flask.

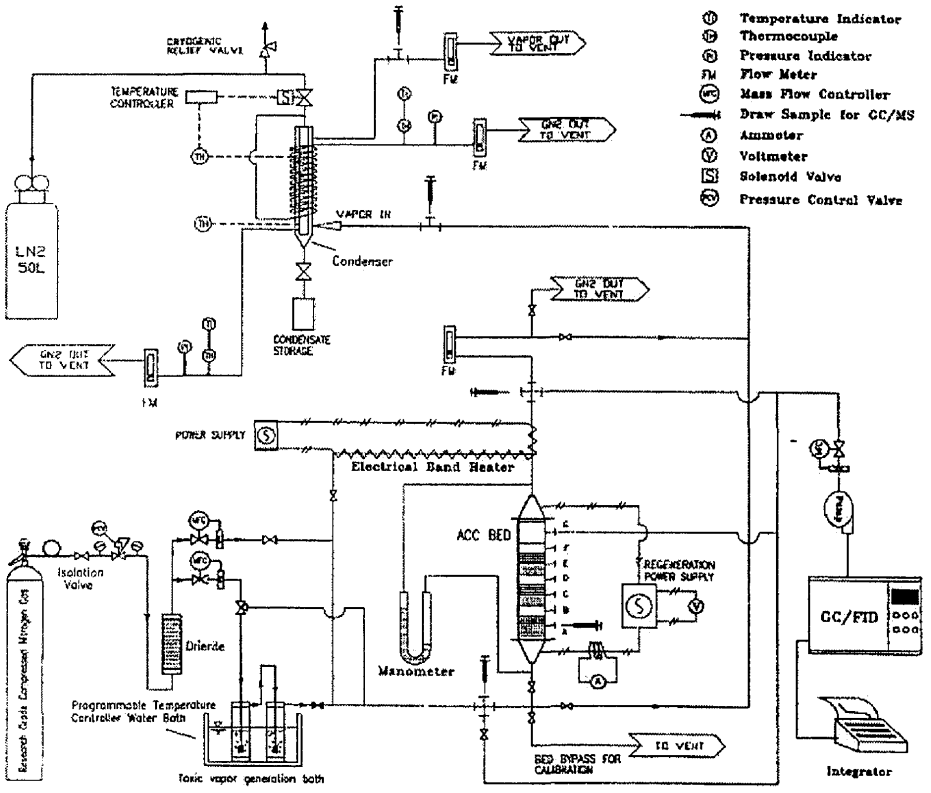

Figure 3.8 Schematic diagram of laboratory-scale ACFC adsorption system

Sample Gas Generation Unit

The gas generation unit is shown in Figure 3.7. Ultra-high purity (UHP) N_2 gas passes through a purifier desiccant (Drierite, model L68GP) where any trace water and organic vapors are removed. Then the purified nitrogen is branched to two separate streams controlled by two mass flow controllers (Tylan models FC-260 and FC-280). One of the N_2 gas streams passes through two fritted glass bubblers connected in series and immersed in a temperature controlled water bath. The bubblers contain the liquid TVOC, causing the N_2 gas stream to become saturated in TVOC vapor. The saturated gas stream is then mixed with the second pure N_2 gas stream to produce a gas mixture with a desired TVOC concentration and total flow rate.

The gas generation system was calibrated using draw samples and a gas chromatograph/mass spectrometer (GC/MS, Hewlett Packard GC 5890 and MS 5971). In the calibration steps the bed was by-passed. The first calibration point was for UHP N_2 and the second for a Matheson calibrated standard TVOC gas mixture. A linear relationship was assumed between the MS counts and the related vapor concentration values. The calibration procedure was checked using another GC (Hewlett Packard Model 5880A) equipped with a flame ionization detector (FID). The FID signal was calibrated, by passing a continuous stream of the Matheson calibrated standard gas mixture through the GC/FID. A linear relationship was assumed between the FID zero signal and the signal of the standard gas. The concentration of generated gas was stable: at a near isothermal lab condition ($\pm 1\,^{\circ}C$), during 3 hr, a linear

concentration decrease of less than 2.5% was observed for MEK and acetone streams of 5,000 and 10,000 ppmv, respectively, at a flow rate of 5 slpm.

Analytical Gas Measurement

As mentioned above, a GC/MS (Hewlett Packard GC 5890 and MS 5971) and a GC/FID (Hewlett Packard 5880A) were used for gas detection and measurement purposes. The concentration of gas mixture in the ACFC system was measured at several sampling ports. Locations of these sampling ports and the continuous sampling system of GC/FID are shown in Figure 3.7. A 30 ml/min sample gas stream, controlled by a factory calibrated Tylan mass flow controller, was drawn by a Mini Dia-Vac gas pump and directly forced through the GC/FID. Since the FID signal was dependent on the gas flow rate, any fluctuations in the flow rate could produce noise on the FID signal. To reduce the signal noise generated by the pump, the GC was equipped with a 0.4% Carbowax stainless steel packed column. The column was 1/8" in diameter and 12 feet in length. The sample effluent from the column was mixed with hydrogen and air and the mixture was burned in the FID. In a FID, the extent of ionization depends on the nature of the compound and the temperature of the flame. In our set-up with a 30 ml/min gas sample, the maximum FID sensitivity was obtained by mixing the sample with 30 ml/min of hydrogen. The balance of the gas entering the FID consists of 400 ml/min clean, dry air. These gas flows were checked using a Bios Dry-Cal instrument and regulated by mass flow controllers located within the GC. The FID ionization signal was amplified and plotted as a function of time on an attached GC console terminal. As with the gas generation system, the concentration measurements using the GC/MS and GC/FID involved the calibration procedures described in the previous section.

Design of Adsorber

Factors that are important in the design of the adsorber include choosing the type of adsorber, regeneration, TVOC and adsorbent, and the concentration and flow rate of TVOC. A fixed-bed was selected as the type of adsorber for this research. Target adsorbates were selected according to industrial use, governmental regulations and cost effectiveness of adsorption technology as discussed in the previous sections. ACFC was selected as the adsorbent material for this project. Electrothermal regeneration was selected as the type of regeneration. The following subsections describe the procedure for selection of ACFC as the adsorbent type and its utilization in the design of fixed-bed.

Selection of Adsorbent

Selection of the right adsorbent plays an important role on the performance of the adsorption separation process. ACFC was selected as a superior adsorbent for TVOC recovery. ACFC is made of woven activated carbon fibers (ACFs), and is an efficient adsorbent to remove TVOCs from gas streams. ACFs are made by carbonizing and activating fibers of phenolic resin, polyacrylonitrile (PAN), viscose, pitch, or rayon. Compared with activated carbon pellets (ACPs), granular activated carbons (GACs) or powder activated carbons (PACs), ACFCs have a higher specific surface area for a higher specific micropore volume which results in a higher contact efficiency. ACFCs have faster adsorption and desorption rates due to their microporous structure (there are no macropores, no or little mesopore volume, and uniform distribution of

micropores from the external surface to the core of fiber) and small fiber size (Ermolenko et al., 1992; Fuji, 1994). ACFCs rapid adsorption and desorption rates can reduce the required process cycle time and increase the bed adsorption capacity by reducing the length of mass transfer zone (MTZ). ACFC can be installed in different configurational forms inside fixed beds providing desired adsorption and desorption performance as well as specific pressure drop (Pa/g adsorption). Suitability for in-situ electrothermal regeneration and easy handling are other advantages of ACFCs. Examples of commercially available ACFCs and ACFs are listed in Table 3.7.

Table 3.7 List of commercially available activated carbon fiber and cloth (Suzuki, 1994).

Type	Viscose	Phenolic	PAN	Pitch
Company	Toyobo	Kynol	Toho Ryon	Osaka Gas
Brand Name	KF-1000 KF-1500 FK-1500L KF-1600	ACF-10, 15, 20, 25 ACN-10, 15, 20, 25 ACP-304 ACC-10, 15, 20, 25	FX-200, 300, 400, 500, 600	A-7, 10, 15, 20, 25

ACFC samples for this project were obtained from American Kynol, a subsidiary of Nippon Kynol, located in Pleasantville, NY. Kynols ACFCs are made of novoloid fibers (polymerized cross-linked phenolic-aldehyde fibers). Novoloid fibers have an amorphous network structure containing 76% carbon, 18% oxygen, and 6% hydrogen (Hayes, 1981). These fibers are woven by conventional textile techniques to produce a novoloid cloth. The cloth is then carbonized and activated in an O_2 free atmosphere using steam or CO_2 at 900 °C in a one step process to produce ACFC. Pore volume and pore size of the ACFC increase with increasing duration of activation.

Kynol ACC-5092 (150 g/m^2 areal density) and ACC-519 (250 g/m^2 areal density) samples were identified as suitable ACFC adsorbents for the experiments. ACC-5092 showed much better structural stability than ACC-519. Furthermore, ACC-5092 was selected due to its high surface density (150 g/m^2) and its structure stability. Specific surface area, total micropore volume, average micropore size, and elemental analysis of ACC-5092 are given in Table 3.8.

Adsorption capacities of ACC-5092-15, ACC-5092-20 and ACC-5092-25 were determined from Freundlich isotherms using the coefficients given by Cal (1993 and 1995). Modeled adsorption capacity of these ACFCs for 10,000 ppmv acetone were 442, 589 and 364 mg/g, respectively. ACC-5092-20 was thus selected as the preferred adsorbent due to its higher adsorption capacity. The higher adsorption capacity of ACC-5092-20 is mainly due to the existence of a high specific pore volume and high volume ratio for pore widths in the supermicropore and transitional ranges between supermicropores and mesopores. SEM (Scanning electron microscopy) micrographs of the ACFC sample are provided in Figure 3.9. The cumulative pore size distribution of the ACFC sample in comparison with some other adsorbents is given in Figure 3.10.

Table 3.8 Physical properties of Kynol ACC-5092 (Foster et al., 1992).

Kynols Brand	BET, SurfaceArea	Mean Pore Size	Pore Volume	Elemental Analysis, wt%		
	m^2/g	Å	cm^3/g	C	H	O
ACC-5902-10	760	4.9	0.49	94.7	0.86	4.44
ACC-5092-15	900	5.7	0.64	92.8	1.04	6.12
ACC-5092-20	1600	7.0	0.73	95.4	0.68	3.92
ACC-5092-25	2400	8.4	0.92	95.4	0.59	3.97

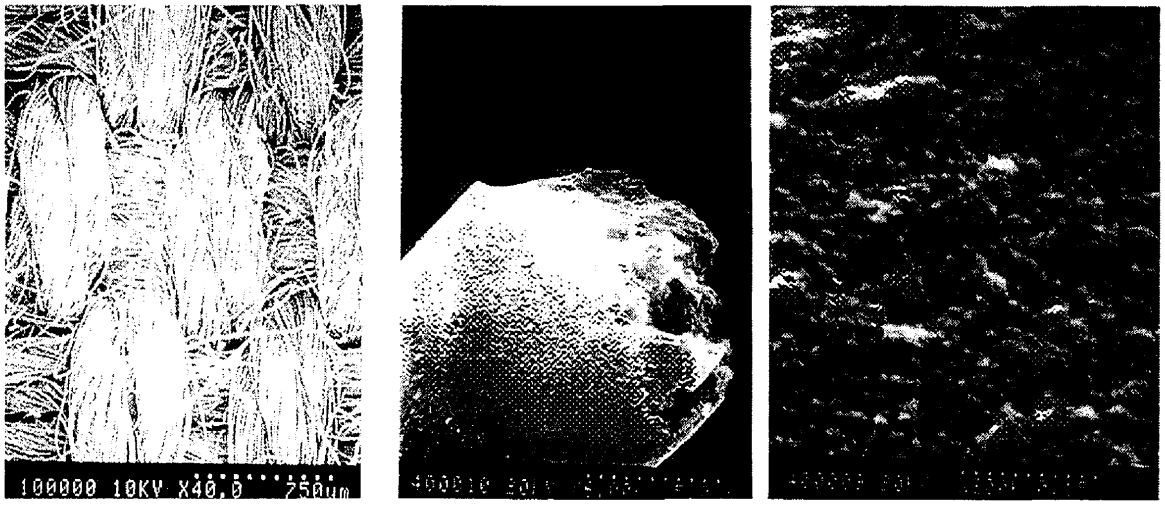

Figure 3.9 SEM micrographs of ACC-5092-20

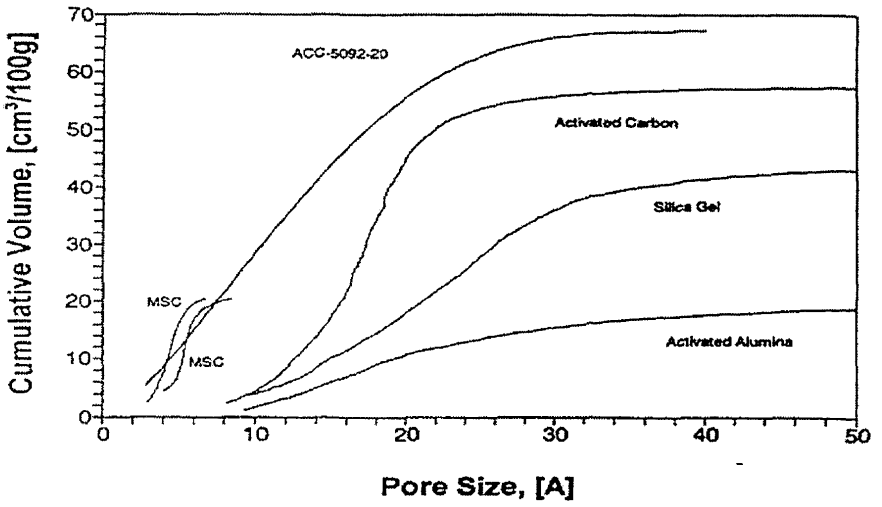

Figure 3.10 Cumulative pore size distribution for ACC-5092-20 and for some other adsorbents (Tang, 1987).

The adsorption characteristics of the ACC-5092-20 sample were measured by the Brunauer-Emmett-Teller (BET) adsorption method using a Micromeritics ASAP 2400 surface area analyzer. The surface areas were determined from the calculation of a monolayer adsorption using the BET equation at the relative pressure of 0.01 to 0.25. These measurements were necessary to insure homogeneity of the ACFC samples within the same lot and reproducibility of experimental results. For example, the BET surface area of two ACC-5092-20 samples from the same lot were measured to be 1592 and 1603 m^2/g (Kynols reported nominal value was 1600 ± 100 m^2/g). The micropore volume was determined to be 0.69 cc/g and 0.72 cc/g. Quantified physical characteristics of ACC-5092-20 are listed in Table 3.9.

Table 3.9 Physical characteristics of Kynol™ ACC-5092-20

Type	Kynol™ ACC-5092-20
Weight:	150 (g/m^2)
Cloth thickness:	0.55 (mm)
Fiber diameter.	10-13 (μm)
Weave:	Modified basket 2 × 1
Construction:	55 × 25 (epi x ppi)
Nominal BET specific surface area:	1600 (m^2/g)
Nominal Langmuir specific surface area:	2000 (m^2/g)
Single point pore volume of pores less than 396 Å at P/Po=0.949:	0.759 (cc/g)
Micropore volume.	0.690 (cc/g)
Average pore diameter (V/4A by Langmuir):	14.5 (Å)
Average micropore width:	6.7 (Å)

Mechanical Design of Adsorber

The fixed-bed was selected as the type of adsorber. Concentrations and flow rates of sample TVOCs in actual industrial gas streams were provided by Liquid Carbonic, Inc. Using this information, the concentration of TVOCs for the system evaluation experiments were selected. Based on the concentration ranges, a suitable ACFC adsorbent was then selected for the tests. The amount of mass adsorption was selected based on the amount of collectable liquid and the overall design configuration and operation of a system that could be scaled up for a full-scale application in the future. The mass of ACFC was estimated using the adsorption capacity modeled with the Freundlich isotherm as was discussed in the previous section. The adsorption cycle time or breakthrough time, t_b, was chosen as 1 hr in the next step. The stoichiometric time was determined by assuming a conservative value of 2/3 for throughput ratio (TPR, the ratio of actual effluent volume to the feed volume that could ideally saturate the fixed-bed). The flow rate of the gas mixture was estimated from the stoichiometric time using the equation 3.1. The length and cross sectional area of the adsorber were selected to satisfy the design conditions (e.g., suitability for the modular configuration and less risk of channeling) and to provide sufficient contact time.

The cloth form of ACFC demands a different adsorber design configuration than the conventional fixed-bed adsorbers (Figure 3.2). The ACFC bed is 16 cm^2 and square in cross section. A square cross section is the most natural form for ACFCs that are placed in a cross flow configuration. Side walls of the fixed-bed were originally made of a nonporous and inert boron nitride ceramic. The brittleness of boron nitride resulted in broken ceramic side walls on two separate occasions. The side walls were then replaced with electrical-grade Teflon sheets. The Teflon is relatively nonporous, inert and excels as electrical insulation. The temperature working range of the Teflon sheet was provided by the manufacturer to be between -195 to 260 °C.

Four pairs of 304 stainless steel frames support the pleated ACFC inside the bed resulting in four separate ACFC modules. Each frame has sixteen 1.14 mm diameter holes, spaced 3.05 mm apart along its top and bottom edges that hold 1.6 mm stainless steel rods to provide uniform spacing between each ACFC pleat. These modules are held into place with grooves along each side of the bed. The modules can easily slide in and out of the bed allowing for installation of the pleated ACFC. In the modules ACFC layers are installed in a pleated cross flow orientation. This allows for flexibility in effective adsorption bed length and apparent packing density. With a 1.14 mm separation distance between each layer, an apparent packing density of 94.5 mg/cm^3 results. The bed packing density can be increased to 600 mg/cm^3.

Four silicon rubber cords, placed in four shallow grooves that were machined in the intersections of the bed side walls, seal the edges of the fixed-bed against leaking gas. The side walls are externally clamped and supported with an aluminum grip arrangement consisting of four separate sections connected by bolts. Tightening the grip provides the compression stress required by the silicon rubber cords and ACFC module sides to seal the bed against gas leaking and internal channeling. Eight tension rods press two stainless steel flanged nozzles against the ends of the fixed-bed and seal those areas. Seven sampling ports, sealed with silicon rubber o-rings, were installed along the length of the ACFC fixed-bed for gas sampling and temperature measurement purposes.

The ACFC fixed-bed was fabricated by University of Illinois Department of Material Sciences and Engineering machine shop. Figure 3.11 shows the fabricated bed in full and

The ACFC fixed-bed was fabricated by University of Illinois Department of Material Sciences and Engineering machine shop. Figure 3.11 shows the fabricated bed in full and partially assembled configurations. Three 155x3.97 cm strips of ACC-5092-20 ACFC were woven into three modules. The modules were placed inside the bed and connected electrically in series.

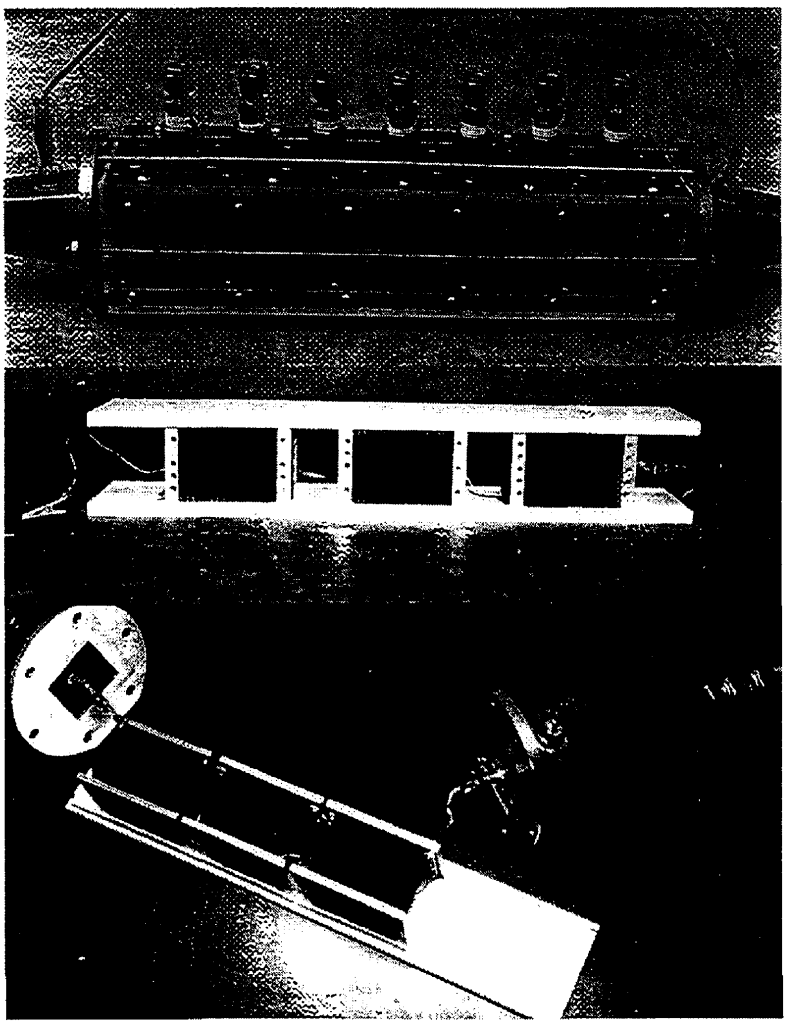

Figure 3.11 ACFC fixed-bed in full and partially assembled configuration

Regenerator

In the fixed bed, the ACFC layers are connected electrically in parallel in three separate modules. The modules are connected electrically in series. The resulting circuit is connected to electrodes of a 120 V a.c. source controlled by a variable a.c. voltage transformer (Variac) and monitored by a voltmeter and an external ammeter. This arrangement was expected to result in a uniform electrical heating and carefully controlled TVOC desorption. The experimental setup for electrothermal regeneration is presented in Figure 3.12.

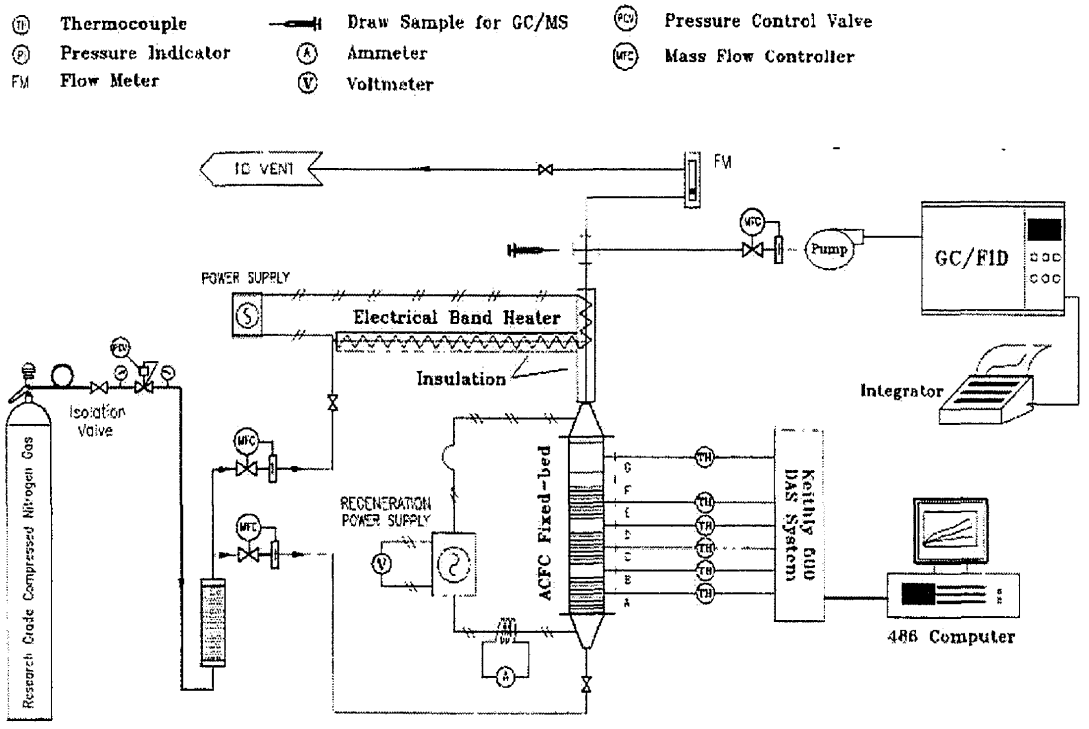

Figure 3.12 Electrothermal regeneration setup.

Condenser

Regeneration of the carbon adsorber provides a concentrated vapor stream at a low gas flow rate which is then sent to the condenser. Using the adsorber as a pre-concentrator improves the operating efficiency of the condenser by increasing removal efficiency and decreasing refrigerant consumption as will be shown later. LN_2 is used as the condenser refrigerant due to its low achievable temperature range and possible re-use capabilities.

The concentrated, reduced flow rate TVOC stream is sent directly to a shell-and-tube countercurrent cryogenic condenser. LN_2 is used as the tube side refrigerant to cool the condenser to temperatures near the freezing point of the organic. TVOC in the N_2 carrier gas is sent through the insulated shell. Condensation of the TVOC occurs on the outer wall of the tube and the inner wall of the shell. The condensed TVOC film is continually washed out of the condenser by gravity.

LN_2 is delivered to the condenser with a self-pressurizing dewar (Cryofab™ model CFPB25-115). The set-point pressure in the dewar is maintained by controlling the amount of LN_2 that passes through a heat exchanger inside the vessel with a cryogenic valve. The LN_2 vaporizes and returns to the liquid storage area. The amount of vaporized LN_2 will control the vessel pressure.

The flow rate of LN_2 controls the temperature of the condenser. Flow rate of LN_2, in turn, is controlled by the pressure of the dewar and by a normally closed cryogenic solenoid valve (Asco Red-Hat series 8264). The cryogenic solenoid valve is controlled using a Gordinier Electronics (model 259) LN_2 temperature controller. A type T thermocouple mounted inside the shell of the condenser entrance provides the temperature feedback for the temperature controller. If the temperature of the condenser at the thermocouple location is above the set-point temperature, the controller opens the solenoid valve for LN_2 delivery.

Inlet and outlet tubing is insulated with polymeric foam insulation wrapped in fiberglass insulation and surrounded by an aluminum radiation shield. Vacuum jacketed delivery lines provide more insulation but cost considerably more (ASHRAE, 1986). ASHRAE (1986) and Davies and Shields (1994) provide a detailed method for selection of appropriate pipe insulation for cryogenic applications.

The cryogenic condenser utilizes a shell-and-tube configuration (see Figure 3.12). The LN_2 refrigerant is passed through the tube and the TVOC laden challenge gas stream transverses

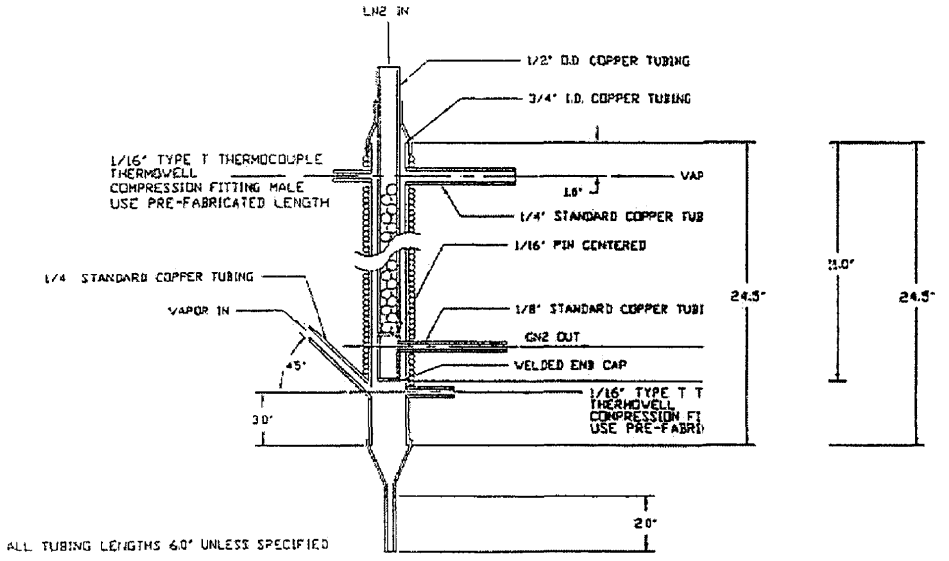

Figure 3.13 Laboratory-scale cryogenic condenser full section with brass bearing packed in the inner tube to aid in heat conduction

the shell casing around the tube, countercurrent to the refrigerant. LN_2 is also circulated through an 1/8 in. copper tube coil jacket wound around the outside shell of the condenser. A radial temperature gradient is thus established. This temperature gradient draws heat from the vapor laden gas stream and forms a radial concentration gradient in which the organic diffuses from the

bulk flow into the condensate film at the wall and condenses. The upper concentration limit is determined by the saturation vapor pressure of the organic vapor at a given temperature.

A shell-and-tube configuration was selected for laboratory use due to the high condensation surface area, better control and classification of condenser response to temperature and the ability to prevent freezing of the organic during continuous process feed flow. Indirect contact condensation also allows for refrigerant re-use. The LN_2 refrigerant is not contaminated with the TVOC in the shell. Therefore the vaporized LN_2 can be used for desorption as an oxygen free (prevent explosion hazards) and water vapor free (prevent ice formation in the condenser) carrier gas. Many other applications may exist for N_2 gas use at a given facility location such as a blanket gas in TVOC transfer lines that have concentrations between the lower explosion limit (LEL) and upper explosion limit (UEL).

Fabrication was conducted at the University of Illinois' Department of Material Science and Engineering machine shop. The laboratory scale condenser has a surface area of 1241 cm^2. The condenser is made of 99.9% pure copper which was selected due to the high thermal conductivity of copper. A 3.8 cm layer of polymeric foam insulation covers the outside of the condenser with an aluminum and vinyl foam insulation around the polymeric insulation as a radiative heat shield.

The TVOC challenge gas stream temperature is monitored using type K thermocouples at the condenser inlet, mid-point and outlet. The thermocouples are connected to a Metrabyte DAS8/EXP16 data acquisition board. The temperature is digitally recorded using Labtech Notebook version 6.2.0. The N_2 refrigerant flow rate is monitored at the outlet using a BIOS DC-2 DRYCAL Flow Calibrator in continuous operation. The mass of LN_2 used during operation can thereby be determined.

4. SYSTEM EVALUATION EXPERIMENTS

Individual processes of the system (adsorption, electrothermal regeneration, and condensation) were characterized by separate experiments. Integration tests were also conducted to demonstrate performance of the system. The experiments performed are discussed in this section.

Evaluation of Adsorption Process

Several adsorption experiments were performed to characterize the adsorption dynamics within the ACFC fixed bed. Some experiments were also performed with a packed bed of ACFC to determine adsorption capacity of ACFC for higher concentration levels than the available measured data (Cal, 1995). The packed-bed results can also be compared against the fixed-bed results to quantify the effect of packing density on the dispersion of concentration front and utilization of ACFC. Adsorption equilibrium tests using a gravimetric balance were also performed to provide an extra means for checking the fixed-bed and packed-bed adsorption capacity measured.

Adsorption breakthrough tests for acetone with ACFC fixed-bed

The experimental setup for these tests was the same as shown in Figure 3.8. The initial steps were to regenerate the ACFC fixed-bed, cool the bed to the ambient temperature, generate the sample gas, calibrate and monitor the concentration for a steady-state condition. The fixed-bed was electrothermally regenerated under a stream of UHP N_2 The regeneration step was shifted to the cooling step when no contaminant could be detected by GC/FID. Cooling was achieved by heat transfer from the walls of the adsorber to the surroundings and heat sweeping by forced convection of a low flow rate UHP N_2 gas through the fixed-bed. The gas generation system was calibrated using draw samples and the GC/MS. In the calibration steps the bed was by-passed. The first calibration point was for UHP N_2, and the second for 1% acetone in a Matheson calibrated gas standard. A linear relationship was assumed between the MS counts and the related vapor concentration values. Prior to the start of each experiment, the GC/FID was also calibrated in a similar fashion.

After the calibrations, the generated TVOC gas mixture was passed through the ACFC fixed-bed. The effluent acetone concentration from the ACFC bed was monitored both continuously by the GC-FID and intermittently by draw sample using a gas-tight syringe and injection into the GC-MS. The temperature upstream and downstream of the bed fluctuated slightly around room temperature throughout the experiment. Experimental breakthrough results describing how acetone concentration changed with time and location are presented in Figures 4.1 to 4.4. For each test, the total gas flow rate through the bed was 5 lpm at standard temperature and pressure (STP: 25 °C, 101,325 Pa). Superficial gas velocity was 5.21 cm/s. The bed contained three modules of pleated ACC-5092-20 for a total mass of 27.05 g ACFC at a packing density of 94.5 mg/cm^3.

Figure 4.1 shows how the concentration at each sampling port along the ACFC bed changed with respect to time. Ports A, C, and E are located in the middle of each module. Ports B, D, and F are located in the void spaces between the modules. Sampling from port D was not performed because that was the location for temperature monitoring during the initial electrothermal regeneration runs. The concentration profiles are in the form of diffusion-limited S shape. Due to similarity in the positions of ports A, C, and E, their concentration profiles show some similarity. Concentration profiles for ports B and F also show some similarities due to their positions. The absence of complete agreement between the concentration profiles is due to several factors, including the entrance transient condition, the temperature rise in the adsorption bed, mixing effects and dilution, and differing contact times and heat transfer rates.

Figure 4.2 demonstrates development and movement of MTZ inside the ACFC bed.

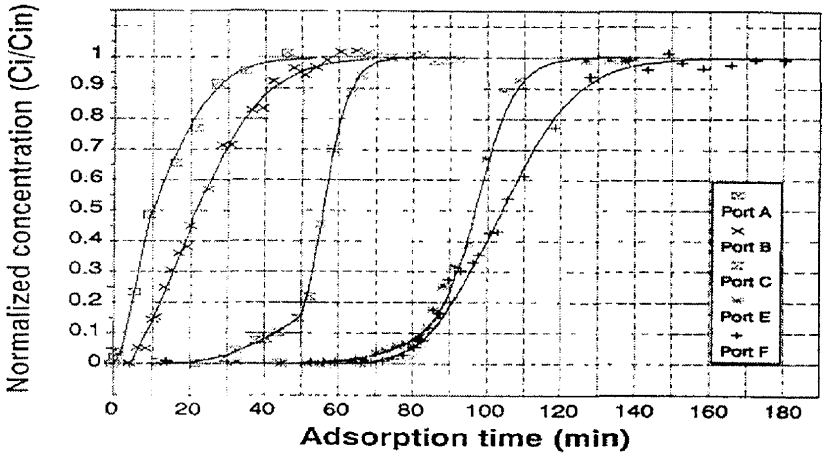

Figure 4.1 Acetone concentration profile development at sampling ports of ACFC fixed-bed as a function of time. Inlet acetone concentration = 1% and total flow rate = 5slpm.

Behind the MTZ, the ACFC is saturated with acetone, whereas in front of MTZ, the bed is virtually free of acetone. Exponential concentration decay at initial stages of the test is observed from the concentration profile at 10 min. The concentration profile at 70 min shows the concentration distribution close to break point. It is observed that the MTZ thickness is almost equal to the length of 1.5 modules (the length of each module is 2.18 in).

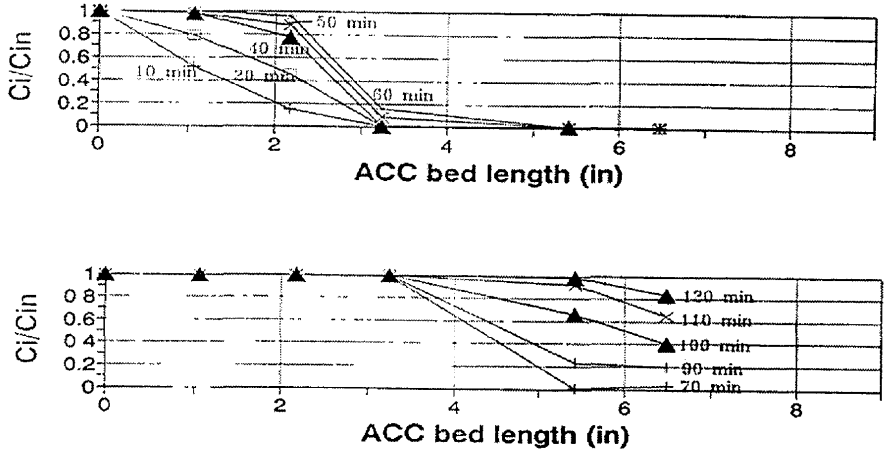

Figure 4.2 Acetone concentration profile as a function of location from the inlet of the ACFC fixed-bed. Inlet acetone concentration = 1% and total flow rate = 5 slpm

Figure 4.3 shows the BTC results for four different runs. Table 4.1 summarizes the key points derived or calculated from the experimental results.

Reproducibility of these results can be seen from the presentation of these curves in a non-dimensional form (Figure 4.4). In the figure, where t is the adsorption time and t_s is the stoichiometric time.

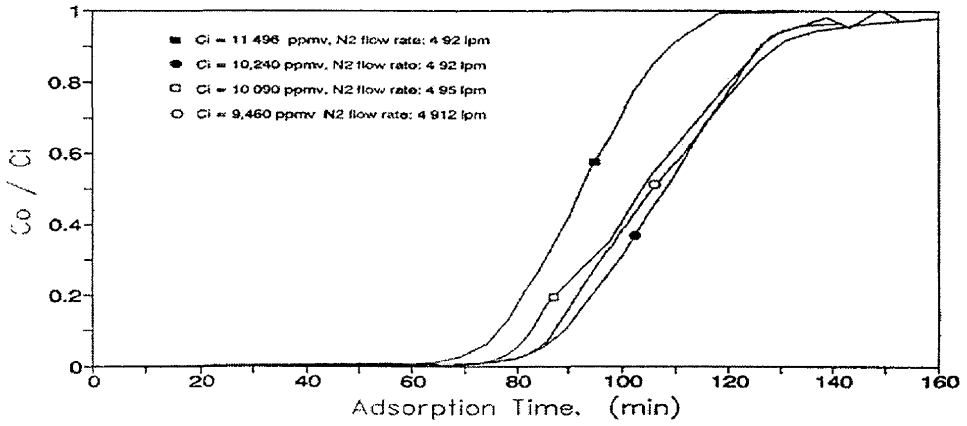

Figure 4.3 Adsorption breakthrough curves for acetone experiments

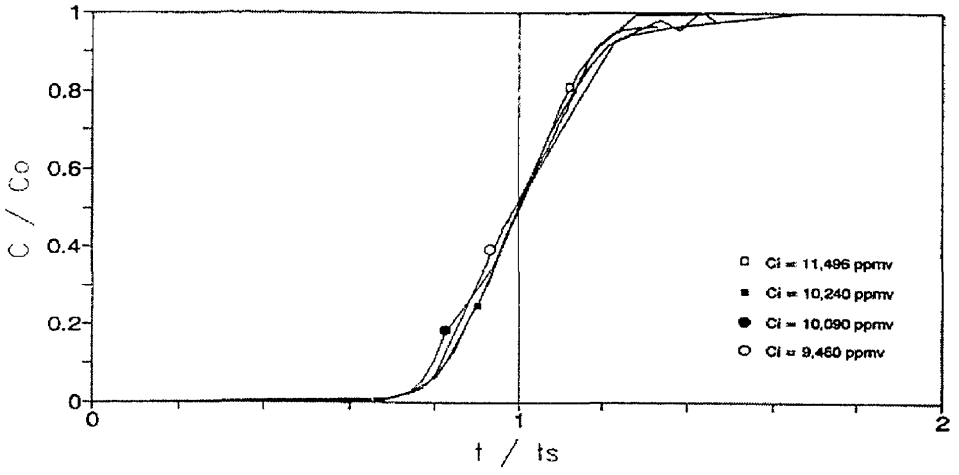

Figure 4.4 Normalized breakthrough curves for acetone experiments

The mass of acetone adsorbed was calculated by numerical integration of the breakthrough curve in the form of:

$$(M_{ads})_t = \frac{(PM_W)}{(R_u T)} \int_0^t \left[\left(\frac{dv}{dt} \right)_{in} - \left(\frac{dv}{dt} \right)_{out} \right] dt \qquad (4.1)$$

Where $(M_{ads})_t$ = cumulative mass of adsorption at time t, M_w = molecular weight of acetone, P = total pressure, $(dv / dt)_{in}$ = acetone inlet volume flow rate, $(dv / dt)_{out}$ = acetone outlet volume flow rate. In terms of mole fraction, the above equations can be written in the form of:

$$(M_{ads})_t = \frac{(PM_W Q_{N_2})}{(R_u T)} \int_0^t \left\{ \left[\left(\frac{C}{1-C} \right)_{in} - \left(\frac{C}{1-C} \right)_{out} \right] \right\} dt \qquad (4.2)$$

Where C is the volume or mole fraction of acetone, and Q_{N_2} is the N_2 flow rate. The specific length of unused bed (LUB) was calculated as:

$$LUB = 1 - \left(\frac{M_b}{M_{sat}} \right) \tag{4.3}$$

where $M_b = M_{ads}$ at break point, and $M_{sat} = M_{ads}$ at saturation. The throughput ratio (TPR), the ratio of actual effluent volume to the feed volume that could ideally saturate the fixed-bed, is calculated as the ratio of elapsed run time to breakthrough to stoichiometric time (t_s).

$$TPR = \left(\frac{t_b}{t_s} \right) \tag{4.4}$$

In our experiments, the throughput ratio of the bed was approximately 78% for a 10,000 ppmv acetone in N_2 gas mixture.

For modeling purposes, adsorption breakthrough experiments were performed in a packed-bed of ACFC to determine the adsorption capacities in the range of 1,000 to 10,000 ppmv. Additionally the packed-bed results for 10,000 ppmv were used to research the effect of packing density on the dispersion of MTZ. These tests are described in the next section.

Table 4.1 Summary of acetone adsorption breakthrough tests with ACFC-fixed bed.

Test Number	1	2	3	4
Inlet gas concentration (ppmv)	11,496	10,240	9,460	10,090
Nitrogen flow rate (slpm)	4.92	4.92	4.912	4.95
Ambient temperature (°C)	23.5 ± 1.5	23.5 ± 1.5	23.5 ± 1.5	22 ± 1
Mass of ACFC (g)	27.05	27.05	27.05	30
Breakthrough time ($t_{5\%}$) (min)	72.5	84.4	84.5	79.5
Stoichiometric time ($t_{50\%}$)(min)	92.6	107.9	107	104
Mass of acetone adsorbed (g)	12.5	12.9	12.37	14
Adsorption capacity (mg/g)	462	477	457	467
LUB (%)	22.3	22.8	22.3	26.6
TPR (%)	78.3	78.2	77	76.4

Adsorption Breakthrough Tests for Acetone with the ACFC Packed-Bed

Adsorption breakthrough tests were performed with a packed bed of ACFC to determine the adsorption capacity of ACFC for concentration levels up to 10,000 ppmv. A schematic diagram of the experimental setup given in Figure 4.5. A stream of 1% by volume acetone gas (Matheson Inc. calibrated standard) was diluted with a stream of UHP N_2 to provide a desired concentration of acetone. The flow rates of standard gas and dilution gas were controlled by two Tylan mass flow controllers with 500 and 200 sccm ranges. The prepared gas stream can be passed through the packed-bed or through the by-pass line for calibration purposes. The temperature of the bed was controlled at a near isothermal (NIT) condition by circulating water in a cooling coil that surrounds the bed. Water was supplied from an automatic temperature-controlled water bath unit. The temperature of the bed was monitored by a type K thermocouple connected with a digital readout. The concentration of the gas mixture upstream and downstream of the bed were measured by the GC/FID. Packed-bed configuration was cylindrical with an internal diameter of 1.1cm. Figure 4.6 shows the results of breakthrough tests for 10,000, 5,000, and 3,333 ppmv acetone.

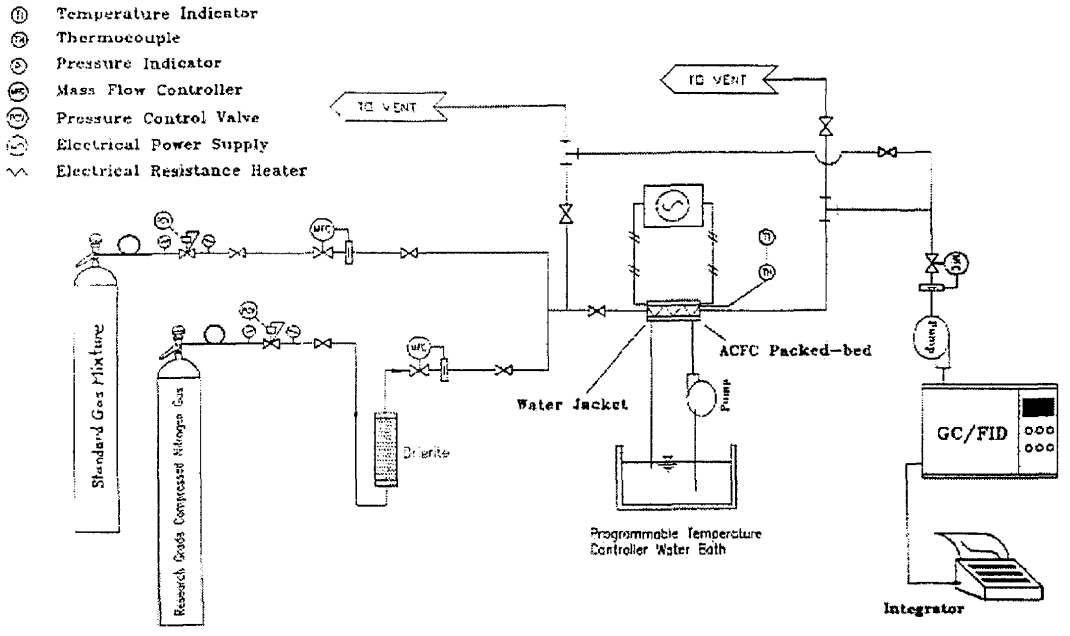

Figure 4.5 Packed bed experimental set-up

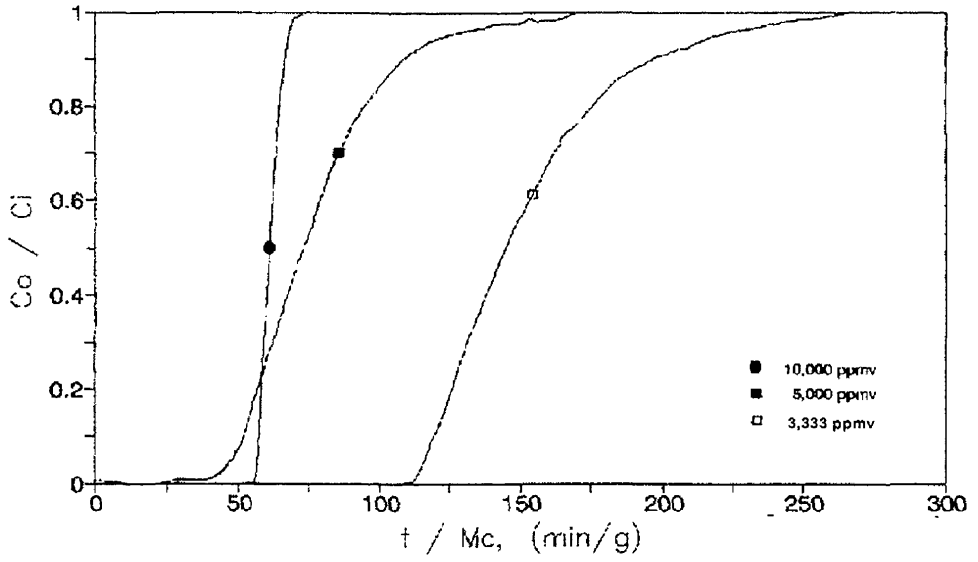

Figure 4.6 Acetone breakthough curves for packed-bed experiments, M_c is the mass of carbon.

To be able to compare the adsorption dynamic behavior of the packed bed with the ACFC fixed bed, the superficial gas velocity for the 10,000 ppmv packed-bed test was set at the same velocity as the fixed bed (5.2 cm/s). The ratio of the ACFC weight in the packed-bed and in the fixed-bed was equal to the ratio of their gas flow rates.

A summary of the experimental conditions and test results is given in Table 4.2. Figure 4.7 shows the BTCs in terms of time normalized by the stoichiometric time. The form of the BTCs illustrate that higher concentration levels and flow rates provide less dispersion and shorter mass transfer zones.

Table 4.2 Summary of acetone adsorption breakthrough tests with ACFC packed-bed.

Test Number	1	2	3
Inlet gas concentration (ppmv)	3,333	5,000	10,000
Ambient temperature (°C)	24 ± 1	24 ± 1	24 ± 1
Mass of ACFC (g)	0.62	0.62	1.6
Total flow rate (slpm)	0.3	0.4	0.297
Stoichiometric time ($t_{50\%}$) (min)	90	45.4	98
Mass adsorbed (mg)	203	231	694
Adsorption capacity (mg/g)	327	372	434

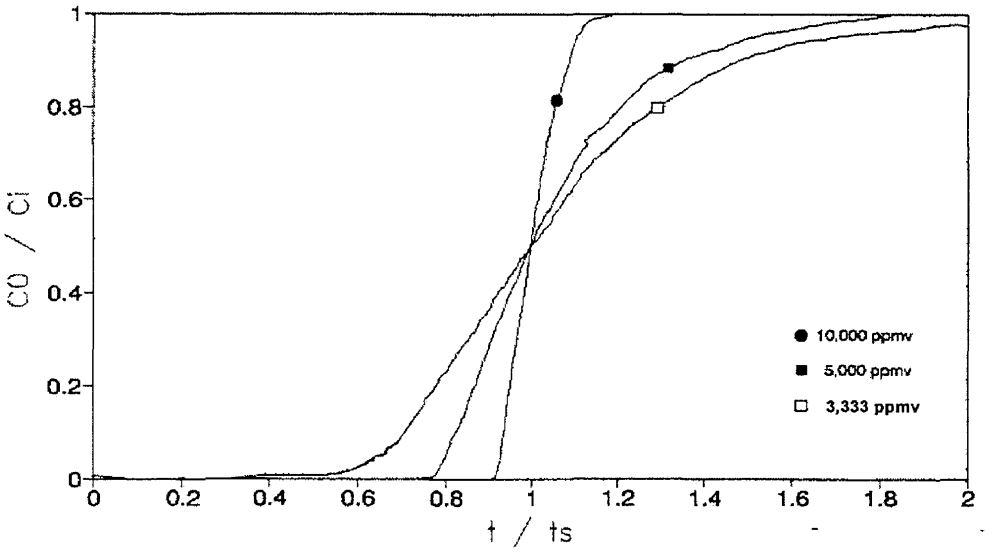

Figure 4.7 Normalized acetone breakthrough curves for packed-bed experiments.

The adsorption capacity for 10,000 ppmv acetone found from packed-bed tests was 512 mg/g while the average adsorption capacity from the fixed-bed experiments was 434 mg/g. To check these results, the adsorption capacity of ACC-5092-20 was measured by a gravimetric method using the same experimental setup used by Cal (1993, 1995). The equilibrium adsorption capacity of acetone for 10,040 ppmv concentration was determined by mass gain of an ACC-5092-20 sample that is exposed to a Matheson calibrated standard acetone gas in a Cahn gravimetric balance (Cahn Model C-2000). From the adsorption data, equilibrium capacity was determined to be 504 mg/g ACFC. From the desorption data, total adsorption capacity was measured to be 489 mg/g ACFC.

Figure 4.8 shows the mass gain sample as a function of time. Two distinct mechanisms are likely to be responsible for total adsorption capacity, one fast and one slow mechanism. The slow mechanism might be due to capillary condensation in the transitional pores between supermicropore and mesopore regions or diffusion into ultra micropores.

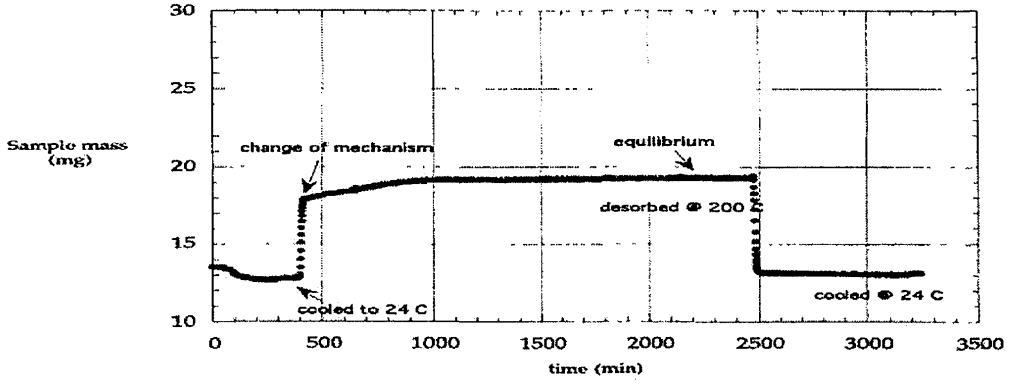

Figure 4.8 Mass gain and loss of ACC-5092-20 using gravimetric techniques.

The equilibrium isotherm for adsorption and desorption of acetone and ACC-5092-20 can be classified as Brunauer, Deming, Deming, and Teller (BDDT) type IV isotherm. The equilibrium micropore adsorption and capillary condensation capacities of the ACFC for 1% by volume acetone were measured from the mass gain of the fast mechanism and the mass gain of the slow mechanism to be 401 mg/g and 93.6 mg/g, respectively.

Effect of packing density on BTC

The effect of packing density on adsorption dynamics is presented in Figure 4.9. Smaller packing density results in a shorter breakthrough time and a larger MTZ due to axial dispersion and mixing effects. Increasing packing density from 94.5 mg/cm^3 to 450 mg/cm^3 increases the breakthrough time from 75 min to 91.7 min. TPR was increased from 78% to 94%. While these are clearly benefits, increased packing density also produces a larger (and more costly) pressure drop. It is possible, however, to find a packing density for optimization of adsorption and pressure drop.

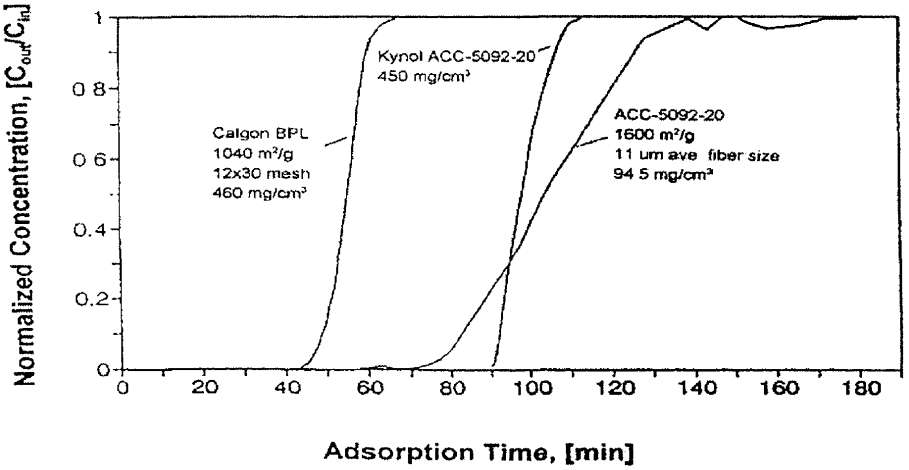

Figure 4.9 Effect of packing density of the characteristics of BTC of acetone adsorbed by ACFC and comparison with BTC of a commercially available activated carbon

To compare adsorption dynamics for the ACFC and a commercially available activated carbon, breakthrough tests were performed with ACFC and then with Calgon BPL 12x30 mesh activated carbon in packed bed configuration (Figure 4.9). To keep conditions similar, the superficial gas velocity through the bed was kept at 5.2 cm/sec for each test. The ratio of adsorbent mass to sample gas flow rate was also kept constant for the tests. The packed bed dynamic adsorption capacity results for the Calgon BPL and the ACFC were determined to be 241 mg/g and 434 mg/g, respectively. The adsorption capacity of the ACFC was almost twice of the adsorption capacity of the BPL. Breakthrough times for the ACFC and BPL adsorbents were 91.7 min and 47.2 min, respectively. The measured adsorption capacity for the BPL sample was in good agreement with modeled values (236 mg/g); using data by McCabe et al. (1993) for a 1% by volume acetone stream at ambient conditions.

Most of the difference in breakthrough times for the two adsorbents is due to the differences in adsorption capacity. The ACFC does demonstrate a sharper slope at the leading

edge of the MTZ suggesting faster mass transfer of the TVOC to the ACFC. At higher flow velocities this rate difference is expected to be amplified.

Adsorption Breakthrough Tests for MEK with the ACFC Fixed-Bed

The experimental setup and conditions for the MEK tests were the same as those for acetone experiments described in previous sections, except that the gas generation system was calibrated for 5,000 ppmv MEK. Figure 4.10 shows the resulting MEK BTCs. The BTCs in normalized form are given in Figure 4.11. The form of the normalized BTCs provides a suitable means for checking the performance of adsorber. For example, the curves with open symbols demonstrate a higher longitudinal dispersion rate than the other tests. This observed dispersion was likely due to a small channeling inside the bed in one case, and the room temperature variability in the other case, as will be discussed later. Channeling inside the bed occurs if the nuts and bolts of the adsorber are not tightened completely. The close overlap of the normalized MEK BTCs in the concentration range of 5,000 to 15,000 ppmv shows that dispersion due to axial molecular diffusion is not an important factor in this concentration range.

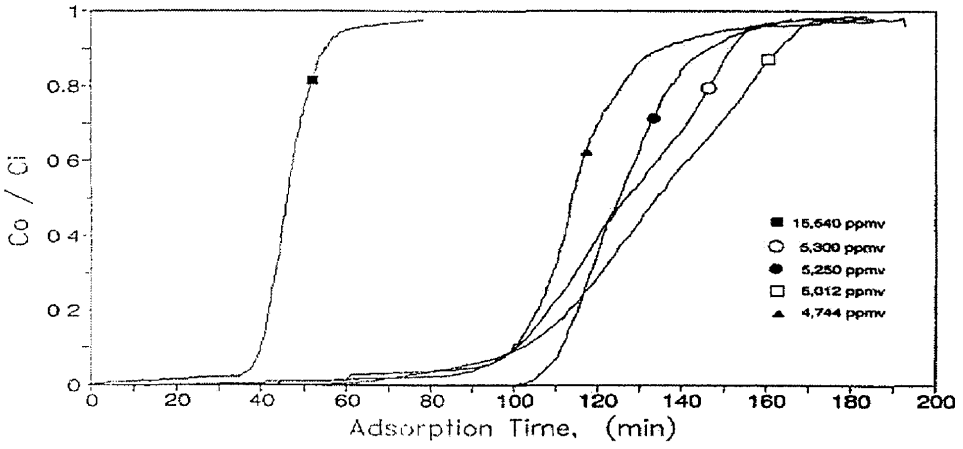

Figure 4.10 Adsorption breakthrough curves for MEK experiments.

Table 4.3 summarizes the conditions of experiments and key points derived or calculated from the experimental results. The TPRs for the three properly performed tests are greater than 80%. TPRs greater than 90% can be achieved by increasing the bed depth. Figures 4.12 to 4.14 show the normalized temperature variation versus normalized time for three different runs. Positions of thermocouples are shown in Figure 3.10. Thermocouple tips, for ports B, D, and G, are located at the middle of bed cross section and after each ACFC module. A, C, and E thermocouples are located close to the wall and in the middle of ACFC modules. At the locations where adsorption takes place, the heat of adsorption is released and results in a rise of temperature. Movement of the concentration wave generates a thermal wave inside the adsorber. For a normal run, the maximum temperature measured at port B is higher than those at the other ports, because it is located in the region of minimum bed length (MBL) and away from the entrance region. Temperatures measured at ports A, C, and E are lower than B, D, and G because they are close to the wall and heat transfer is faster.

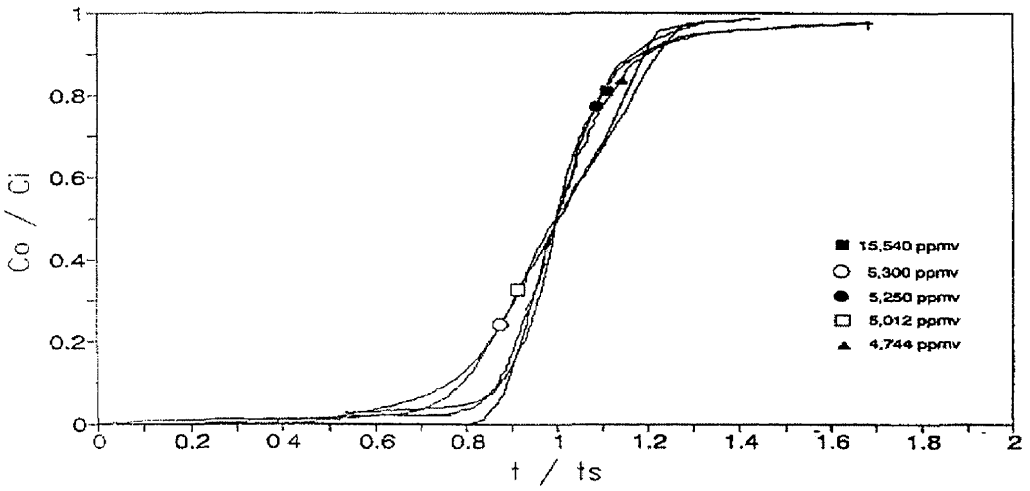

Figure 4.11 Normalized breakthrough curves for MEK experiments

Table 4.3 Summary of MEK adsorption breakthrough tests with ACFC fixed-bed.

Test Number	1	2	3	4	5
Inlet gas concentration (ppmv)	15,540	5,300	5,250	5,012	4,744
Nitrogen flow rate (slpm)	5.0	4.916	4.993	4.99	4.99
Ambient temperature (°C)	25	20.5	24	27	23.6
Mass of ACFC (g)	19.2	19.2	19.2	19.2	19.2
Breakthrough time ($t_{5\%}$) (min)	38	92.7	108.3	87.3	92.4
Stoichiometric time ($t_{50\%}$) (min)	46	126.9	125.2	134.5	114.2
Mass of MEK adsorbed (g)	10.93	9.72	9.78	9.81	8.17
Adsorption capacity (mg/g)	569	506	509	511	426
Mass adsorbed at breakpoint (g)	8.7	7.1	8.3	6.4	6.4
LUB (%)	20	27	15	35	22
TPR (%)	83	73	86	65	81

The occurrence of maximum temperature at point D and the high noise seen on the temperature curves that is seen in Figure 4.12 is indicative of channeling in the bed. Channeling shifts the location of maximum temperatures toward the end of the fixed-bed. This temperature shift and the mixing effects from channeling disperse the BTC more than its normal form (as seen in the normalized concentration curves). Dispersion effects on the BTC of test number 4 are

not likely from channeling. This can be concluded from temperature data for this run as presented in Figure 4.13. On the day of the experiment, the ambient laboratory temperature changed from a starting temperature of 27 °C to an ending temperature of 30.5 °C. This problem contributes to the dispersion of the BTC by reduction of adsorption capacity, decrease in throughput ratio, and increase in length of unused bed. A well behaved temperature profile, as is seen in Figure 4.14 and Table 4.3, accompanies a less dispersive breakthrough curve, shorter MTZ and LUB, as well as a higher TPR.

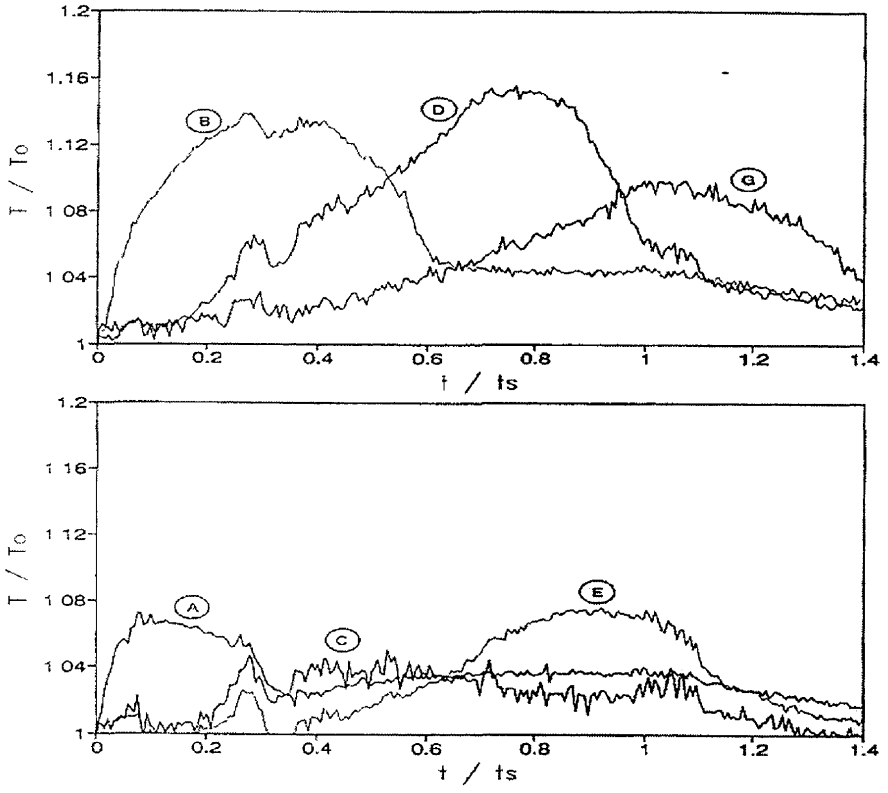

Figure 4.12 Temperature history of adsorption breakthrough experiment for 5,300 ppmv. Letters identify sampling adsorption bed sampling ports in Figure 3.8.

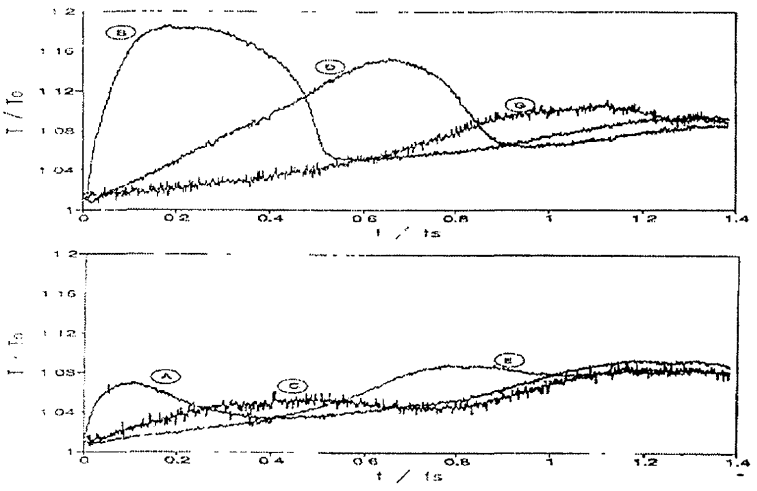

Figure 4.13 Temperature history of adsorption breakthrough experiment for 5,012 ppmv MEK. Letters identify sampling adsorption bed sampling ports in Figure 3 12.

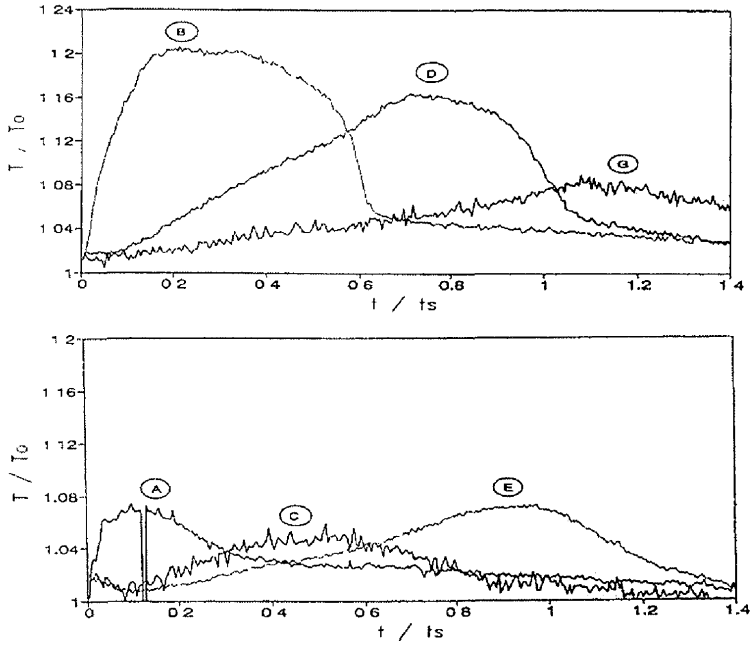

Figure 4.14 Temperature history of adsorption breakthrough experiment for 5,250 ppmv MEK.. Letters identify sampling adsorption bed sampling ports in Figure 3.12.

Modeling of Adsorption Equilibrium

According to Dubinin (1986), the physical adsorption of vapors in micropores can be described by the theory of volume filling of micropores. In general, adsorption capacity of microporous carbons can be conveniently expressed by the Dubinin-Astakhov (DA) equation (Dubinin, 1975) in the form of

$$W = W_O \exp\left[-\left(\frac{A}{\beta E_0} \right)^n \right] \qquad (4.5)$$

where W = pore volume filled at temperature T, and relative pressure P_0/P, W_0 = total micropore volume, $A = R_u T \ln (P_0/P)$, R_u is the universal gas constant, β, E_0, and n are characteristic parameters of the adsorbent/adsorbate. E_0 is the characteristic energy of adsorption for a reference adsorbate and β is a coefficient expressing the ratio of the characteristic adsorption energy of the adsorbate to that of the reference adsorbate. By definition, β has a value of 1 for the reference adsorbate, benzene. The exponent n reflects the width of pore energy distribution. For a variety of microporous carbons, it has been shown that n = 2 (which reduces the DA to the Dubinin Radushkevich (DR) equation).

Using data for $\ln(W)$ versus $\ln(P_0/P)$ and a nonlinear regression method, optimum $R_uT/\beta E_0$ and n can be found for a given adsorbate and adsorbent system. A plot of lnW versus $\ln^n (P_0/P)$ should provide a straight line with a slope $-(R_uT/\beta E_0)^n$ and an intercept $\ln (W_{0})$.

Results of the acetone and MEK adsorption tests for ACC-5092-20 were used to determine DA and DR parameters. Results included data obtained using the ACFC fixed-bed and packed-bed for high concentrations (1,000 to 10,000 ppmv) and data from Cal (1993,1995) for lower concentration levels (50 to 1,000 ppmv). The parameters found are given in Table 4.4, and plots of experimental data versus modeled DA and DR isotherms are given in Figures 4.15 and 4.16. The DA model fits the data more closely than DR. For acetone, the DR equation underestimates the adsorption capacity for a concentration level greater than 1,500 ppmv. For MEK, the DR and DA equations provide similarly accurate results for concentration levels greater than 100 ppmv and less than 5,000 ppmv.

Table 4.4 DA and DR parameters for adsorption of acetone and MEK with ACC-5092-20.

Adsorbate	Parameters	DR	DA	DA (weighted)
ACETONE	n	2	1.304	1.448
	W_0, (mg/g)	578	1500	1137
	$\beta E_0 / R_u T$	5.2382	3.1326	3.664
	R^2	0.98	0.992	0.994
MEK	n	2	2.356	--
	W_0, (mg/g)	643	591	--
	$\beta E_0 / R_u T$	6.171	6.472	--
	R^2	0.98	0.983	--

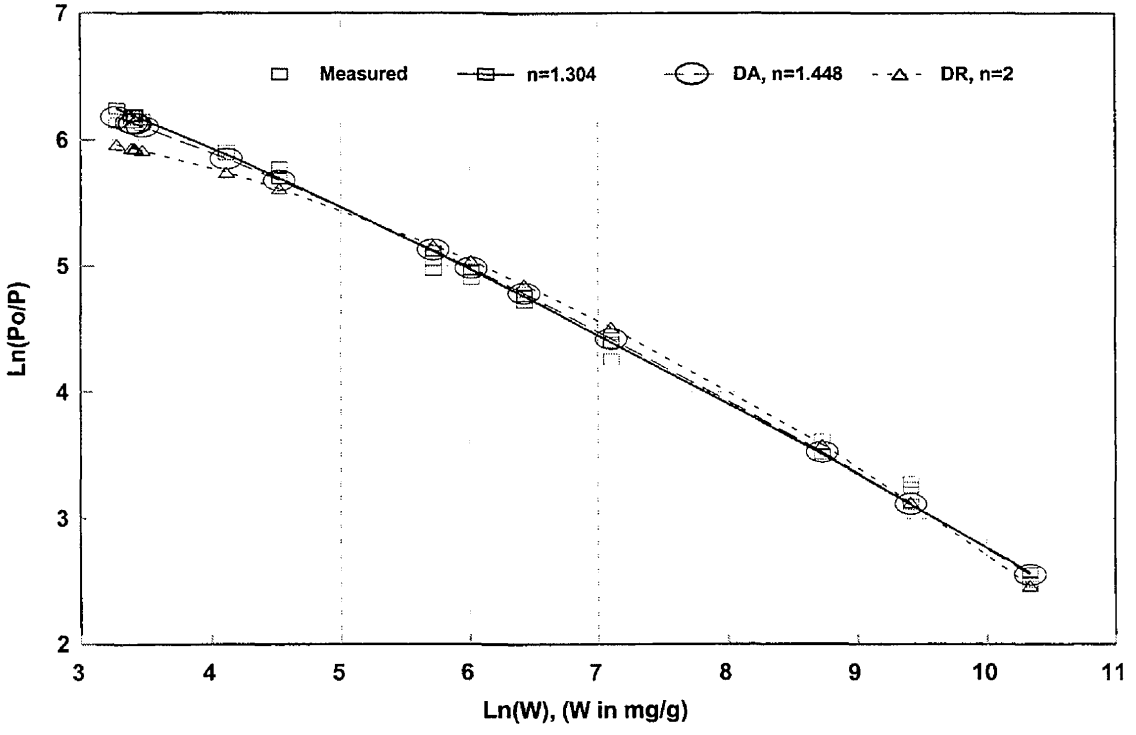

Figure 4.15 Modeled DA and DR isotherms for adsorption of acetone by ACC-5092-20.

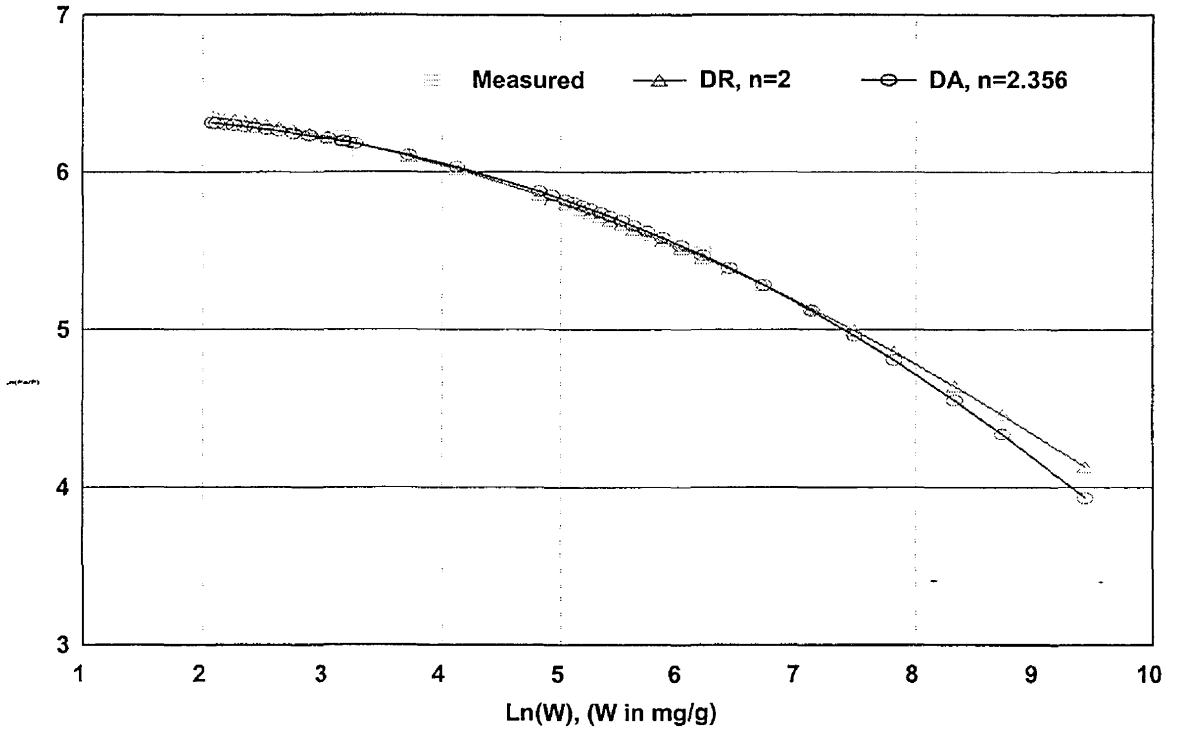

Figure 4.16 Modeled DA and DR isotherms for adsorption of MEK by ACC-5092-20

Modeling of Adsorption Dynamics

Numerous models with different degrees of mathematical sophistication have been introduced for adsorption dynamics in fixed-beds over the years. Usually the adsorption dynamic models predict the BTC. Then data such as stoichiometric time, breakthrough time, TPR, length of MTZ or LUB are extracted from the predicted BTC. More rigorous models use numerical schemes to solve a series of coupled partial differential equations that describe conservation laws of systems such as mass, momentum, species, and energy. In some situations, depending on the design of the adsorber, it is possible to decouple the equations and solve them separately or disregard the effect of some of them. For systems with simple hydrodynamic and NIT conditions, it may be sufficient to solve concentration equations derived from the conservation laws of mass and species. The NIT condition prevails in a situation where either heat of adsorption is small or heat transfer between fluid and solid is slow enough to cause additional broadening of the concentration front. In NIT conditions, heat transfer from adsorbent and walls of adsorber is fast enough to prevent the formation of a distinct thermal wave in the adsorber. Application of a developed model for NIT conditions is restricted to conditions with geometric and thermo-hydrodynamic similarities. In addition to the NIT assumption, further simplifying assumptions can be made to linearize equations describing gas and solid phase concentrations. For example, it is often assumed that the mass transfer film coefficient and the effective adsorbent diffusitivity are constant.

Assuming a polynomial of second order as the deriving force for mass transfer, the rate of change of adsorbate mole fraction (volume concentration) at the bed outlet can be written in the form of:

$$\left(\frac{dC}{dt}\right) = K_1 C + K_2 C^2 \qquad (4.6)$$

with boundary conditions: $(t = 0, C_o/C_i = 0)$, $(t = t_s, C_o/C_i = 0.5)$ and $\lim (C_o/C_i) = 1$ as $t \rightarrow \infty$

Solution of eq. 4.6 is in the form of:

$$C_o/C_i = \{ 1 + \exp[K(t_s - t)] \}^{-1} \quad (4.7)$$

Yoon and Nelson (1984) used concepts of probability to relate the rate of mass transfer to the product of the probability for adsorption and probability for breakthrough and derived the same equation.

Using regression analysis for data range of $0.1 < C/C_0 < 0.9$, optimum sets of K and t_s can be determined. This method was applied to model the BTCs for acetone and MEK. Table 4.5 provides the K and t_s values for each set of experiments. Figures 4.17-18 show the modeled BTCs. Very good agreement exists between modeled and experimental results.

Table 4.5 K and t_s coefficients for the BTC dynamic model.

BTC Experiment	$(t_s)_{measured}$ (min)	$(K)_{model}$	$(t_s)_{modeled}$ (min)	R^2
Acetone, 11,496 ppmv	92.6	0.125	92.6	0.998
Acetone, 10,240 ppmv	107.9	0.103	108.5	0.995
Acetone, 9,460 ppmv	107	0.096	106.7	0.975
Acetone, 10,090 ppmv	104	0.097	103.9	0.99
MEK, 15,540 ppmv	46	0.283	46.5	0.99
MEK, 5,300 ppmv	127.2	0.074	127.5	0.99
MEK, 5,250 ppmv	125.2	0.121	126.2	0.988
MEK, 5,012 ppmv	133.4	0.066	134.4	0.99
MEK, 4,744 ppmv	114.2	0.132	115.2	0.98

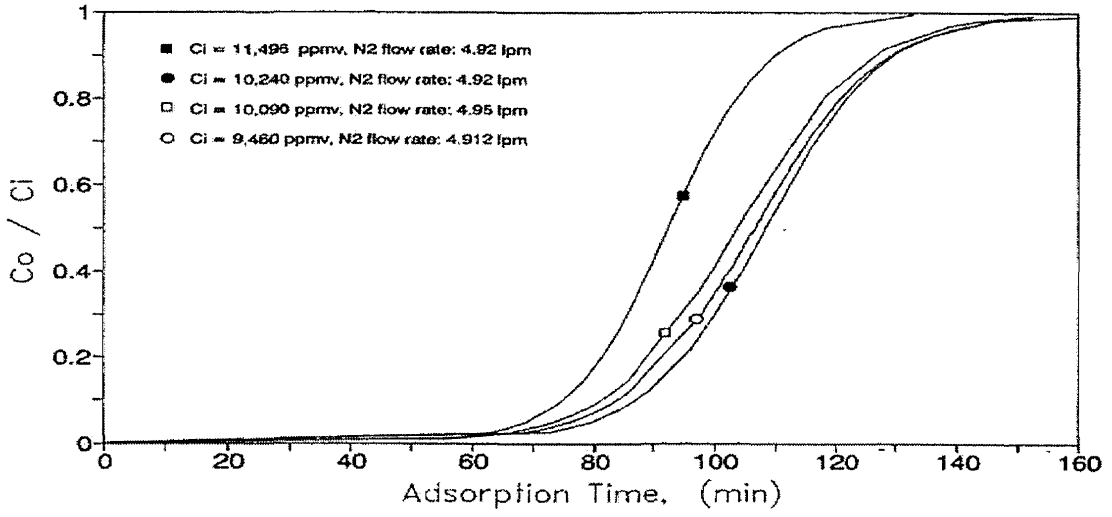

Figure 4.17 Results of modeled breakthrough curves for acetone experiments

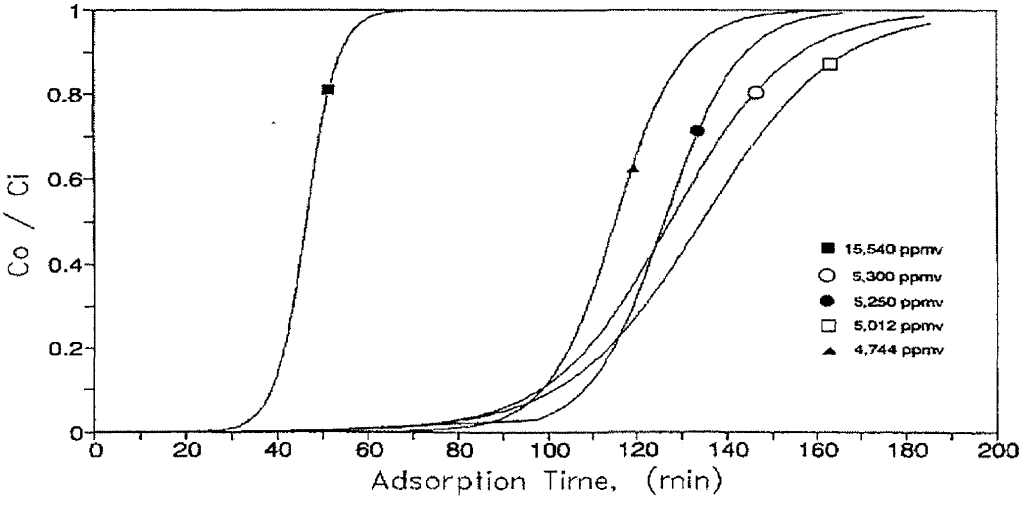

Figure 4.18 Results of modeled breakthrough curves for MEK experiments

Electrothermal Regeneration Experiments

After completion of each breakthrough test, the saturated ACFC fixed-bed was electrothermally regenerated. In a full-scale system, the fixed-bed can be conveniently made of several separate modules placed in series. This enables regeneration of each module in a fully saturated condition. Regeneration of a saturated bed increases the thermal efficiency of the condenser as well as increasing concentration of adsorbate during regeneration. Moreover, the adsorption capacity of the bed is also fully utilized and a TPR greater than 99% can be obtained.

Regeneration of Acetone from ACFC Fixed-Bed

The experimental setup for electrothermal regeneration tests is shown in Figure 3.12. Due to the high energy rates transferred to the adsorbate in this regeneration method, supersaturated vapor streams were produced at the stages of desorption. Supersaturation caused condensation in the pipelines downstream of the adsorber and affected the concentration measurement by the GC/FID and GC/MS. This problem was solved by diluting the desorption stream to a level below the saturation level with addition of a heated UHP N_2 stream. The concentrations of the resulting diluted mixtures were measured with the GC/FID by the same procedure as discussed before. The measured concentrations were corrected using:

$$C_c = \frac{(C_d Q_{N_2,t})}{(C_d Q_{N_2,d} + Q_{N_2,c})} \qquad (4.8)$$

Where C_c = concentration of the concentrated TVOC, C_d = diluted TVOC concentration, $Q_{N_2,t}$ = $Q_{N_2,d} + Q_{N_2,c}$ = total nitrogen in the diluted stream, $Q_{N_2,c}$ = flow rate of nitrogen carrier gas in the fixed-bed, $Q_{N_2,d}$ = flow rate of dilution nitrogen added to effluent.

Regeneration tests for a saturated fixed bed of ACFC were performed to evaluate the effect of applied electrical power (Figure 4.19). N_2 gas flow rate through the bed was controlled at 1 slpm for three tests and 0.5 slpm for two tests. Electrical voltage for each test was set at select values to observe the effect of applied electrical power profile on the resulting effluent TVOC concentration and bed temperature profiles. Effluent maximum TVOC concentrations during desorption ranged from 18% to 63% by volume. TVOC concentration profile and desorption time were readily controlled by carrier gas flow rate and applied electrical power. Increasing TVOC concentration was observed with decreasing carrier gas flow rate and increasing applied power. Figure 4.20 shows the temperature profiles measured at different locations of the bed. The temperature profiles shown in Figure 4.19 display the temperature history at port D, the location of maximum temperature during regeneration. In all five tests, more than 65% of the adsorbed acetone was regenerated at a bed maximum temperature of < 50 °C and an effluent concentration of > 10% by volume. During this time, gas phase bulk temperature change was minimal (< 10°C). Low temperature changes are indicative of an efficient energy transfer.

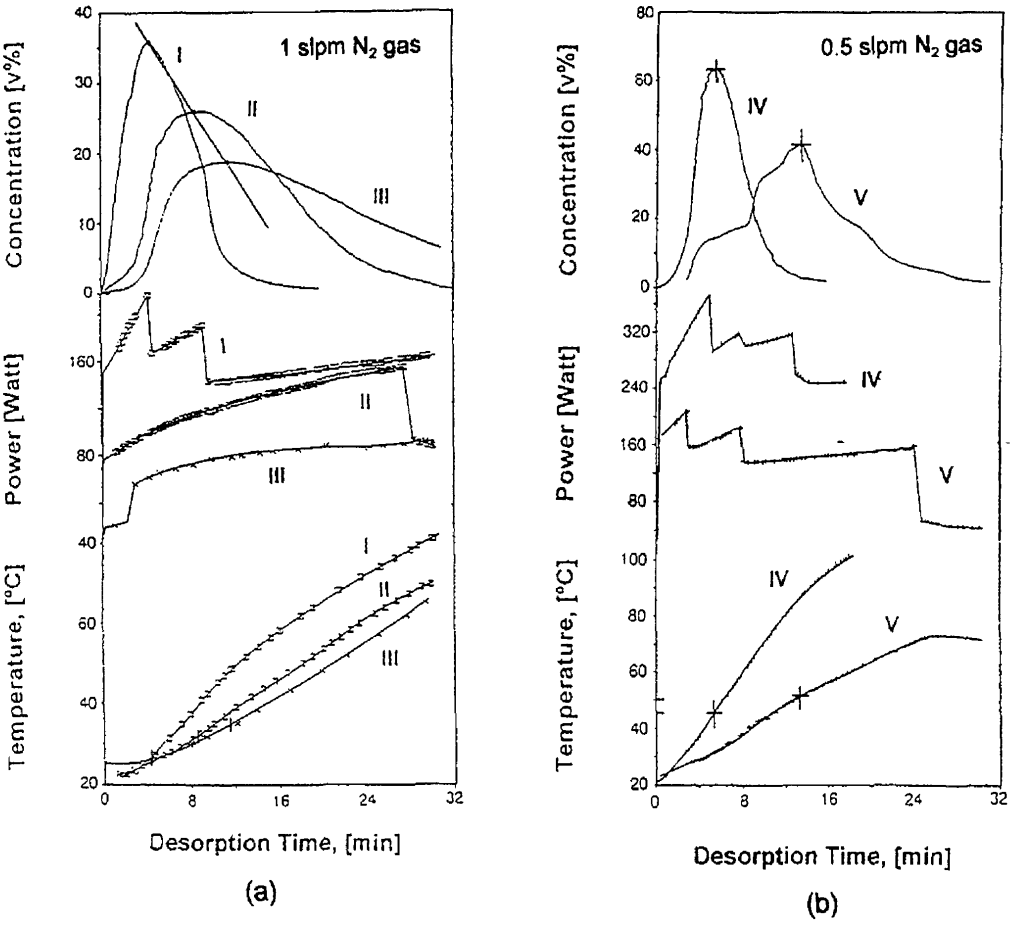

Figure 4.19 Regeneration results for desorption of acetone from ACFC fixed-bed

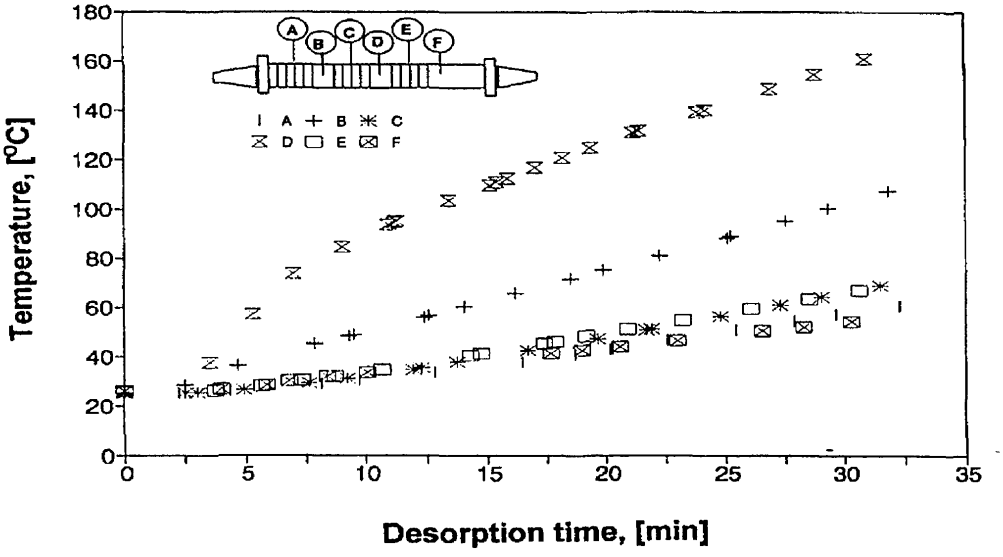

Figure 4.20 ACFC fixed-bed temperature history as a function of sampling location for desorption of acetone, profile IV

Mass of acetone desorbed was calculated by numerical integration of the concentration profiles in the form of:

$$\left(M_{des}\right)_t = \frac{\left(PM_W Q_{N2}\right)}{\left(R_u T\right)} \int_0^t \left[C/\left(1-C\right)\right]_{out} \, dt \qquad (4.9)$$

Applied energy was calculated by integration of the power from experimental data, where: v = voltage, i = current, and E_t = energy applied until time t. Note that due to assumption of ideal gas in the above equations, some inaccuracies might be introduced for high

$$E_t = \int_0^t v \, i \, dt \qquad (4.10)$$

concentration values. Mass desorbed and energy supplied as functions of time are presented in Figures 4.21-22. The profiles that are marked as I, IV, and V provide supersaturated concentration. These profiles show 30-35% less mass desorption than the initial amount of adsorption. The difference between initial amount of adsorption and final amount of desorption was less than 10% for the profiles marked as II and III. The maximum concentration levels of these two profiles were less than the saturation vapor pressure. Another hypothesis for the observed mass loss might be due to dissociation of adsorbate on the surface of ACFC when high electrical power is supplied to the bed. This problem should be further investigated in the future. If these reasons are the cause of the differential mass measured, it is better to normalize the regeneration curves based on total mass desorbed at a baseline steady-state condition. Figures 4.23-24 show such curves.

As the results indicate, increasing carrier gas flow rate increases desorption rate but reduces concentration of acetone in the gas stream. Increasing electrical power increases both

desorption rate and acetone concentration. Therefore, it should be possible to find an optimum set of conditions for electrical power, carrier gas flow rate, and temperature to minimize the overall energy consumption of the system.

Table 4.6 summarizes the conditions of the acetone regeneration experiments and key points derived or calculated from the experimental results.

Table 4.6 Summary of regeneration tests for desorption of acetone from ACFC-fixed bed

Test Number	1	2	3	4	5
Maximum generated concentration, C_{max} (%)	41.13	63.2	35.64	26	18.62
Time of C_{max}, t_{max} (min)	13.3	5.36	4.26	9.26	11.15
Mass regenerated by t_{max} (g)	4.15	3.38	2.91	4	3
Energy spent to t_{max}, E_{max} (KJ)	118.4	90.8	38.7	51.4	37.8
Maximum bed temperature at C_{max} (°C)	51.5	46	27	33.5	35
Concentration at 50% regeneration (%)	25.7	53.5	28.9	23.9	17.14
Time of 50% regeneration $t_{50\%}$ (min)	15.5	6.7	6.35	12	15.7
Mass regenerated at $t_{50\%}$ (g)	5.55	5.75	6.08	6.2	5.41
Energy spent to $t_{50\%}$. $E_{50\%}$ (KJ)	136	116.7	66.5	71	60
Maximum bed temperature at $t_{50\%}$ (°C)	55.2	52.2	33	38.5	43
Ambient temperature (°C)	22±1	25±1	22±1	22±1	20±1
Carrier gas flow rate (slpm)	0.5	0.5	1	1	1

Regeneration of MEK from ACFC Fixed-Bed

The experimental setup and dilution process was the same as those for the acetone experiments. Regeneration results for desorption of MEK from ACFC-fixed-bed are presented in Figures 4.25-28 and Table 4.7.

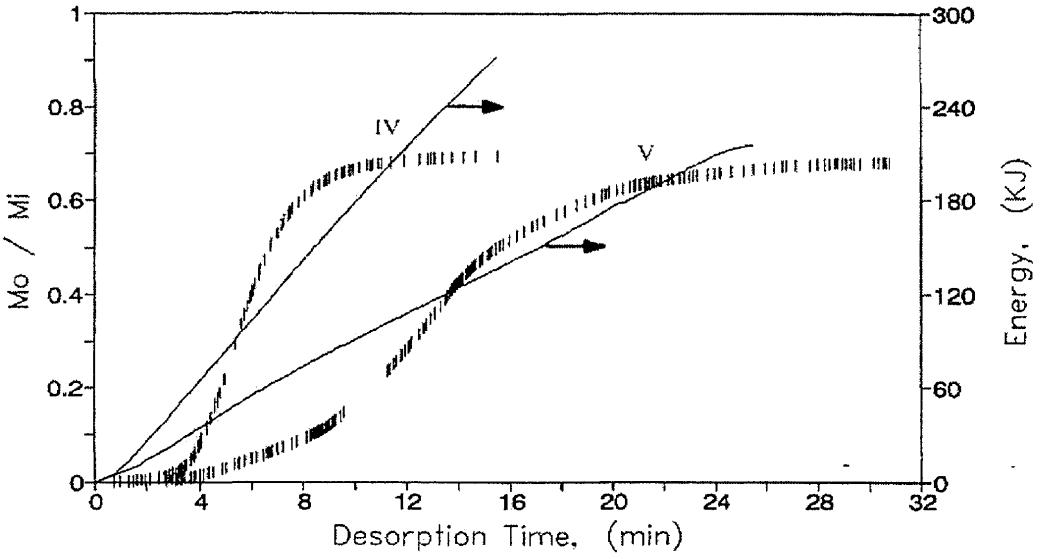

Figure 4.21 Normalized mass desorbed and cumulative energy consumed as a function of time for acetone experiments. Nitrogen flow rate = 0.5 slpm

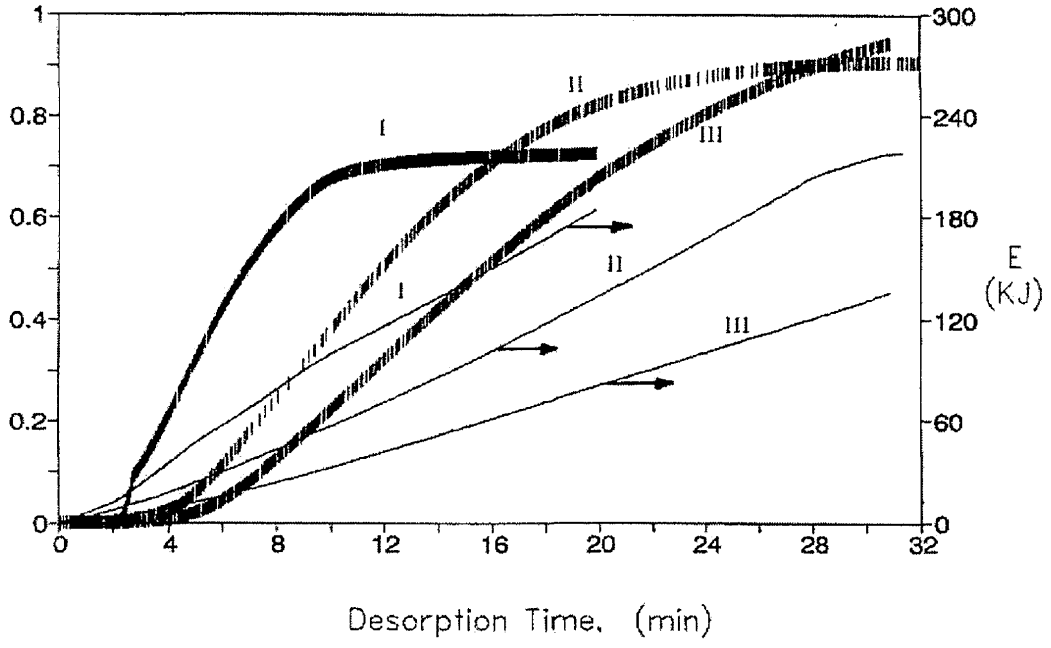

Figure 4.22 Normalized mass desorbed and cumulative energy consumed as a function of time for acetoneexperiments. Nitrogen flow rate = 1 slpm

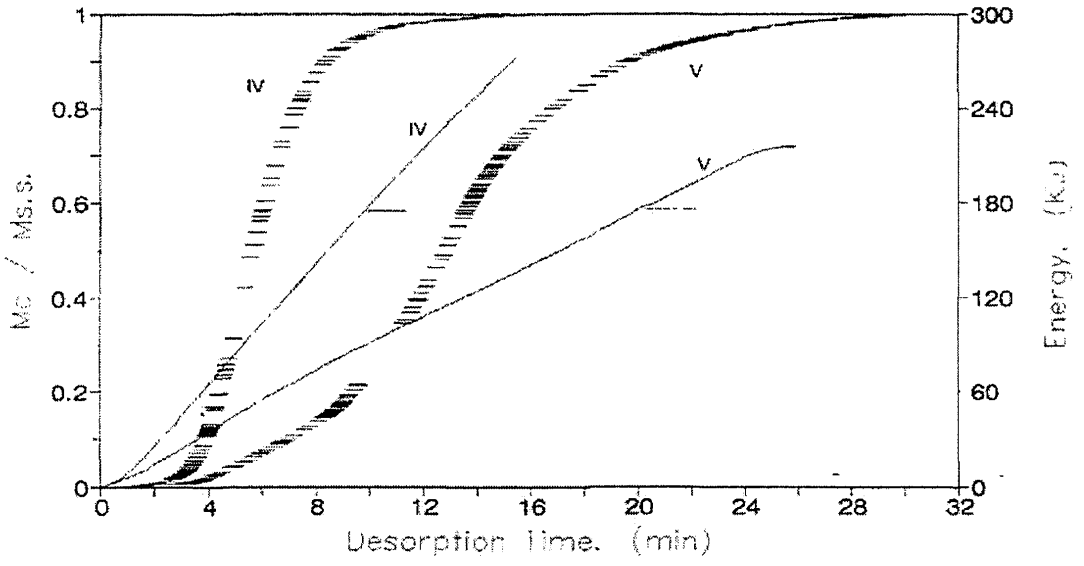

Figure 4.23 Corrected normalized mass desorbed and cumulative energy consumed as a function of time for acetone experiments. Nitrogen flow rate = 0.5 slpm

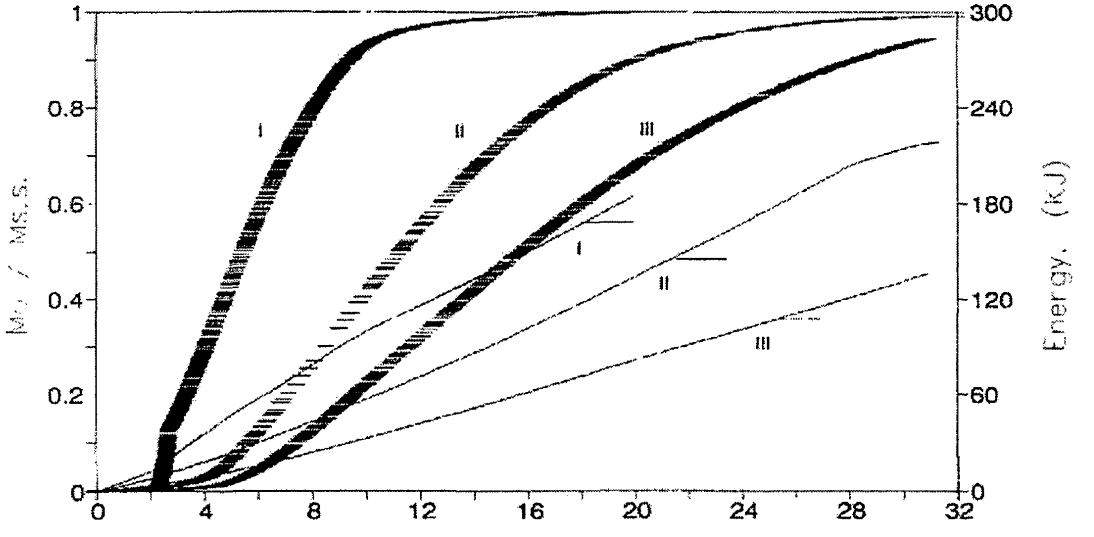

Figure 4.24 Corrected normalized mass desorbed and cumulative energy consumed as a function of time for acetone experiments. Nitrogen flow rate = 1 slpm

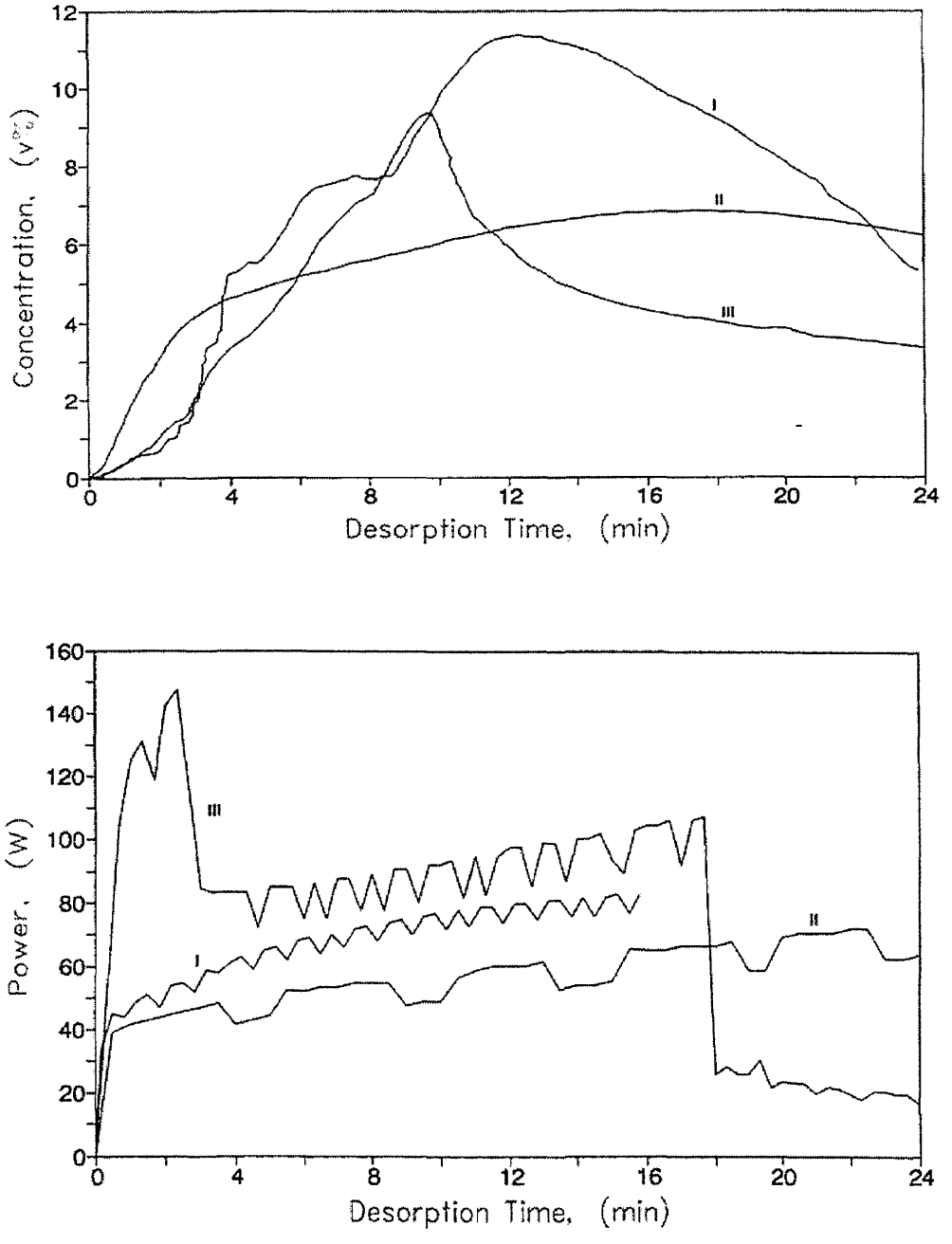

Figure 4.25 Resulting concentration profiles for regeneration of ACFC fixed-bed saturated with MEK

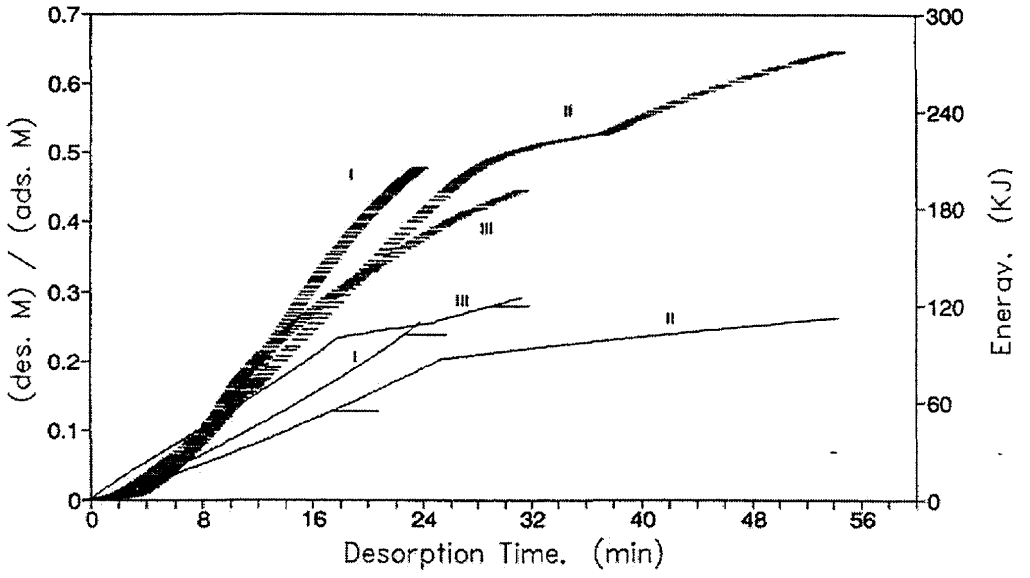

Figure 4.26 Normalized mass desorbed and cumulative energy consumed as a function of time for MEK experiments

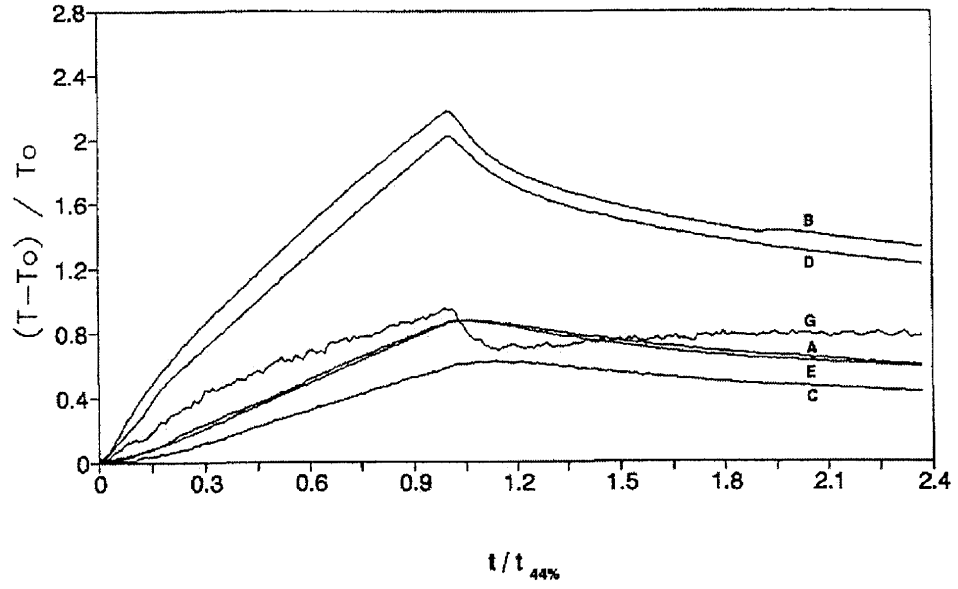

Figure 4.27 ACFC fixed-bed temperature history as a function of sampling location for desorption of MEK, profile II

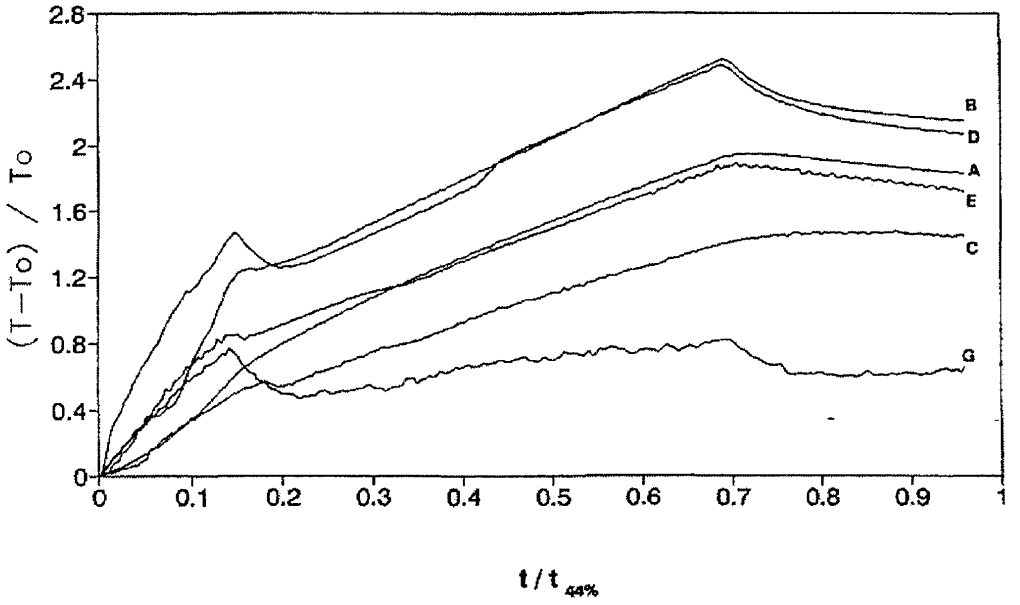

Figure 4.28 ACFC fixed-bed temperature history as a function of sampling location for desorption of MEK, profile I

Table 4.7 Summary of regeneration tests for desorption of MEK from ACFC-fixed bed

Test Number	1	2	3
Maximum generated concentration, C_{max} (%)	6.83	9.37	11.37
Time of C_{max}, t_{max} (min)	17.7	9.7	12.4
Mass regenerated by t_{max} (g)	2.77	1.19	2.21
Energy spent to t_{max}, E_{max} (KJ)	55.8	53.6	47.7
Maximum bed temperature at C_{max} (°C)	79	75	43
Carrier gas temperature at t_{max} (°C)	56	60	26
Concentration at 44% regeneration (%)	1.25	2	7
Time of 44% regeneration $t_{44\%}$ (min)	25.5	30.8	21.6
Mass regenerated at $t_{44\%}$ (g)	4.3	3.7	4.83
Energy spent to $t_{44\%}$. $E_{44\%}$ (KJ)	87.5	123.8	96
Maximum bed temperature at $t_{44\%}$ (°C)	95	94	58
Carrier gas temperature at $t_{44\%}$ (°C)	62	66	29
Ambient temperature (°C)	27	23.6	25
Carrier gas flow rate slpm	0.5	0.5	1.0

The ACFC fixed-bed was regenerated with less electrical power to avoid overheating the bed. Due to higher MEK molar energy of adsorption, more electrical power was required to produce high concentration levels comparable to the ones observed for the acetone experiments. Higher supplied electrical power for profile III resulted in lower concentration levels and different shapes of concentration profile. This might be due to dissociation or polymerization of MEK on the surface of ACFC that needed further investigation.

Effect of Electrothermal Regeneration on the ACFC

Effect of electrothermal regeneration on the physical properties of the ACFC was judged by measuring specific surface area and effective micropore volume of the ACFC samples after up to 50 adsorption/desorption cycles. The measurements were done after every ten cycles. These evaluations were done on a single layer of ACFC attached to electrodes in a glass reactivation cell (Figure 4.29) developed and operated by Brett Covington of the University of Illinois.

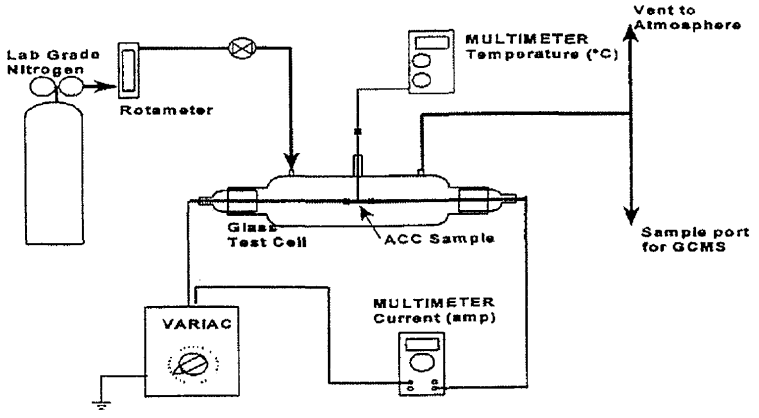

Figure 4.29 Schematic of the setup for the cyclic adsorption/electrothermal regeneration experiments

The glass test cell was 40 cm long and 1.7 liters in volume with two opposing aluminum electrodes that act to support the cloth sample as well as provide electrical connections. A Variac, (model W10MT3), provided a potential difference across the sample and current was monitored by a Fluke 77 multimeter. The bulk temperature of the ACFC was monitored by a type K thermocouple detected by a digital multimeter (Omega 881C). Laboratory grade N_2 (99.95 % pure) was used to purge air and contaminants from the test cell.

The ACFC layer was saturated with the TVOC and then regenerated electrothermally. During the regeneration, N_2 flow was set at 0.5 lpm and the sample was heated at a bulk sample temperature of 140 ± 10°C for 20 min. This required a voltage between 8 and 12 volts and a current between 0.7 and 1.1 amperes for a typical sample of 100 to 150 mg. This procedure was repeated up to 50 cycles. The samples were analyzed using the Micromeritics ASAP 2400 surface area analyzer to determine the specific surface areas and micropore volumes after the completion of 10, 20, 30, and 50 cycles. The baseline for surface areas and pore volumes were determined by analyzing the ACFC samples prior to the start of adsorption/desorption cycles. The measured N_2 isotherms were converted into specific surface area and effective micropore

volume by use of the BET (Brunauer et al., 1938), DR (Dubinin, 1989), and Harkins Jura (HJ) (Harkins and Jura, 1943, Lowell and Shields, 1984) equations.

Acetone and benzene were used for these experiments. For the benzene tests, the changes in the adsorption properties of the ACC-5092-20 were 2.2 % increase for BET specific surface area and 2.4 % increase for HJ effective micropore volume for the 12 hour electrothermaly regenerated sample, 2.6 % increase for BET specific surface area and 3.1 % increase for HJ effective micropore volume for 50 cycles. For the acetone tests, the changes in the adsorption properties of the ACC-5092-20 were 3.9 % increase for BET specific surface area and 3.8 % for single point effective micropore volume for 50 cycles. All of these values were within the experimental error of 5.5% for BET specific surface area and 8.4 % for HJ effective micropore volume. For benzene tests, the largest changes were an increase in the BET specific surface area by 7.7 % and the HJ effective micropore volume by 8.49 %. Likewise the cycles of acetone saturation with electrothermal regeneration showed similar results with surface area increase of 3.9 % and single point effective micropore volume increase of 3.8 %. These variations can be considered negligible when compared to error values of more than 10 % reported by Dubinin (1989).

Cryogenic Condensation Modeling

The Wagner equation (equation 3.2) provides a method to determine the TVOC saturation concentration based on a given temperature assuming vapor/liquid equilibrium. In order to apply the Wagner equation, temperature needs to be determined and sufficient condenser surface area must exist for the TVOC vapor to reach equilibrium with its liquid condensate. Fundamental numerical modeling provides a method to determine condenser temperature and equilibrium conditions based solely on gas stream, refrigerant and condenser characteristics.

Two levels of modeling are considered: 1) thermodynamic coupled with the Wagner equation (Appendix C) and 2) mass transfer (Appendix D). Thermodynamic modeling provides outlet TVOC vapor concentration, required refrigerant flow rate and final condenser temperature assuming no heat or mass transfer resistance and equilibrium conditions. Mass transfer modeling incorporates mass transfer resistances into the thermodynamic model. However, such an approach assumes no heat transfer resistance. The condenser surface area required to reach a desired outlet TVOC concentration equilibrium can be obtained with this technique. The minimum TVOC gas phase concentration occurs at a condenser surface area in which equilibrium between the liquid condensate and the vapor is achieved.

Thermodynamic Model

Thermodynamic modeling coupled with the Wagner equation provides a predictive method to determine outlet TVOC concentrations, required refrigerant flow rates and final condenser temperature. This model is based on equilibrium and assumes no heat loss. This model does not provide condenser sizing information (e.g., condenser surface area). The model balances the latent and sensible heat gained by the LN_2 refrigerant with the latent heat of condensation lost by the organic vapor, the sensible heat lost by the vapor laden gas stream and the sensible heat lost by the condensate film.

The thermodynamic model is developed for condensation of VOCs in a non-condensable carrier gas. The following assumptions are made in the development of the model:

1) Thermodynamic equilibrium between the refrigerant and challenge gas stream is achieved,
2) no mass or heat transfer resistance, and
3) no system heat loss except from condensate wash-out.

The energy balance equation can be obtained from the first law of thermodynamics. The energy gained by the refrigerant equals the energy lost by the challenge gas stream. One benefit of cryogenic condensation is that the latent heat of vaporization for LN_2, as well as the specific heat change of the gaseous N_2, is an available heat sink (Figure 4.30). The first law of thermodynamics can be stated in words for this system as:

$$\left\{\begin{array}{c}\text{LN}_2\text{ Latent Heat}\\ \text{of Vaporization}\end{array}\right\}+\left\{\begin{array}{c}\text{GN}_2\text{ Sensible}\\ \text{Heat Change}\end{array}\right\}=\left\{\begin{array}{c}\text{VOC Latent}\\ \text{Heat of}\\ \text{Condensation}\end{array}\right\}+\left\{\begin{array}{c}\text{VOC \& Carrier}\\ \text{Gas Sensible}\\ \text{Heat Change}\end{array}\right\}+\left\{\begin{array}{c}\text{VOC Condensate}\\ \text{Sensible Heat}\\ \text{Change}\end{array}\right\}$$

or written in integral form as:

$$M_{LN2}\,\Delta h_{LN2}+m_{GN2}\int_{T1}^{T2} C_{P,\,N_2}\,dT=m_{LA}\,\Delta h_A+m_{a\text{-}N2}\int_{T2}^{T3} C_{P,A-N_2}\,dT+M_{LA}\int_{T2}^{T3} C_{P,LA}\,dT \qquad (4.13)$$

where,

m_{LN2} = mass flow rate of liquid nitrogen
Δh_{LN2} = enthalpy of vaporization for LN_2
m_{GN2} = mass flow rate of gaseous N_2
$C_{p,N2}$ = specific heat of carrier gas
m_{LA} = mass flow rate of condensed VOC
Δh_A = enthalpy of condensation for VOC
$m_{A\text{-}N2}$ = mass flow rate of carrier gas and TVOC gas stream
$C_{p,A\text{-}N2}$ = combined specific heat of carrier gas and TVOC vapor
$C_{p,LA}$ = specific heat of TVOC liquid condensate
T1 = temperature of LN_2 (77.4 K)
T2 = final temperature of the LN_2 refrigerant and carrier gas and TVOC gas stream
T3 = initial temperature of the challenge gas stream.

$$A_{con}=\frac{H_{load}}{U\,\Delta T_{LM}} \qquad (4.14)$$

Condenser surface area based on heat transfer can be estimated from (USEPA[b], 1991):

where,

A_{con} = condenser surface area
H_{load} = heat load determined from the enthalpy loss of the vapor and carrier gas
U = assumed overall transfer coefficient, 20 BTU/hr ft^2 °F (from USEPA[b], 1991)
ΔT_{LM} = log-mean temperature difference between coolant, vapor and equilibrium temperatures

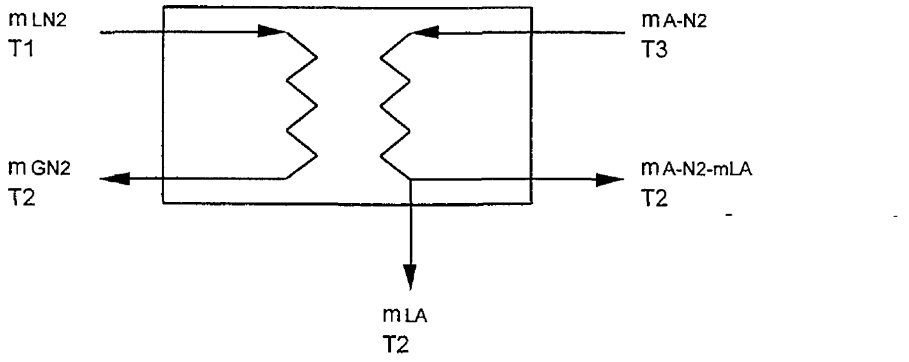

Figure 4.30 Schematic of thermodynamic model element

The thermodynamic model is coupled with the Wagner equation (eq. 3.2) to provide the saturation concentration at the equilibrium temperature. The complete model including mass and flow conservation is listed in Appendix C and was written in EES version 3.7. The model is written for LN_2 refrigerant and acetone in N_2 challenge gas stream. To analyze other VOCs or carrier gas streams, only the gas and liquid material properties need to be changed. A wide variety of material properties for many gases and liquids can be found in Reid et al. (1977).

Results of the thermodynamic model are presented with experimental data in this section. For design purposes, the model can be used to estimate LN_2 requirements, removal efficiency, outlet TVOC concentrations and outlet gas temperature. The typical input data required are inlet temperature, inlet gas flow rate, inlet concentration and inlet gas temperature. However, a wide variety of variables can be evaluated. For instance, a required removal efficiency may be input to determine the required LN_2 refrigerant flow rate.

Mass Transfer Model

The thermodynamic model coupled with the Wagner equation, used to determine the saturation TVOC concentration, provides a method to estimate outlet concentration, removal efficiency and refrigerant requirement . However, this model assumes thermodynamic equilibrium and no mass resistance. Assuming no mass transfer resistance may yield condenser designs in which equilibrium between the TVOC vapor and the corresponding condensate film is not achieved. Outlet concentrations will be higher in undersized non-equilibrium condensers. The thermodynamic model is not dependent on the physical shape and size of the condenser, which is an important design consideration.

Two transfer mechanisms influence the selection of condenser size based on desired TVOC removal: 1) mass transfer surface area required to achieve the desired mass removal (Chilton and Colburn, 1934) and 2) heat transfer surface area required to achieve the desired condensation temperature, thus mass removal (Colburn and Hougen, 1934). These mechanisms

should be coupled together with momentum transport and the fundamental thermodynamics of the system. Condenser size based on desired mass removal is determined from the surface area required to transport the desired mass to the surface (mass transfer) and the surface area required to achieve the desired condenser temperature (heat transfer and thermodynamics).

Mass transfer coupled with momentum transport and thermodynamics can be evaluated independent of heat transfer if the condenser temperature profile is assumed or if an average condenser temperature is determined directly from the thermodynamic model described above. Determining the condenser temperature from thermodynamic equilibrium assumes that heat transfer resistance is negligible. The effect of heat transfer resistance is to increase the temperature (thus outlet TVOC concentration) of the challenge gas stream predicted from the thermodynamic model.

Mass transfer condensation is modeled for an indirect contact condenser in which the refrigerant gas stream is not mixed with the challenge gas stream. The challenge gas stream is modeled as forced convection of a vapor in a non-condensable gas condensing into a liquid film. Essentially all condensation in a shell-and-tube heat exchanger is filmwise as opposed to dropwise (Wilbur, 1985). Mass transfer occurs from the bulk gas flow of the challenge gas stream to the condensate film. A gas film is established between the bulk flow and condensate layer which resists mass transfer as discussed in section 3.

The mass transfer driving force results from a concentration gradient in the gas film (Figure 4.31). The temperature at the gas/condensate interface is lower than in the bulk challenge gas stream. The lower temperature results in a lower saturation concentration at the interface than in the bulk flow if the vapor is at the saturation point. This concentration gradient induces mass transport to the condensate surface where condensation occurs (Chilton and Coulburn, 1934).

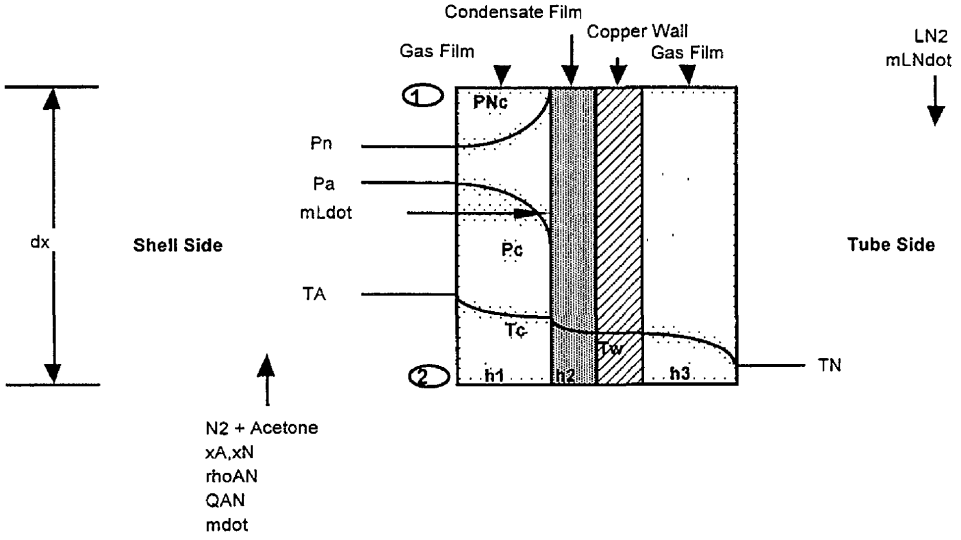

Figure 4.31 Condenser element used for mass and heat transfer models.

The mass transfer model incorporates the thermodynamic model discussed above with the radial mass transport of the vapor to the condensate surface. The following assumptions are made in addition to the assumptions made in the thermodynamic model development:

1) laminar challenge gas flow (Re < 2400)

2) adiabatic conditions
3) temperature at the condensate film is the thermodynamic equilibrium temperature T2 from the thermodynamic model if this module is used
4) condensation surface is modeled using the flat plate assumption (Rosenow et al., 1985)
5) gas and liquid properties are dependent on temperature, composition and concentration only
6) complete vaporization of the LN_2
7) temperature and concentration gradients are log-mean (Wilbur, 1985)
8) vapor equilibrium concentration exists at the gas/condensate interface (Kern, 1950) (found from the Wagner equation)
9) condensation occurs at the condensate surface only (Rosenow et al., 1985)
10) no condensate surface waves; waviness increases mass transfer (Siddique et al., 1994)
11) uniform condensate film thickness (wash-out is equal to mass condensed)
12) driving mass transfer force is from the concentration gradient between bulk challenge gas and condensate film (Chilton and Coulburn, 1934)
13) the TVOC mass entering the gas film boundary layer is condensed (Kern, 1950)

To determine axial concentration of a vapor in the condenser, radial mass transfer is determined from a mass transfer coefficient. The mass transfer coefficient, Kg, is developed from the Chilton and Coulburn analogy between and mass transfer (1934):

$$Kg = \frac{h_l \left(\frac{C_{p,AN}\, \nu_{AN}}{\kappa_{AN}} \right)^{2/3}}{C_{p,AN}\, P_{n,gf}\, MW_{AN,ave} \frac{\nu_{AN}}{\left(\rho_{AN,ave}\, k_d \right)^{2/3}}} \qquad (4.15)$$

where,

h_l = heat transfer coefficient for laminar flow with the entrance length correction
$C_{p,AN}$ = specific heat of the VOC-carrier gas challenge gas stream
ν_{AN} = viscosity of the VOC-carrier gas challenge gas stream
k_{AN} = thermal conductivity of the VOC-carrier gas challenge gas stream
$P_{n,gf}$ = log-mean partial pressure of carrier gas in the mass transfer boundary layer
$MW_{AN,ave}$ = average molecular weight of the challenge gas stream
$\rho_{AN,ave}$ = average density of the challenge gas stream
k_d = diffusion coefficient of TVOC in carrier gas using the Gilliand equation

This equation is shown to conservatively hold for flow inside tubes, flow across a single tube and flow along plane surfaces (Kern, 1950). The appropriate value for h_l is substituted into the equation depending on the flow conditions. Determination of the convective heat transfer coefficient involves the Nusselt analysis. The Nusselt number is given as (Incropera and DeWitt, 1990):

$$Nu = \frac{h_l D_e}{\kappa_{AN}} \tag{4.16}$$

Seider and Tate (1936) showed that for laminar flow inside circular tubes with a constant surface temperature, the Nusselt number is given as:

$$Nu = 1.86 \left(\frac{D_e G_{ave}}{\nu_{AN}} \frac{C_{p,AN} \nu_{AN}}{\kappa_{AN}} \frac{D_e}{dx} \right)^{1/3} \left(\frac{\nu_{AN}}{\nu_{AN,c}} \right)^{0.14} \tag{4.17}$$

where T_c is constant and:

$$0.48 < \frac{C_{p,AN} \nu_{AN}}{\kappa_{AN}} < 16{,}700$$

$$0.0044 < \left(\frac{\nu_{AN}}{\nu_{AN,c}} \right) < 9.75$$

D_e = effective heat transfer shell-and-tube diameter,
G_{ave} = average radial mass flow rate of TVOC to the condensate surface,
dx = condenser element length,
$\nu_{AN,c}$ = VOC-carrier gas viscosity at the condensate surface and
T_C = temperature of condensate film.

Equation 4.18 includes the combined entry length correction. This correction is used for condensers in which the challenge gas stream does not have fully developed velocity and thermal profiles at the entrance. Whitaker (1972) recommends this equation for:

$$\left(\frac{D_e G_{ave}}{\nu_{AN}} \frac{C_{p,AN} \nu_{AN}}{\kappa_{AN}} \frac{D_e}{dx} \right)^{1/3} \left(\frac{\nu_{AN}}{\nu_{AN,c}} \right)^{0.14} \geq 2 \tag{4.18}$$

Otherwise, fully developed flow exists in the majority of the shell in which the challenge stream transverses, and an approximation for the Nusselt number is (Incropera and DeWitt, 1990):

$$Nu = 3.66 \tag{4.19}$$

The mass transfer model in Appendix D is written for the entrance length correction. Equating (4.16) and (4.17) and solving for h_l results in the convective heat transfer coefficient:

$$h_l = 1.86 \frac{\kappa_{AN}}{D_e} \left(\frac{D_e G_{ave}}{\nu_{AN}} \frac{C_{p,AN} \nu_{AN}}{\kappa_{AN}} \frac{D_e}{dx} \right)^{1/3} \left(\frac{\nu_{AN}}{\nu_{AN,c}} \right)^{0.14} \tag{4.20}$$

The diffusion coefficient (kd) in eq. (4.2) is determined from the empirical Gilliand equation for the diffusivity of one gas through another (Gilliand, 1934):
where,

$$k_d = 0.0166 \frac{\left(\frac{T_{A1} + T_{A2}}{2} \right)^{3/2}}{P \left(\nu_N^{1/3} + \nu_A^{1/3} \right)^2} \left(\frac{1}{MW_N} + \frac{1}{MW_A} \right)^{1/2} \quad (4.21)$$

T_{A1} = temperature of bulk challenge gas at the element entrance
T_{A2} = temperature of bulk challenge gas at the element exit
P = ambient pressure
ν_N = viscosity of the carrier gas in the challenge gas stream
ν_A = viscosity of the TVOC in the challenge gas stream
MW_N = molecular weight of carrier gas in the challenge gas stream
MW_A = molecular weight of the TVOC in the challenge gas stream

The amount of TVOC condensed for each element can be determined from a mass balance of the TVOC entering the gas film. Based on the assumption that all of the mass of TVOC entering the gas is condensed, the mass transfer coefficient can be used to determine the mass condensed (Kern, 1950):

$$M_{LA} = K_g \, dP_{lm,vapor} \, SA \, MW_{vapor} \quad (4.22)$$

where,

M_{LA} = mass of acetone condensed
K_g = mass transfer coefficient
$dP_{lm,vapor}$ = log-mean vapor partial pressure difference between the bulk VOC-carrier gas flow and condensate film
SA = condensation surface area
MW_{vapor} = molecular weight of acetone

The required condensation surface area can be determined from eq. (4.14).

The model in Appendix D was written using acetone as the adsorbate and N_2 as the carrier gas. Different compounds may be evaluated by substituting the appropriate material property equations and constants into the model. The list of variables found in Appendix B details the constants used in determining material properties. The fundamental mass transfer coefficient, K_g, diffusion coefficient, k_d, heat transfer coefficient, h_1, and thermodynamic equations are applicable as long as the above assumptions are adequate for evaluation purposes. Also, modeled specific heats, conductivities and visocities were verified with experimental data presented in literature (Carmichael, 1996).

The mass transfer model provides a method of determining condenser mass removal performance, refrigerant flow rate and required surface area based on mass transfer. Typical inputs to the model include inlet gas temperature, inlet gas flow rate, inlet TVOC concentration and either outlet concentration or refrigerant flow rate. The refrigerant flow rate will establish the condenser temperature profile, and thus from the Wagner equation and mass transfer, the axial concentration profile. Therefore if the refrigerant flow rate is defined then the condenser axial concentration is found or vice versa. Defining an outlet concentration will fix the refrigerant flow rate required and the axial concentration profile. Another option is to circumvent the thermodynamic module and input the temperature profile directly.

If the refrigerant flow rate is used, the model determines a condenser temperature based on thermodynamic equilibrium. The modeled bulk gas temperature in the condenser will be lower than the actual temperature due to heat transfer resistance that is not considered in this model. Using the thermodynamic model will under predict the axial concentration at any point in the condenser. Higher refrigerant flow rates will be required to counter heat transfer resistance and achieve the desired condenser temperature (thus outlet concentration).

The outlet mole fraction was determined as a function of condenser surface area for a gas stream with the following characteristics:

Inlet acetone mole fraction	=	0.05 to 0.8
Inlet gas temperature	=	294 K
Inlet challenge gas flow rate	=	1 actual lpm
Temperature of the condensate	=	195 K
Temperature of outlet gas	=	200 K

Thus, the temperature profile was directly input in lieu of allowing the thermodynamic module to determine the condenser temperature. This was done to determine the refrigerant flow rate required to achieve these condenser conditions. The average condenser temperature is assumed log-mean (Kern, 1950).

The minimum TVOC outlet concentration is predicted at approximately 1000 cm^2 for an inlet acetone mole fraction of 0.25 (Figure 4.32). The LN_2 flow rate was found to be 10.1 g/sec to achieve the inputted condenser temperature profile. Results show that outlet TVOC concentration cannot be changed appreciably at large condenser surface areas. This is a result of the bulk acetone vapor concentration approaching the saturation equilibrium concentration at the condensate temperature.

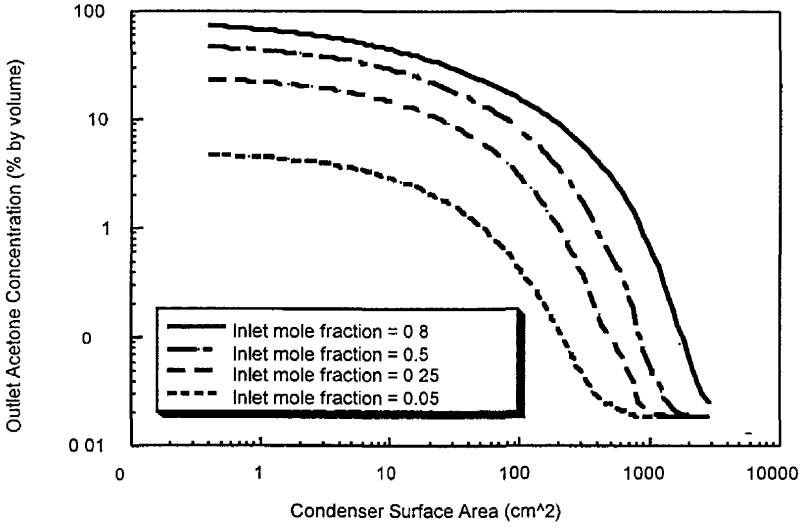

Figure 4.32 Modeled outlet acetone volume fractions for various condenser lengths. Inlet temperature = 294 K, outlet temperature = 200 K, condensate film temperature = 195 K and challenge gas stream flow rate = 1 lpm.

A modeled plot of acetone mole fraction versus condenser surface area for specific process conditions can be made for design purposes. Knowing the desired outlet concentration, the required mass transfer condensation surface area and refrigerant flow rate can be determined to achieve the desired outlet concentration (removal efficiency).

Modeling provides an analysis of condensers that can be used in determining an optimum design. The thermodynamic model provides insight into removal efficiencies, outlet concentrations and required refrigerant flow rates given process conditions. Incorporating mass transfer with the thermodynamic model provides a method for determining the condensation surface area required to achieve the desired outlet concentration

Cryogenic Condensation Modeled and Experimental Results

The objective of developing the bench-scale cryogenic condensation system is to evaluate the feasibility of condensing TVOC vapors using LN_2 as a refrigerant. Experimental results are presented in this section to evaluate the performance of the cryogenic condensation system. The condenser outlet TVOC concentration is experimentally determined for various flow rates, inlet concentrations and condenser temperatures. Also, initial and optimized test results are presented for the integrated ACFC adsorption/cryogenic condensation system. Model results from the thermodynamic and mass transfer models already presented in this report are also presented.

CO_2 Refrigerant Results

A preliminary TVOC condensation test was conducted to evaluate the outlet acetone vapor concentration using an alternative refrigerant. Solid carbon dioxide (CO_2, dry ice) was

chosen because of its low temperatures and ease of handling and delivery. A flow rate of 3 actual lpm of house air was passed through the center of a 61 cm length × 7.6 cm diameter hollow cylinder packed with dry ice. The total flow rate of refrigerant (house air and sublimed CO_2) was 5.5 actual lpm. This flow was passed through the inside tube of the condenser. The condenser was cooled to 264 ± 1 K without the vapor laden gas stream passed through the shell. A 500 sccm gas flow of 85.8 ± 2.0% N_2 and 14.2 ± 2.0% acetone was then introduced counter currently into the shell. The temperature measured at the outlet of the challenge gas stream was 273 ± 5 K. The outlet concentration of acetone in gaseous N_2 was monitored using syringe samples drawn at the condenser outlet and injected into the GC/MS (Figure 4.33). After approximately 11 min, the average outlet concentration was 8.1 ± 0.6% by volume. The maximum theoretical concentration using the Wagner Equation at 273 K is 9.1% (Figure 3.3). The mean mass removal efficiency was 45.6% with CO_2-air refrigerant.

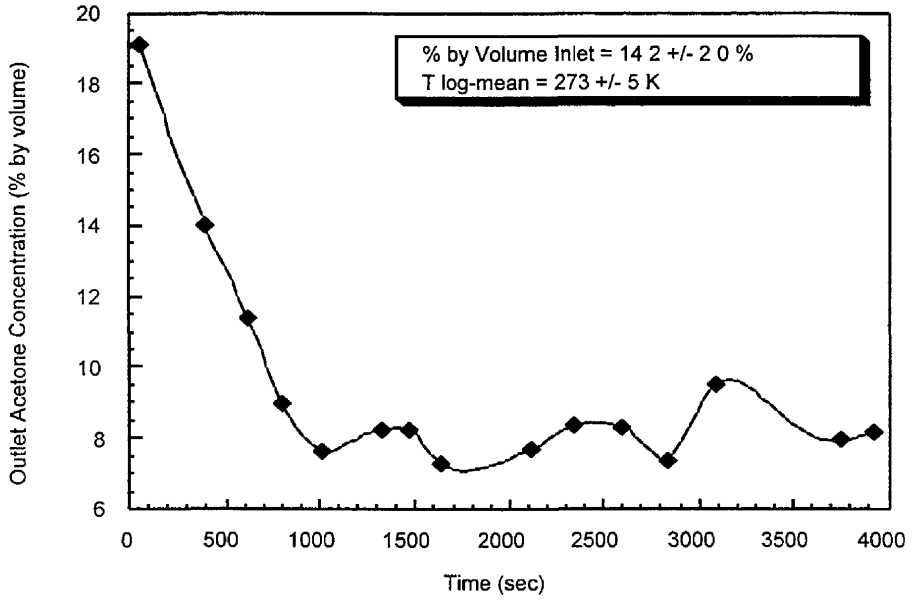

Figure 4.33 Condenser outlet acetone concentration using CO_2 and compressed air as the tube refrigerant. Flow rate = 0.5 actual lpm, condenser shell pressure = 745 mm Hg and ambient temperature = 294 K.

The outlet concentration was near the acetone equilibrium saturation concentration at the temperature of the outlet challenge gas stream. This demonstrates that using air passed over solid CO_2 does not achieve temperatures low enough to condense large quantities of acetone unless the inlet acetone gas concentration is above the saturation concentration at ambient temperature. The high outlet acetone concentrations and low removal efficiency excludes this type of refrigerant from many applications. If the concentration of acetone is below the saturation concentration at 273 K then little or no acetone will be condensed.

Condenser Temperature Characteristics

The use of LN_2 as a refrigerant provides the cooling capacity to achieve temperatures near the freezing points of many organic compounds (Figure 3.3). At these temperatures, TVOC saturation concentrations are much lower than for the saturation concentrations at temperature ranges for refrigerants such as water, dry ice or ethylene glycol/water mixtures.

Another advantage for the use of LN_2 over other refrigerants is that the LN_2 undergoes a phase change from a liquid to a gas. The latent heat of vaporization and gaseous sensible heat are utilized for cooling the TVOC and carrier gas. Other refrigerants typically do not undergo a phase change and therefore only sensible heat is utilized for cooling capacity.

An initial test was conducted on the shell-and-tube condenser to determine the time to reach the set-point temperature and to determine the temperature frequency and amplitude of the temperature control system. UHP nitrogen was sent through the shell side at 0.995 slpm in lieu of the vapor laden gas stream. LN_2 was then delivered through the tube at a liquid mass flow rate of 5.9 g/min. The pressurized dewar was set at 20 pounds per square inch. The temperature control system was set at 185 K. The temperature of the inner tube wall was measured as a function of time (Figure 4.34).

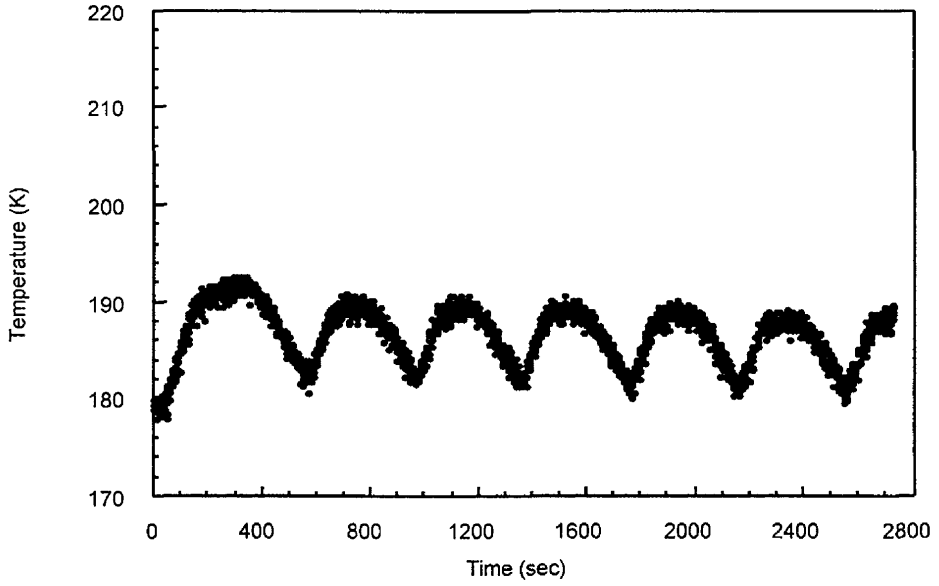

Figure 4.34 Temperature cycling of the condenser using the temperature control system at a set-point of 185 K.

The set-point temperature was reached after 5490 sec at which time the solenoid valve began cycling (Figure 4.35). The valve remained open for an average of 300 sec and closed for an average of 92 sec per cycle. The temperature was controlled within +6 K and -5 K of the set-point temperature.

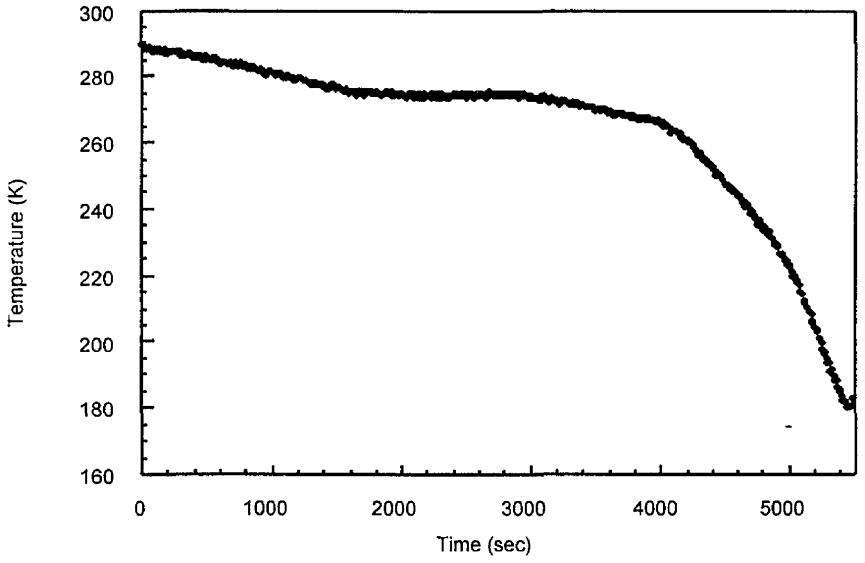

Figure 4.35 Condenser cool-down to set point cycling

Modeled and Experimental Refrigerant Requirements

Theoretical and experimental LN_2 refrigerant requirements were evaluated as a function of inlet acetone concentrations (Figure 4.36). The theoretical mass of LN_2 per unit mass of acetone condensed was determined from the thermodynamic model developed in section 4. Experimental LN_2 mass was determined from the outlet gas flow rate of N_2.

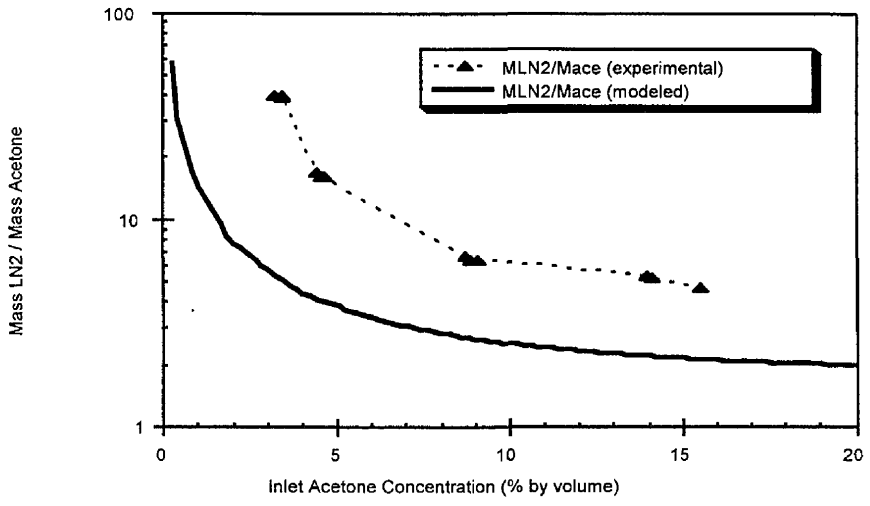

Figure 4.36 Modeled and experimental LN_2 requirements as a function of inlet acetone concentration

With the desired inlet acetone concentration flowing through the shell, the condenser was cooled to steady-state temperature cycling. The temperature and flow rate of the N_2 gas were measured at the condenser outlet and corrected to 298 K and 1 atm. An average flow rate was determined for one complete cycle in which the solenoid valve was opened and closed. The mass of LN_2 was calculated for each complete temperature cycle using the volume expansion ratio for LN_2 to gaseous N_2 (1:696) at standard conditions (298 K and 1 atm). The mass of acetone condensed was determined by measuring inlet and outlet acetone gas concentrations, flow rate and time for each temperature cycle. The mass of condensed acetone is thereby determined from:

$$\text{mass acetone condensed} \sim (C_{in} - C_{out}) \times Q_{in} \times t \tag{4.21}$$

where,

C_{in} = inlet acetone concentration
C_{out} = outlet acetone concentration
Q_{in} = flow rate of the inlet gas stream
t = one complete temperature cycle

Deviations of the experimental data from the modeled data are most likely due to heat entering the condenser from the outside. The model assumes adiabatic conditions in which heat is not transferred into or out of the system except from the liquid condensate washing out. The condenser system insulation does not completely eliminate all heat transfer.

Modeled and experimental results show that at low inlet concentrations more LN_2 is required to condense a unit mass of acetone (Figure 4.36). For instance, at an inlet concentration of 2.0% by volume acetone, 10 kg of LN_2 is theoretically required to condense 1 kg of acetone. However, at an inlet concentration of 20% by volume acetone, only 2 kg of LN_2 is required to condense 1 kg of acetone. Experimental results show the same general trend. This supports the earlier statement that higher concentration vapor streams result in more efficient use of LN_2. High outlet TVOC concentrations can generally be obtained from desorption of activated carbon after breakthrough of the TVOC has been achieved. The use of a carbon adsorber upstream of the condenser facilitates the more efficient use of LN_2.

Condenser Performance Evaluation

Condenser outlet acetone gas concentrations were measured for various different possible operating conditions to gain better insight into condenser performance. Modeled results are presented along with experimental results where applicable. Condenser temperature data are presented with the performance curves due to the dependence of the outlet concentration on temperature (Wagner equation).

Condenser outlet acetone gas concentration was measured for highly variable inlet acetone concentrations. Ambient temperature and pressure were 294 K and 743 mm Hg, respectively, with a 0.5 actual lpm challenge gas flow rate passing through the condenser shell. The condenser was cooled to steady-state temperature cycling prior to the introduction of the challenge gas stream (Figure 4.37). LN_2 was not passed through the outside cooling coil for this experiment to compare results with tests that utilize the coil. Inlet acetone gas concentrations were varied between 2% and 20% by volume acetone to determine the condenser outlet acetone concentrations (Figure 4.38).

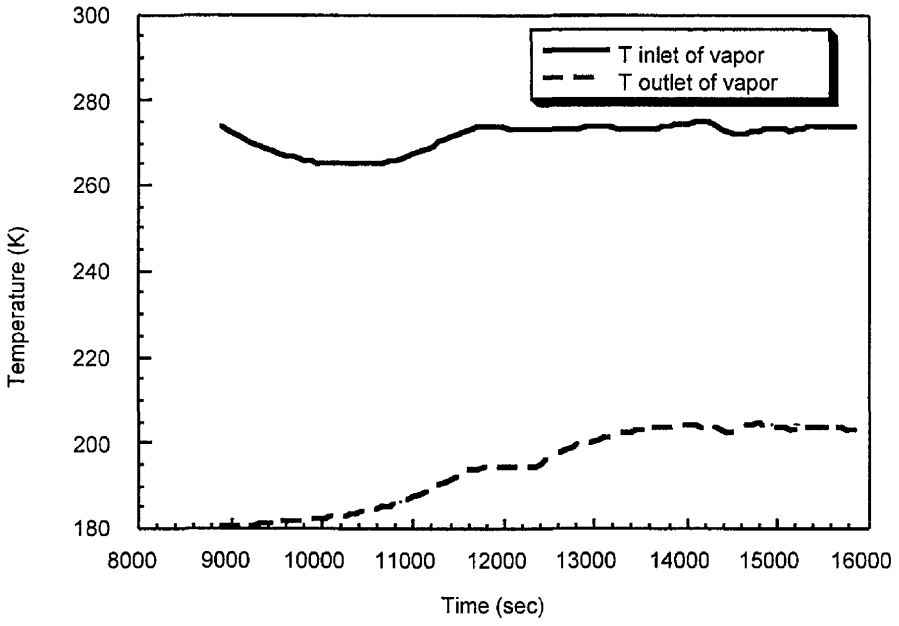

Figure 4.37 Condenser temperature profile for variable inlet acetone concentrations

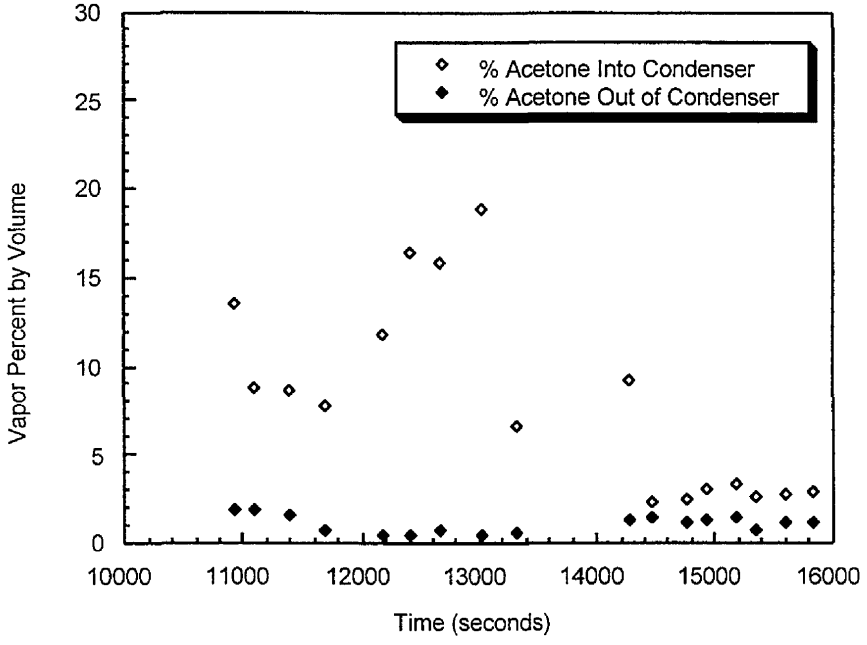

Figure 4.38 Condenser inlet and outlet concentrations for variable inlet acetone concentrations

The outlet acetone gas concentration remained fairly constant for abrupt changes in inlet concentration (Figure 4.38). The outlet acetone gas concentrations ranged between 0.4% and 1.9% by volume corresponding to concentrations between 0.1% and 2.0% predicted by the Wagner equation. The relatively high outlet acetone concentrations are due to the relatively high

condenser temperature at the vapor inlet. To create a more uniform condenser temperature profile, 3/8 inch diameter spherical brass packing was packed in the condenser tube. The packing provides mass that resists temperature change, and the brass material conducts heat from the relatively warmer vapor inlet to the cooler vapor outlet. A more uniform temperature profile was achieved as will be shown later with the packed heat exchanger. The limiting condenser temperature is the freezing temperature of the TVOC or H_2O if H_2O exists in the gas stream. Lower log-mean condenser temperatures can be achieved by bringing the inlet and outlet condenser temperatures closer together. In effect, the lower temperature is raised and the higher temperature is lowered. Because the lower temperature is raised, higher mass flow rates of LN_2 can be utilized to decrease the lower condenser temperature back near the freezing point of the VOC, while the higher temperature is decreased overall. The TVOC therefore has a higher residence time in a lower overall condenser temperature profile, thereby promoting further condensation of VOC.

Another test was conducted with conditions similar to that outlined in the previous test. Ambient temperature was 294 K and ambient pressure was 748 mm Hg. The challenge gas inlet flow rate was 0.5 actual lpm. Step inlet acetone gas concentrations ranging from 9.5% to 3.0% by volume were passed through the condenser shell. LN_2 was passed through the tube packed with the brass spheres. LN_2 was also passed through the outside shell coil. The objective of this experiment was to determine if the temperature profile and outlet acetone concentration could be reduced.

The condenser temperature at the inlet of the vapor was reduced by 15 ± 10 K utilizing the brass packing and the cooling coil (Figure 4.39). Correspondingly, the outlet acetone concentrations were reduced from a range between 2.0% and 0.1% by volume down to a range between 0.3% and 0.04% by volume (Figure 4.40). The average outlet acetone gas concentration is 0.19% by volume. The Wagner equation predicts an acetone concentration of 0.20% by volume for a log-mean condenser temperature of 221 K.

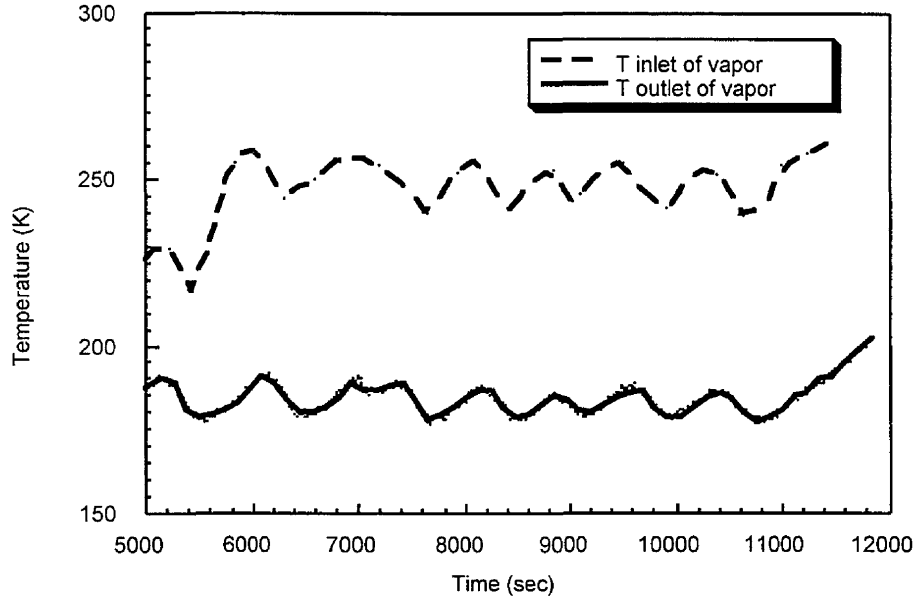

Figure 4.39 Condenser temperature profile for step acetone inlet concentrations

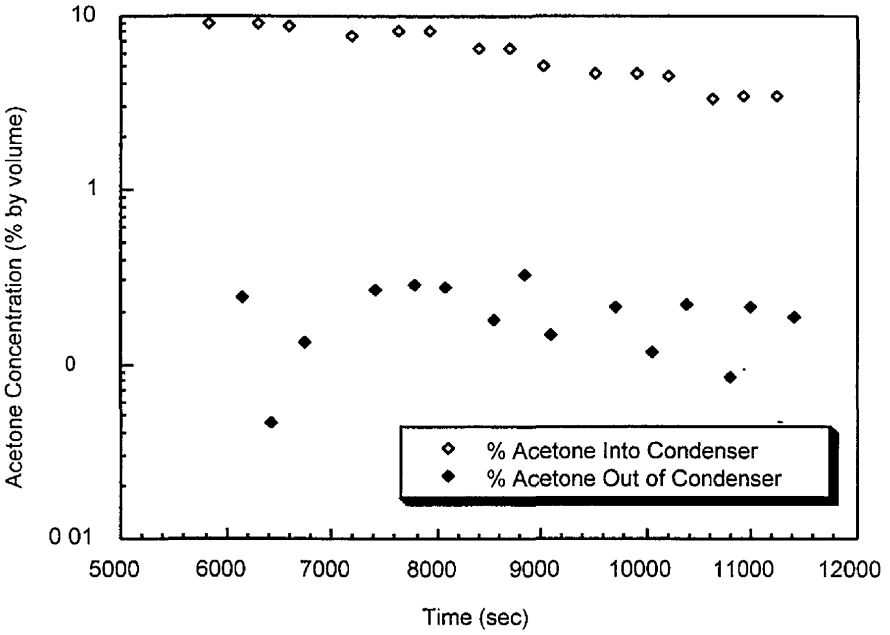

Figure 4.40 Condenser inlet and outlet acetone concentrations for step inlet concentrations

Condenser TVOC outlet concentrations were also measured for varying TVOC inlet concentrations between 0.25% and 18.3% by volume to determine TVOC removal efficiencies (Figure 4.41).

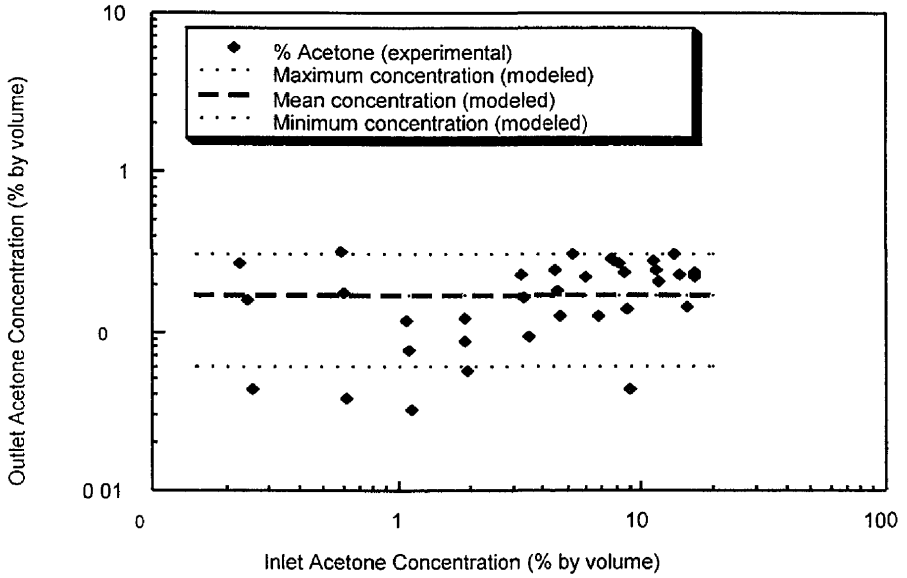

Figure 4.41 Outlet versus inlet acetone concentrations. Modeled maximum, mean and minimum concentrations are the saturation equilibrium concentrations at 225 K, 215 K and 206 K, respectively (experimental condenser temperature range).

The challenge gas flow rate was 0.5 actual lpm and at an ambient temperature of 294 K and ambient pressure of 745 mm Hg. The condenser was pre-cooled to an equilibrium log-mean temperature of 215 ± 10 K for each experiment. Over the entire range, outlet acetone concentrations remained fairly constant near the equilibrium vapor concentration of 0.17% at 215 K as predicted by the Wagner equation. Removal efficiencies are therefore higher for higher inlet concentrations. For instance, the removal efficiency found for an acetone inlet concentration of 18.3% was found to be 98.8%. However, the removal efficiency for an inlet acetone concentration of 0.6% was 70.5%.

The inlet and outlet acetone gas concentrations from the above experiment were used to determine removal efficiencies (Figure 4.42). Removal efficiency was also modeled using the thermodynamic model coupled with the Wagner equation. The experimental log-mean condenser temperatures and inlet acetone gas concentrations were input into the model to determine outlet concentrations and refrigerant mass requirements.

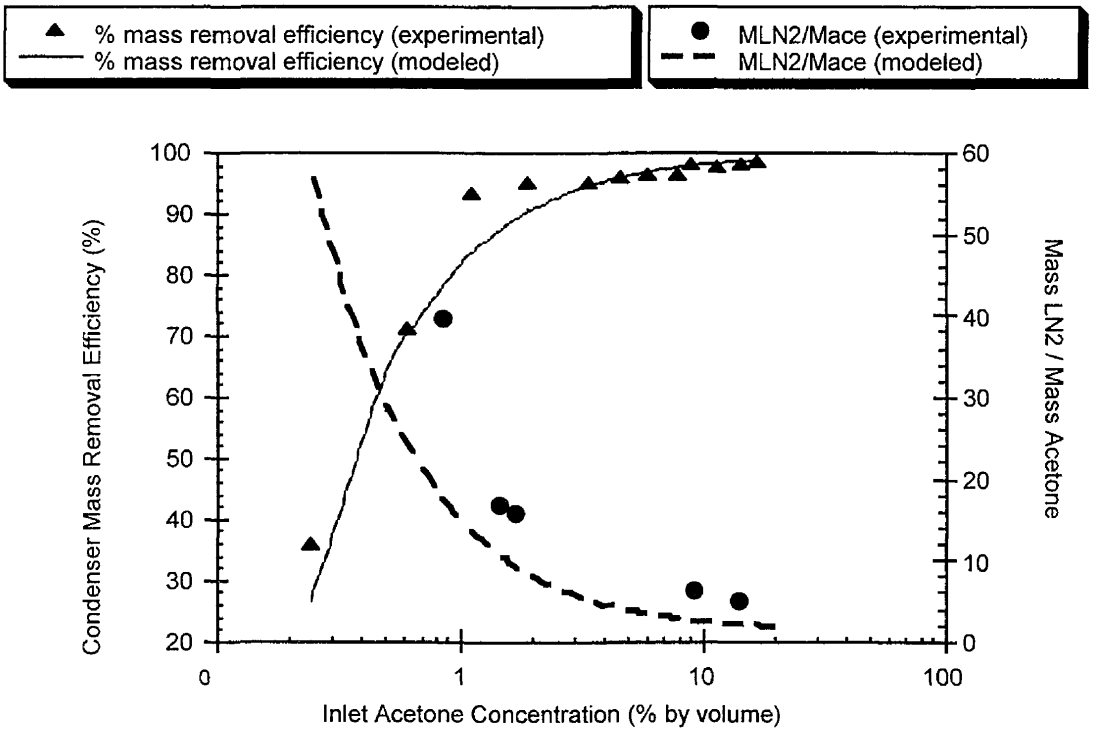

Figure 4.42 Modeled and experimental mass removal efficiencies and refrigerant requirements as a function of the condenser inlet acetone gas concentration

Removal efficiency increases as the inlet concentration of the acetone increases. Also, the mass of LN_2 required to condense a unit mass of acetone decreases as inlet acetone gas concentrations increase. Therefore, higher inlet acetone gas concentrations result in higher removal efficiencies and more efficient use of the LN_2 refrigerant. Industrial TVOC gas streams typically contain low TVOC concentrations at high flow rates (Ruddy and Carroll, 1993). At low TVOC concentrations, the condenser's removal efficiency decreases and requires elevated refrigerant requirements. However the use of a carbon adsorber prior to condensation can result in concentrated TVOC levels during desorption. Pre-concentrating the TVOC increases removal efficiency and decreases the amount of LN_2 required to condense a unit mass of VOC. As

discussed earlier, pre-concentrating the TVOC can also decrease the carrier gas flow sent to the condenser. The decreased flow reduces the condenser sizing requirements by increasing residence time. Overall, carbon adsorption/desorption prior to condensation results in: 1) increased removal efficiency, 2) efficient refrigerant use, and 3) reduction of condensation surface area by 1) increasing the TVOC concentration and 2) reducing the flow rate.

The effect of flow rate on condenser outlet acetone gas concentration was determined for flow rates between 0.5 actual lpm and 3.0 actual lpm. Ambient temperature and pressure were 295 K and 746 mm Hg, respectively. An inlet acetone concentration between 9.1% and 9.5% by volume was passed through the shell of the condenser. The average temperature at each flow rate was determined from thermocouple measurements for modeling purposes (Figure 4.43).

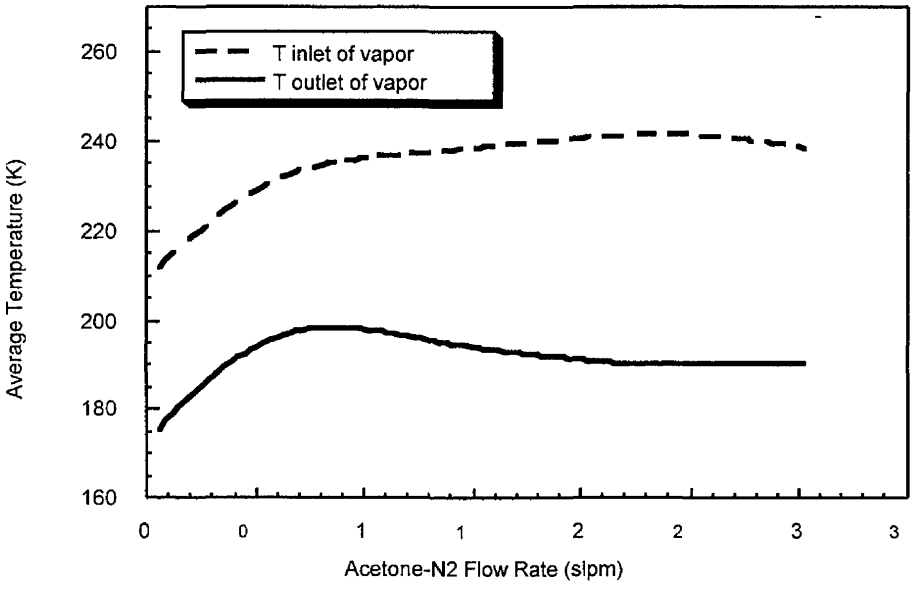

Figure 4.43 Average condenser temperature profile for each flow rate in which inlet and outlet acetone gas concentrations were sampled

The outlet gas concentration remained fairly constant over the flow rate range examined (Figure 4.44). The lower modeled and experimental acetone outlet concentrations for flow rates under 0.5 actual lpm are a result of lower log-mean condenser temperatures. The lower temperatures result in lower saturation concentrations (Wagner equation). The relatively constant outlet acetone concentrations show that the bench-scale cryogenic condenser can be operated at variable flow rates ($25 < Re < 1300$) without affecting condensation performance. In addition, the constant outlet concentrations indicate that sufficient condensation surface area exists for the vapor to be in equilibrium with its condensate liquid film.

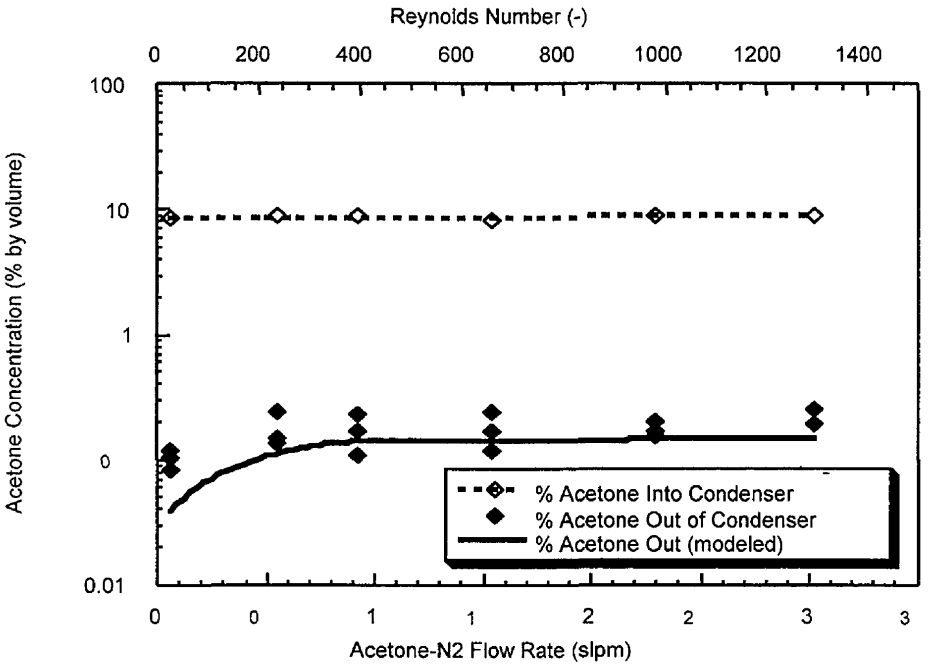

Figure 4.44 Condenser outlet acetone concentrations for various challenge gas flow rates

The condenser was also evaluated for acetone removal performance at various condenser equilibrium temperatures (Figure 4.45). Ambient temperature and pressure were 296 K and 750 mm Hg, respectively. A 10% by volume acetone challenge gas stream at 0.5 actual lpm was sent through the condenser at log-mean temperatures ranging from 209 K to 271 K. The measured

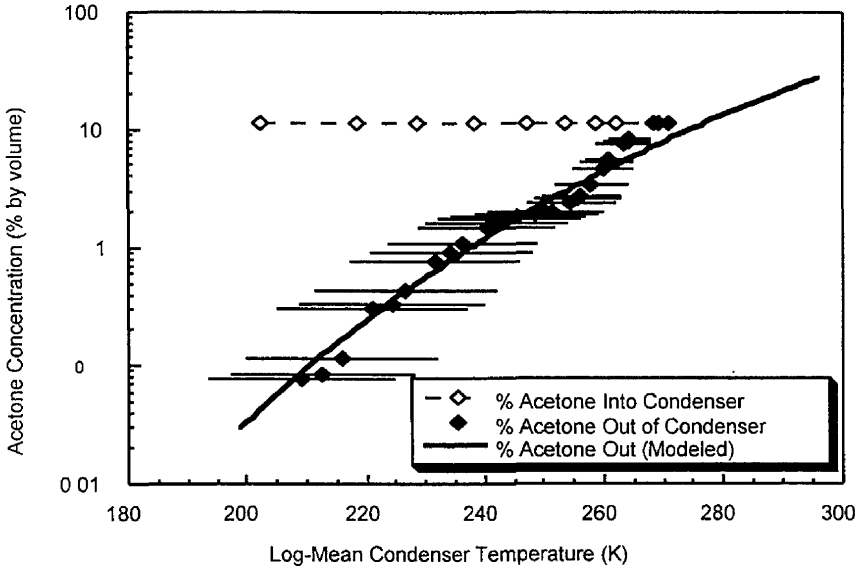

Figure 4.45 Inlet and outlet acetone concentrations for various log-mean condenser temperatures.Error bars are the condenser temperature ranges for each experimental data point

outlet concentrations closely approximated the theoretical equilibrium vapor concentration as predicted by the Wagner equation. This indicates that the acetone bulk vapor concentration reached equilibrium at the liquid-vapor surface on the condenser walls. The model provides a predictive method of determining the outlet concentration given temperature or vice versa.

Outlet concentrations of MEK were also examined for various condenser temperatures (Figure 4.46). Ambient temperature and pressure were 295 K and 746 mm Hg, respectively. A 0.5 actual lpm challenge gas stream was passed through the condenser shell after the desired equilibrium temperature was achieved. Generation of a constant MEK concentration challenge gas stream proved difficult using the dual-bubbler gas generation system. The inlet MEK concentration varied from 8.4% to 18.1% for the duration of the experiment.

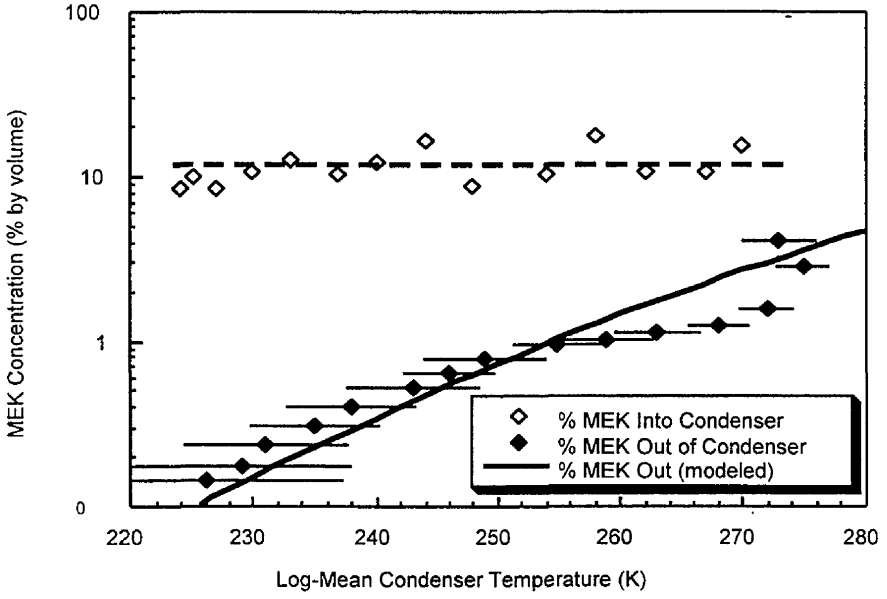

Figure 4.46 Inlet and outlet MEK concentrations for various log-mean condenser temperatures. Error bars are the condenser temperature ranges for each experimental data point

Outlet MEK gas concentrations closely approximated the theoretical modeled saturation curve. This provides evidence that adequate condenser surface area is present for MEK to reach equilibrium with its liquid condensate at each temperature. If sufficient condensation surface area exists for equilibrium between the vapor and liquid to be reached, the modeled saturation curve provides a predictive method to determine the outlet concentration based on a known condenser temperature. Conversely, for design purposes, a known outlet concentration can be used for determining the required condenser temperature.

Integrated Results

Condenser performance evaluation shows that condensation is enhanced at high inlet concentrations. Carbon adsorption/desorption provides a method to concentrate VOCs prior to condensation. This extends the range in which condensation can be used for TVOC recovery to low TVOC concentrations. The objective of integrating a bench-scale ACFC fixed bed with the cryogenic condenser is to determine if condenser performance is similar to the performance found using a generated challenge gas stream.

Prior to the introduction of the challenge gas desorption stream, the condenser was cooled to the steady-state temperature. Brass packing was not inserted into the condenser tube, and LN_2 was not passed through the outside shell cooling coil. The purpose of not enhancing a uniform temperature profile was to compare the condenser temperature profile with previous temperature profile results (Figure 4.37) and outlet acetone concentrations (Figure 4.38).

A 0.5 slpm gaseous N_2 stream was passed through the ACFC fixed bed during desorption and sent directly to the inlet of the condenser. A condenser temperature profile was observed similar to the previous test in which the cooling coil was not utilized (Figure 4.47). Condenser temperature difference between the inlet and outlet of the vapor averaged 79 K with a log-mean condenser temperature of 236 K. The relatively high condenser inlet temperature reduces the amount of acetone condensed.

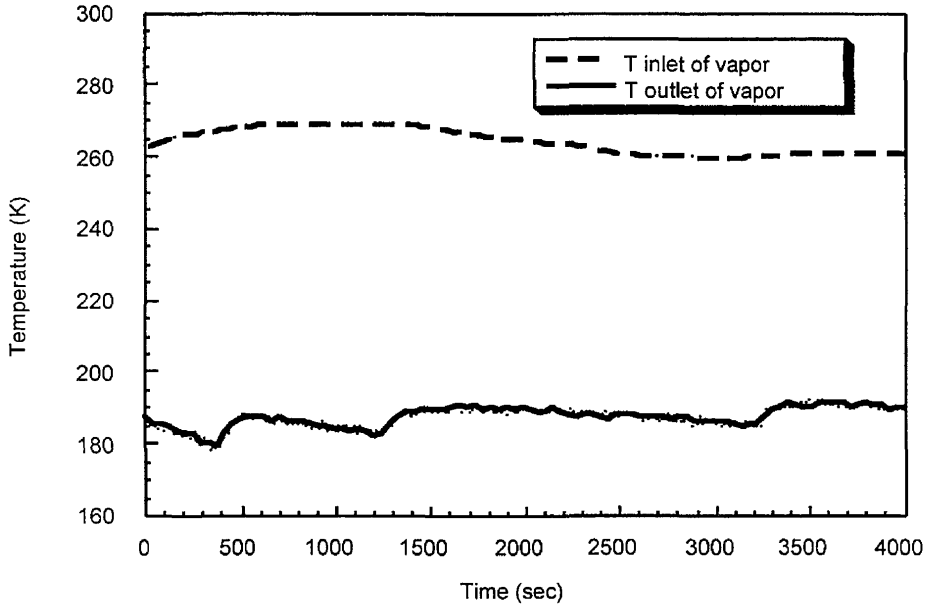

Figure 4.47 Condenser temperature profile for desorption challenge gas stream without tube packing or utilization of cooling coil

The condenser inlet acetone gas concentration reached a maximum 11.8% by volume (Figure 4.48). Outlet acetone vapor concentrations ranged from 0.5% and 3.9% by volume resulting in a TVOC mass removal efficiency of 73.6% in the condenser. This outlet concentration range is similar to the acetone concentration range between 0.4% and 1.9% by volume for the generated inlet challenge gas stream (Figure 4.38). The low removal efficiency

can be attributed to the large temperature difference between the inlet and outlet condenser temperatures.

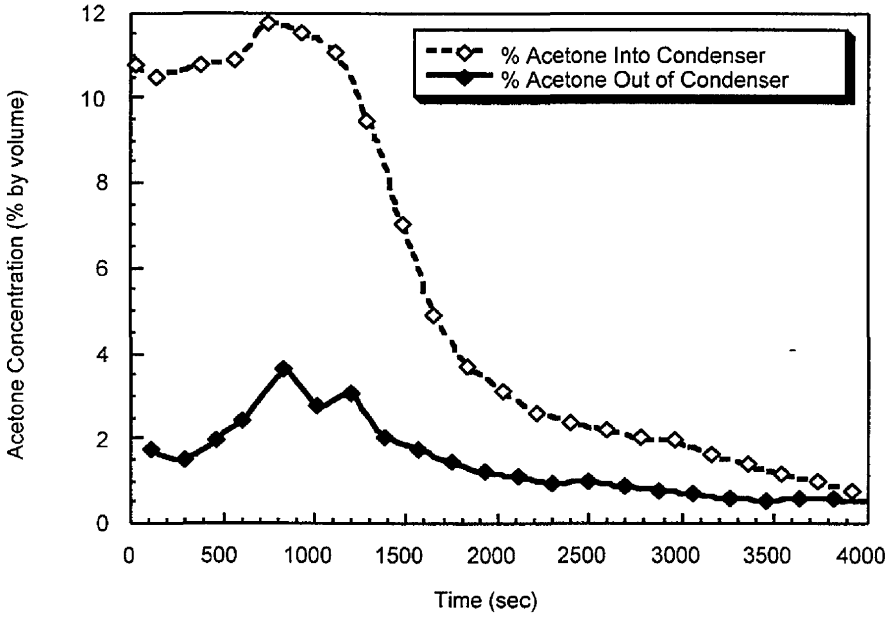

Figure 4.48 Condenser inlet and outlet acetone concentrations for a high inlet condenser temperature

Condenser outlet acetone vapor concentration was also evaluated with the brass packing in the condenser tube and LN_2 circulated through the cooling coil. The acetone was electrothermally desorbed from the ACFC fixed bed in a 0.5 slpm N_2 carrier gas. Ambient temperature and pressure were 295 K and 745 mm Hg, respectively.

The condenser temperature difference between the vapor inlet and outlet was reduced from the 79 K without the utilization of the bearings and coil to an average temperature difference of 65 K (Figure 4.49). The lower temperature difference resulted in the ability to lower the condenser to a log-mean temperature of 220 K or 16 K cooler than without the bearings and cooling coil.

The lower condenser temperature profile resulted in lower outlet acetone concentrations ranging from 1.6% to 0.05% by volume (Figure 4.50). The mass removal efficiency increased from 73.6% from the previous results to 95.0% using the brass packing and cooling coil.

To further optimize condenser performance, the LN_2 delivery line was extended in the tube to the midpoint of the condenser. This reduces by half the length that heat must be transfered to the coldest portion of the condenser. Conditions closer to an isothermal condenser temperature profile were achieved (Figure 4.51). The average temperature difference between the condenser midpoint and vapor inlet was further reduced to 40 K with a log-mean temperature of 206 K.

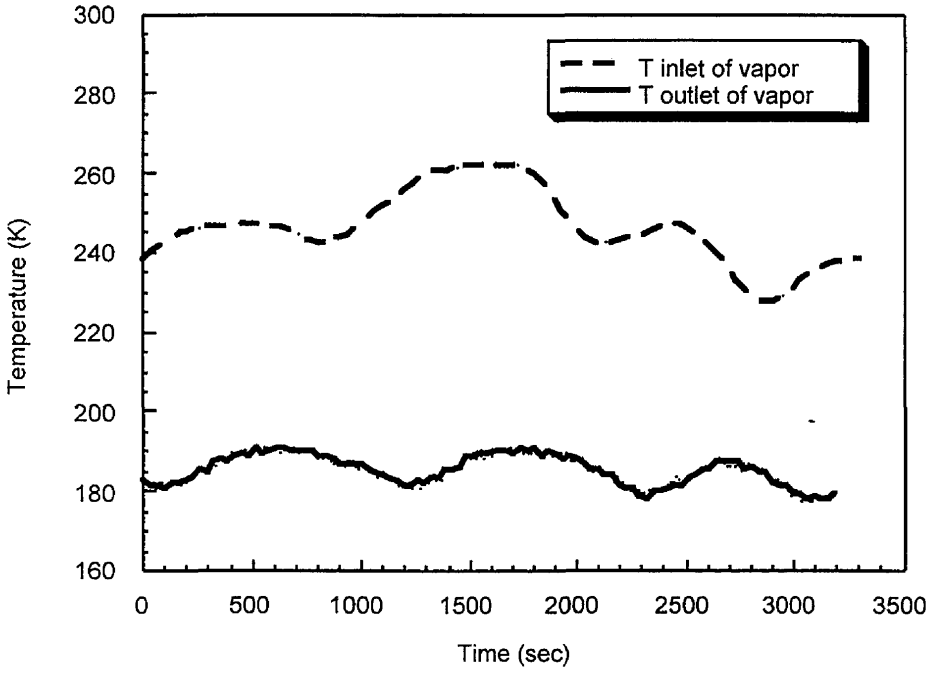

Figure 4.49 Condenser temperature profile using brass packing in the condenser tube and LN_2 passing through the outside shell cooling coil

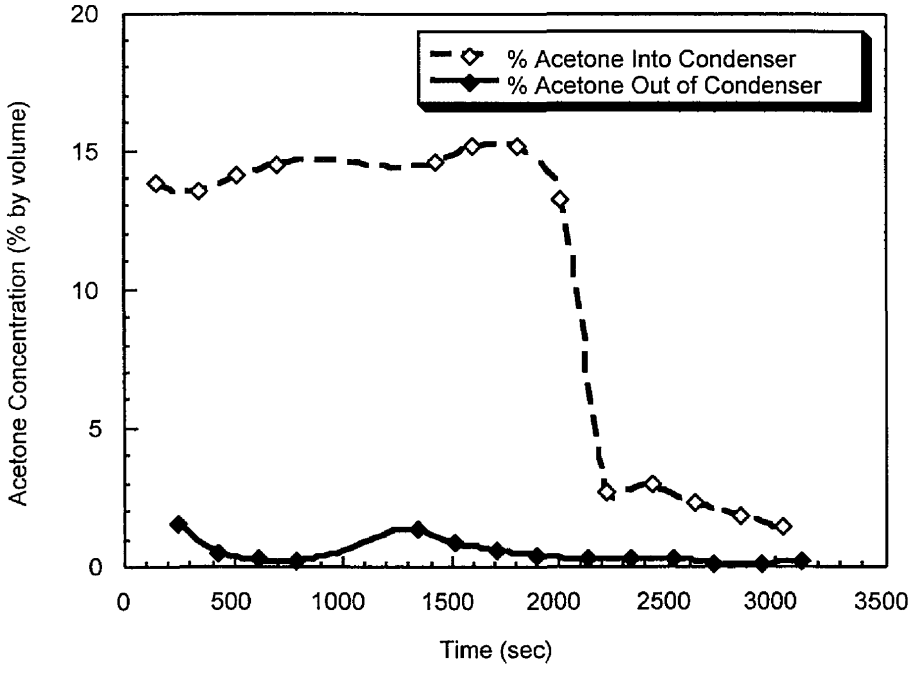

Figure 4.50 Desorption inlet acetone concentration and outlet acetone gas concentration using brass packing in the condenser tube and LN_2 passing through the outside shell cooling coil

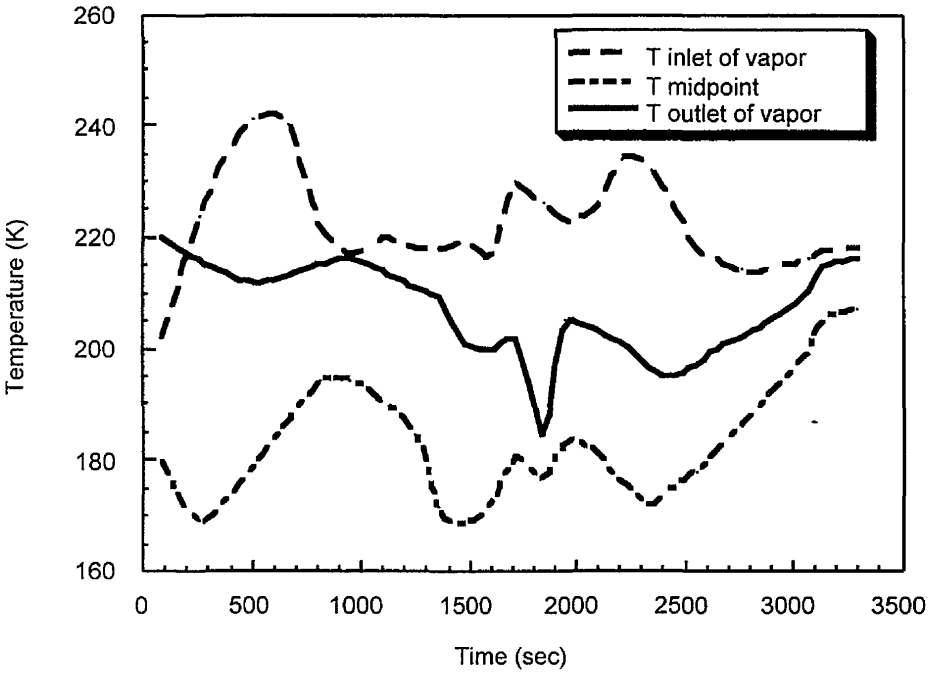

Figure 4.51 Optimized condenser temperature profile for LN_2 delivery in the tube at the condenser midpoint

The acetone vapor concentration at the condenser outlet remained low and fairly constant throughout the desorption cycle (Figure 4.52). At desorption times between 150 sec and 1000 sec the desorbed acetone concentration was greater than the equilibrium vapor saturation concentration. As the vapor cooled in the lines to the condenser, the acetone condensed to the equilibrium vapor concentration of 24% at an ambient temperature of 296 K. The condenser further cooled the vapor to concentrations between 0.028% to 0.21% by volume. Condenser mass removal efficiencies were found to be 98.2% for the condensation system and 99.8% for the combined carbon adsorption/cryogenic condensation system. During the adsorption/desorption cycle, the acetone in the 1% by volume and 5.0 slpm challenge stream was concentrated from 1% to approximately 60% by volume, and the carrier gas flow rate was decreased from 5.0 to 0.5 slpm.

Condenser outlet concentrations were also evaluated for a high flow desorption/condenser inlet challenge gas stream. After partial ACFC saturation, the ACFC was electrothermally desorbed in a 4.1 slpm gaseous N_2 purge stream. The desorbed gas stream was sent directly to the condenser cooled to the optimized temperature profile (Figure 4.53). Condenser outlet acetone concentrations were greater than the saturation concentrations predicted from the Wagner equation (Figure 4.54). This suggests that equilibrium between the acetone vapor and its condensate was not achieved at the condenser outlet due to the high flow rate (low residence time).

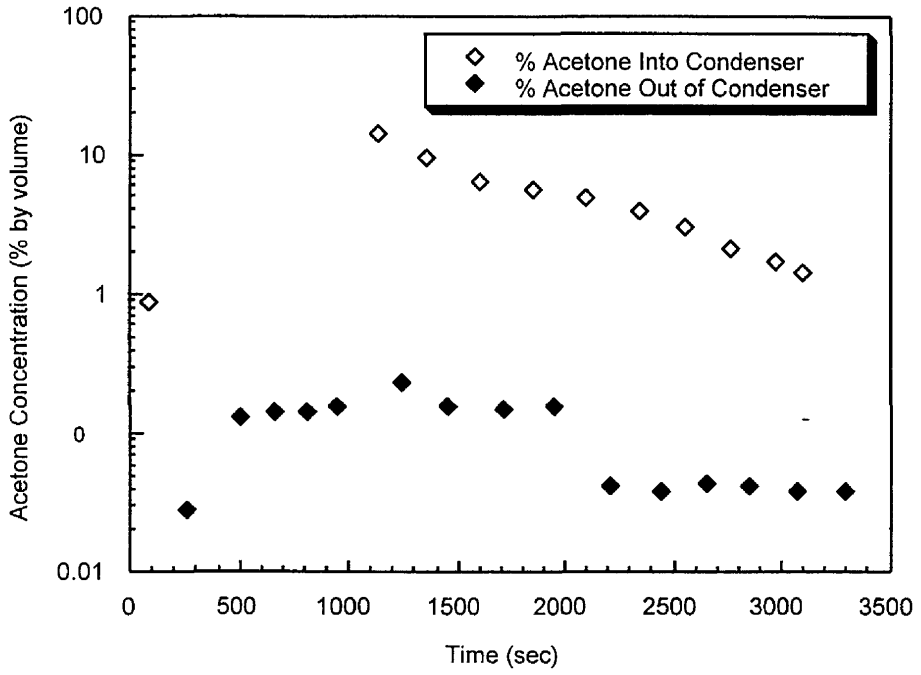

Figure 4.52 ACFC desorption / condenser inlet acetone concentrations and outlet acetone concentrations for an optimized temperature profile

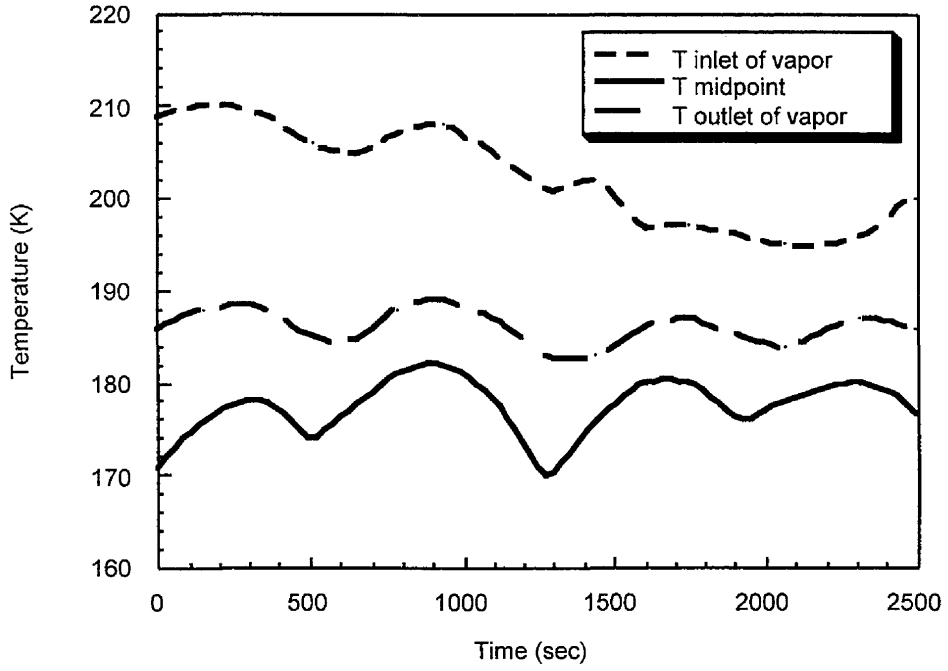

Figure 4.53 Condenser temperature profile for a high flow rate ACC desorption/condenser inlet flow rate

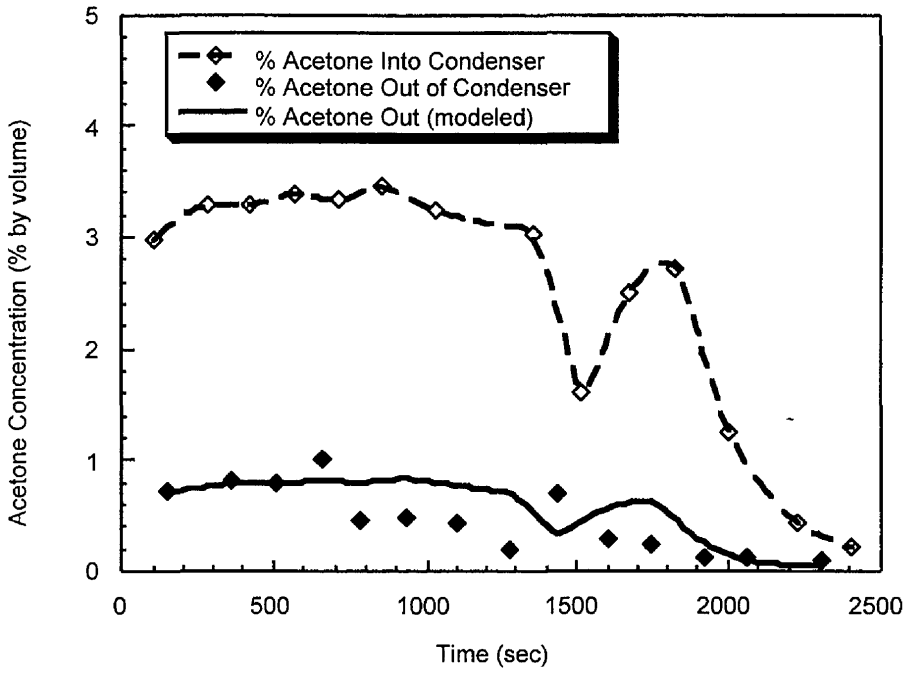

Figure 4.54 ACFC desorption/condenser inlet acetone concentrations and experimental and modeled outlet acetone concentrations

The mass transfer/thermodynamic model was utilized to evaluate this hypothesis. Results from the model show that the acetone does not theoretically achieve the equilibrium saturation concentration (as predicted by the Wagner equation) for the experimental flow rate and condenser length (Figure 4.55). To compare experimental outlet acetone concentrations with the model, the following data was input into the model:

1) gas stream temperature = log-mean experimental temperature profile (from Figure 4.53)
2) concentration = experimental inlet acetone concentrations (Figure 4.54)
3) flow rate = 4.1 slpm, model calculated actual conditions and the flow rate increase from acetone desorbed into the gas stream (concentration dependent)
4) ambient temperature and pressure = 295 K and 746 mm Hg, respectively

Modeled results approximate the experimental acetone outlet concentrations (Figure 4.54).

Condenser mass removal efficiency was also evaluated for MEK. A simulated 0.5 actual slpm desorption MEK in N_2 challenge gas stream was generated using the dual-bubbler system. The challenge stream was sent directly to the condenser operating at steady-state temperature cycling (Figure 4.56). Ambient temperature and pressure were 295 K and 750 mm Hg, respectively.

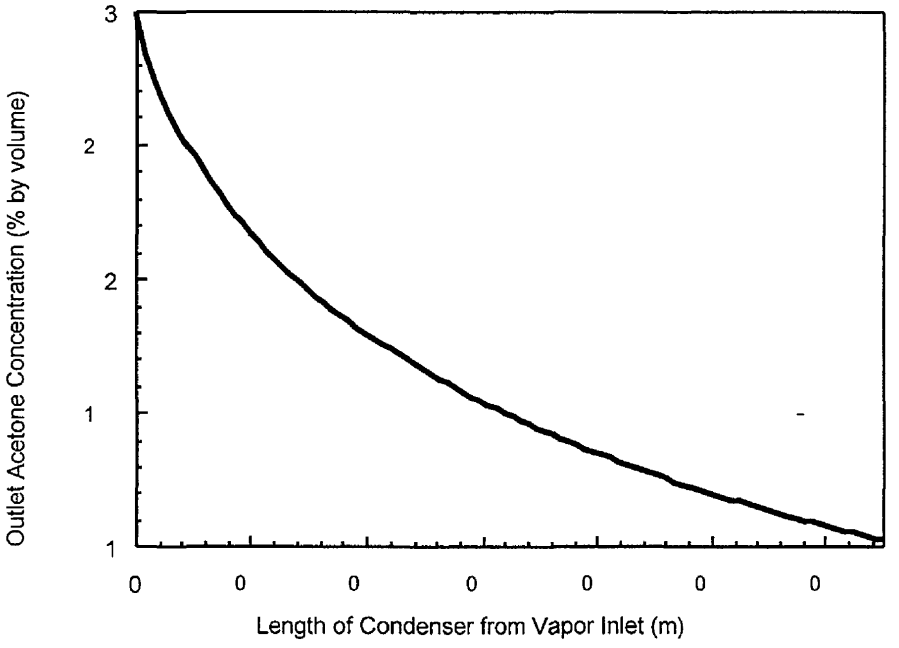

Figure 4.55 Outlet acetone concentration profile along the length of the bench-scale condenser predicted from the mass transfer/thermodynamic model

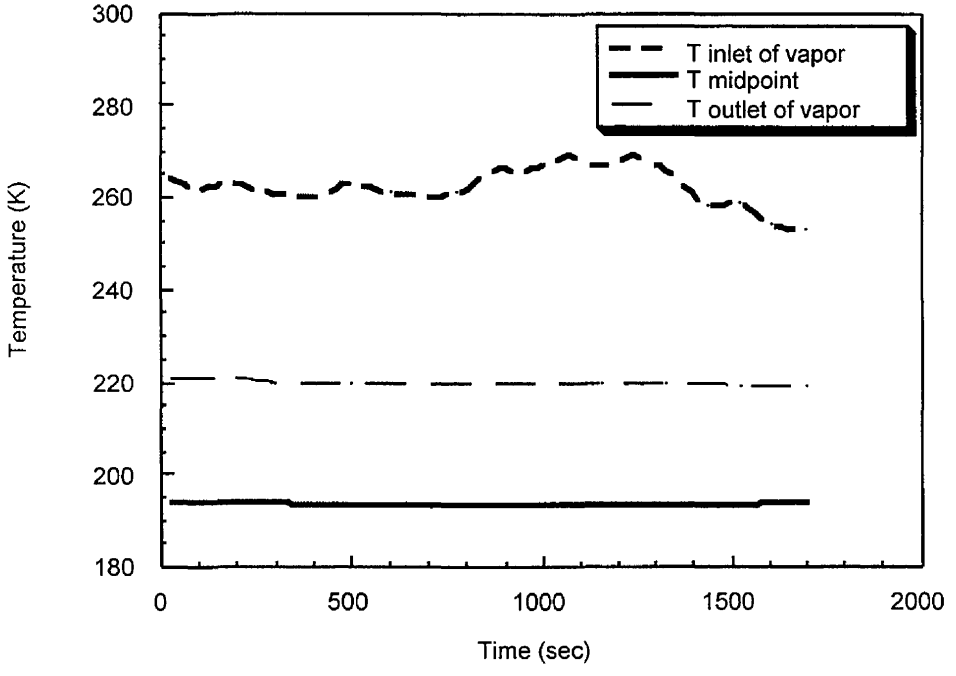

Figure 4.56 Condenser temperature profile for a low flow rate MEK challenge gas stream

Outlet MEK concentrations remained near 1% by volume for simulated desorption inlet concentrations ranging from 23.8% to 1.5% by volume (Figure 4.57). Saturation concentrations predicted from the Wagner equation range from 0.0019% to 2.7% by volume for the condenser temperature range. The condenser mass removal efficiency was found to be 93.3%.

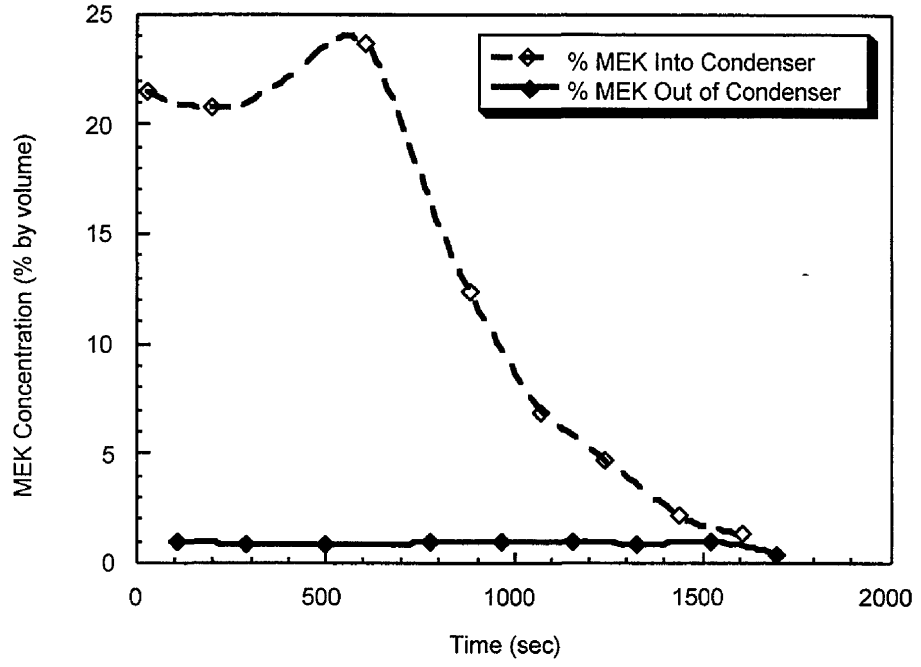

Figure 4.57 Condenser inlet and outlet MEK concentrations for a 0.5 actual lpm challenge gas stream

Acetone and MEK condensation were evaluated using the bench-scale cryogenic condensation system and the integrated ACFC adsorption/desorption/cryogenic condensation system. Condenser outlet vapor concentrations approximate the saturation concentrations at the log-mean condenser temperature as predicted by the Wagner equation. This results in higher removal efficiencies for higher inlet vapor concentrations. Condenser mass removal efficiency exceeds 98% for acetone and 93% for MEK. The removal efficiency of the integrated ACFC adsorption/cryogenic recovery system is 99+%. In addition, modeling and experimental results show that LN_2 is more efficiently utilized for higher concentrations of vapor, thus lower carrier gas concentrations.

Carbon adsorption/desorption prior to cryogenic condensation concentrates the vapor. This results in higher removal efficiencies and lowers the mass requirement of LN_2 per unit mass of TVOC condensed. Carbon adsorption/desorption also decreases the flow rate of gas entering the condenser. Lower flow rates result in the larger residence times, and thus less condensation surface area can be utilized to achieve saturation vapor concentrations.

The thermodynamic and mass transfer models provide a method to estimate outlet vapor concentrations given process gas stream conditions and gas/liquid properties of the process stream constituents. Modeling results approximate the experimental results for LN_2 requirements, outlet acetone concentration, mass transfer and condenser sizing.

The model results, compared with experimental data, show that carbon adsorption/desorption upstream of condensation decreases flow rate and increases the TVOC gas

concentration entering the condenser. The amount of gaseous TVOC condensation is based on the residence time of the gas stream in the condenser. By reducing the flow rate, smaller condensers can be used with the same residence time as larger condensers at higher flow rates. Increasing the gaseous TVOC concentration will be shown to increase mass removal efficiency and decrease the mass of LN_2 required to condense a unit mass of TVOC.

Purity of Recovered TVOC Condensate

Purity analysis of the liquid acetone condensate was conducted at the School of Chemical Sciences Mass Spectrometry Laboratory at the University of Illinois at Urbana-Champaign. Sample condensate (50 ml) was drawn from the bottom of the condenser after ACFC adsorption/desorption and cryogenic condensation. A second acetone sample for comparison purposes was taken from the dual bubbler used for challenge gas generation. The acetone used for analysis is Fisher Chemical Acetone Optima lot A929-4 UN1090 recommended for spectrophotometry and GC use. Total residue after evaporation is reported at 1 ppmv and GC assay resulted in a 99.6% minimum acetone content.

Liquid condensate acetone samples were analyzed using a VG Analytical 70 VSE mass spectrometer manufactured by Fisons Instruments. Analysis for acetone was first conducted to determine the abundance of acetone in a 2.5 μl sample. Analysis of the blank sample drawn from the dual bubblers and the sample drawn after adsorption/desorption/condensation were conducted without detection of the acetone peak to increase the detection limit. The abundance found for the acetone detection was 4.5×10^8 counts.

The blank sample taken from the dual bubbler showed slight traces of high molecular weight compounds at a mass to charge ratios of 71, 85, 111, 131, 145 and 159 (Figure 4.8). The total trace impurities account for 0.39% of the total liquid sample (Table 4.8).

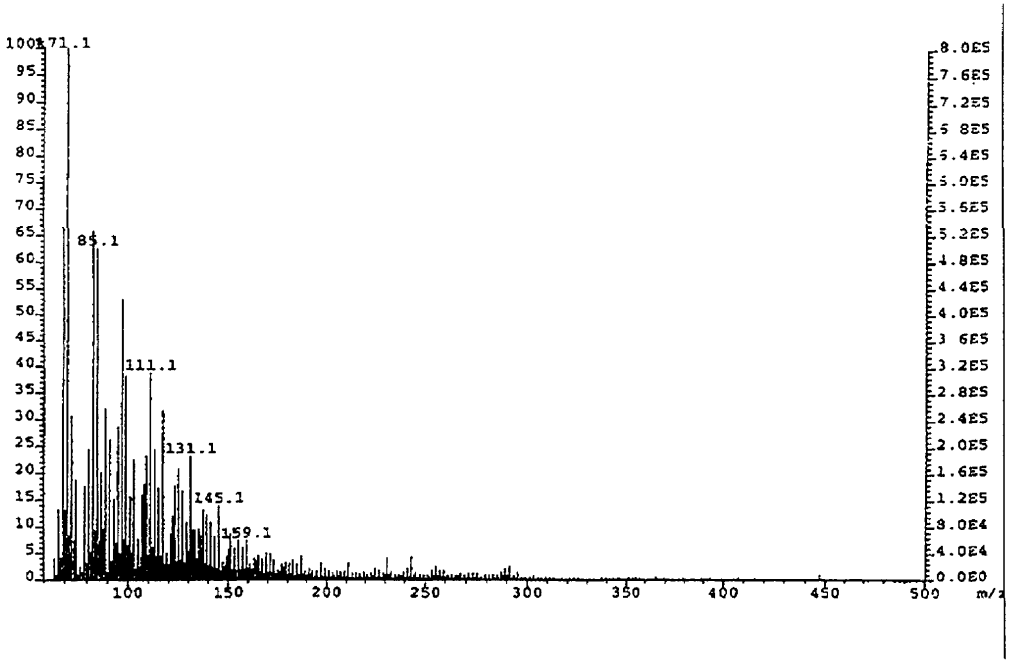

Figure 4.58 Condenser inlet and outlet acetone concentrations for a high inlet condenser temperature

Table 4.8 Percent impurities analyzed relative to acetone abundance for acetone blank sample

Mass/Charge Ratio	Abundance	% Relative to Acetone
71	8.0×10^5	0.17
85	5.5×10^5	0.12
111	3.2×10^5	0.07
131	1.7×10^5	0.03
145	8.1×10^4	trace
159	4.2×10^4	trace
	TOTAL	0.39

The processed sampled taken from the condenser also showed traces of high molecular weight compounds at a mass to charge ratios of 71, 97, 113, 149, 167, 195, 261, 279 and 391 (Figure 4.59). The total trace impurities account for 1.73% of the total liquid sample (Table 4.9).

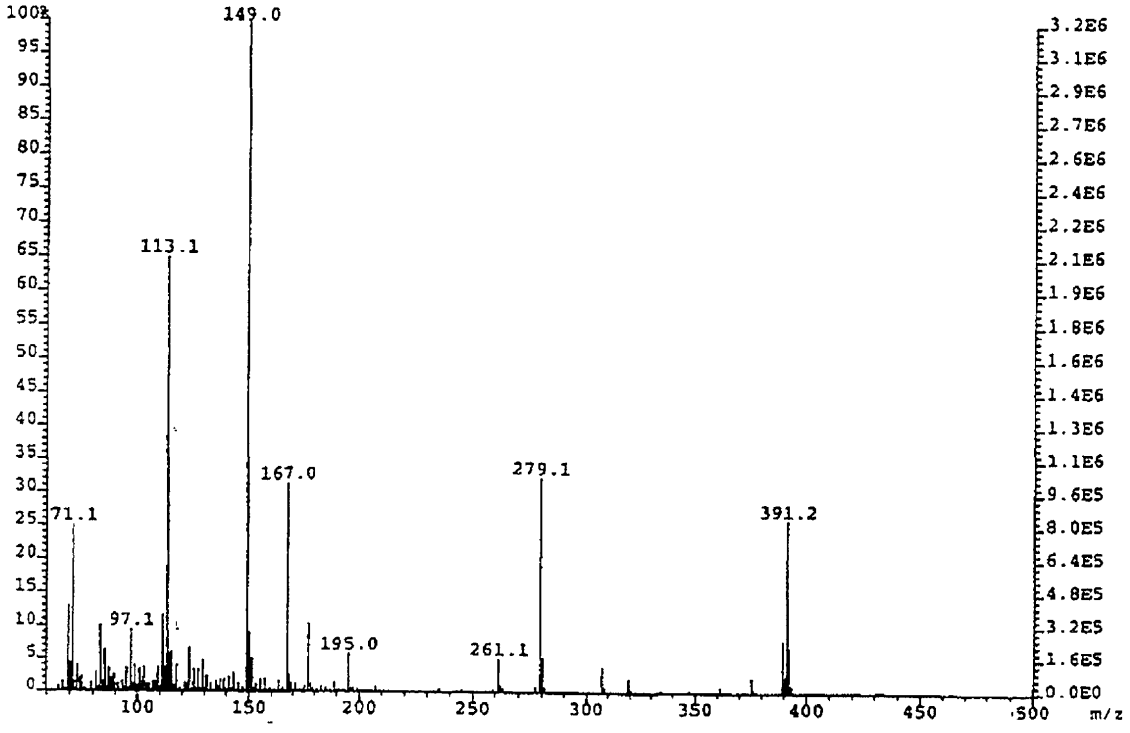

Figure 4.59 Impuritites in processed acetone sample found from mass spectroeter analysis

Table 4.9 Percent impurities analyzed relative to acetone abundance for adsorption/desorption/condensation acetone sample.

Mass/Charge Ratio	Abundance	% Relative to Acetone
71	8.0×10^5	0.17
97	2.7×10^5	0.06
113	2.1×10^6	0.53
149	3.2×10^6	0.71
167	1.0×10^5	0.02
195	1.6×10^5	0.022
261	1.6×10^5	0.022
279	1.0×10^6	0.02
391	8.1×10^5	0.18
	TOTAL	1.73

5. LARGE-SCALE APPLICATIONS OF THE ACFC SYSTEM & COST ANALYSIS

Separation and recovery of volatile organic chemicals and solvents from the Synthetic Organic Chemical Manufacturing Industries (SOCMI), industrial painting processes, and water and wastewater treatment plants are potential areas of targeting application of the ACFC sorption system. This system can be considered for any industrial process exhausting sizable quantities of valuable toxic vapors that can be efficiently recovered by carbon adsorption. Utilization of this system with electrothermal regeneration makes the ACFC system a good substitute for conventional carbon adsorption systems when the waste hot gas or steam are not economically or technically a feasible option for the regeneration. In general, electrothermal regeneration shortens the desorption time and increases the regenerated concentration appreciably; thereby contributing to cost reduction of the condensation unit. Electrothermal regeneration is preferrable compared to steam because steam may contribute to polymerization reactions on the surface of adsorbant. This type of reaction is usually caused by the breakdown of some reactive organic compounds on the surface of carbon in the presence of transitional metals as catalysts (McInnes, 1995). In general, carbon adsorption is not recommended for VOC streams containing ketones. Continued exposure to ketones can produce exothermic reactions that can cause fires in conventional carbon adsorption systems. This reaction can take place in conventional carbon adsorption systems because transitional metals are available in commercial activated carbon adsorbents. Since the ACFC does not contain transitional metals (Table 3.8), the ACFC sorption system is expected to result in safe recovery of ketones. Feasibility of adsorption, desorption and condensation of acetone and MEK via ACFC were extensively demonstrated in the previous chapters. In the following section, design conditions and cost analysis of an ACFC sorption system are provided for recovery of acetone.

Preliminary Design and Economic Analysis of the ACFC Electrothermal Sorption System

The Net Present Value (NPV) and break-even price analysis of the ACFC electrothermal sorption system was done by Dr. Subhash Bhagwat at the Illinois State Geological Survey. The analysis is based on the flow diagram in Figure 3.1. It includes the adsorption-desorption and condensation stages. A separate analysis of the condensation stage is presented in Section 5..

Table 5.1 summarizes design conditions of the ACFC system. These values were used as input parameters in the economic analysis. The Producer Price Index (PPI) for Capital Equipment published by the U.S. Department of Commerce was used to update the investment data to 1996 status. The scenarios I and II differ from one another primarily due to the price of ACFC mass quoted by two different sources. The base case for the estimation of operating costs assumes that in an industrial setting the plant operations will be automated enough to permit this unit to function - operate and maintain - with 1 hour of labor per shift, 3 shifts per day, 365 days per year. This assumption is subject to a greater degree of uncertainty than the assumptions regarding the prices of electricity and LN_2 consumed in the process. The energy consumption for desorption was calculated to be 144 MJ/hr. The price of electricity for industrial use currently averages about 6 cents/kwh. Liquid nitrogen price of 1991 was updated to 1996 by using the Consumer Price Index (CPI). The operating costs are assumed to increase at a 3% annual rate but revenues from the sale of recovered acetone are assumed to be constant over the ten year period. This is realistic because market competition and alternative sources of chemicals often do not permit price increases.

Table 5.2 presents the NPV analysis for scenario II as the base case. Scenario II is based on the higher of the two price quotes for the ACFC mass and the adsorption cycle time of 2.6 hours. The mass of ACFC required in this case was calculated to be 112.5 kg per reactor vessel or 225 kg total. A reduction in adsorption time to 1 hour would reduce the reactor price from $1,750 to $1,000 per vessel and the mass of ACFC needed from 112.5 kg to 88 kg per vessel.

The NPV analysis determines the price of recovered acetone at which the process pays for itself. We have assumed that all the capital needed has been borrowed at 20 % annual interest rate. The annual cash flows were discounted also at the same rate of 20 %. The rate of 20 % is essential to attract funds to a new technology such as this. The risks assumed by the potential investor must be justified by a higher return on investment than the investment alternatives available to the investor.

The break-even economic analysis indicates that the recovered acetone must be saleable for at least $1.08 per kg. The current market value of acetone is $15.95 per gallon or about $5.40 per kg, assuming a specific gravity of 0.78. The process of adsorption, desorption and condensation thus promises to be highly economical.

Sensitivity Analysis

The economic outcome is highly sensitive to changes in components of the operating costs. For example, if the labor requirements increase from 1 person-hour per shift to 2 person-hours, the break-even price of recovered acetone increases by 26 cents to $1.34/kg. Similarly, an increase in electricity price from 6 cents to 10 cents per kwh raises the break-even price by 13 cents to $1.21/kg. The effect is cumulative if both costs go up at the same time.

The process economics are also highly sensitive to the price of the ACFC mass. The break-even price of acetone declines from $1.08/kg to $0.91/kg if the price of the ACFC mass declines from $120 to $20 per kg. A reduction in adsorption cycle time from 2.6 hour to 1 hour makes the process less sensitive to the price of ACFC mass. At 1 hour adsorption cycle time and an ACFC price of $20/kg, the break-even price of recovered acetone is $0.89/kg. It rises to $0.93/kg if the price of ACFC mass rises to $120/kg. This price is 15 cents/kg lower than the base case with an adsorption cycle time of 2.6 hours. Finally, the lowering of the interest and discount rates from 20 to 15% results in a 10% decline in break-even acetone price from $1.08 to $0.97 per kg.

In conclusion, the NPV analysis of the entire system including adsorption, desorption and condensation indicates excellent prospects for an economically profitable process of recovering acetone. The sensitivity analysis shows the effect of component cost changes on the total break-even price of recovered acetone. The components of the annual operating cost are more important than the initial investment level in influencing the total cost. Efforts to reduce the labor requirements for operation and maintenance and the energy required for desorption would pay highly. The cost of ACFC, although treated here as investment, is a variable of considerable significance. Reducing the adsorption cycle time will not only reduce total cost but also make the total cost less sensitive to changes in ACFC price. Overall, the preliminary economic analysis offers several opportunities for future process development and optimization. A detailed economic analysis with refined data and a comprehensive sensitivity analysis is recommended. Caution should be exercised in transposing the results to other TVOCs because each substance will have a different response to the process.

Table 5.1 Mass transfer/thermodynamic model results for scale-up condenser design

Adsorption system	Electrothermal Swing Adsorption
Number of adsorbers	2
Type of toxic volatile organic chemical	Acetone in dry air
Molecular weight of the toxic gas	58
Density of liquid TVOC (g/cc)	0.786
Flow rate, Q (m^3/min)	10
Inlet adsorber temperature (K)	298
Bed operating Pressure (Pa)	101325
Inlet adsorber concentration (ppmv)	10000
Inlet adsorber concentration (g/m^3)	23.72
Superficial gas velocity (cm/s)	20
Packing density (mg/cm^3)	300
Desired cross sectional area of fixed bed (cm^2)	8333
Form of the bed cross section	square
Adsorber internal configuration	square metal frames pressing ACFC
Desired width or radius of the fixed bed (cm)	91.3
Selected width or radius of the fixed bed (cm)	90
Cross section of the fixed bed (cm^2)	8100
Fixed bed throughput ratio (%)	70
Breakthrough time (hr)	2.5
Stoichiometric time (hr)	3.6
Mass of adsorption till breakthrough (Kg)	35.58
Mass rate of TVOC recovered (Kg/hr)	14.232
Required bed adsorption equilibrium capacity (Kg)	50.829
ACC-5092-20 adsorption equilibrium capacity (g/g)	0.452
Mass of ACC-5092-20 required per each bed (Kg)	112
Total mass of ACC-5092-20 required, Creq (Kg)	225
Volume of each fixed bed required (cm^3)	374845
Length of the fixed bed required (cm)	46.3
Selected bed length (cm)	42
Approximate adsorber vessel surface area (cm^2)	22680
Estimated vessel cost (C_v), Fall 1989 $	3254.86
Electrical energy requirement per unit mass of acetone recovered (KJ/g)	10.1
Nitrogen flow rate during regeneration, m^3/min	1
Energy requirement per hour (MJ/hr)	144

Table 5.2 Activated Carbon Fiber Cloth (ACFC) Fixed Bed Adsorber and cryogenic condenser for Toxic Volatile Organic Compounds (TVOC)

	Scenario I	**Scenario II**
Price of two ACFC vessels	3500	3500
Mass of ACFC in two vessels(Kg)	225	225
Price of ACFC ($ per Kg.)	20	120
Cost of ACFC ($)	4500	27000
Cost of condensor ($)	8000	8000
Cost of auxiliary equipment ($)	20000	20000
Total investm.Adsorber+Condenser		
Instrumentation, controls, sales	36,000	58,500
taxes, freight etc. (58% of Inv.)	20880	33930
Installation (31% of Inv.)	11160	18135
Total investment (1988 dollars)	68040	110565
PPI 1988-96 Capital Equipment	1.254	1.254
Total investment (1996 dollars)	**85,322**	**138,649**
Operating Costs		
Labor (hrs/shift)	1	
Shifts/day	3	
Workdays/yr	365	
Labor wage ($/hr)	13	
Wages/Yr ($)	14235	
Overheads for		
admn.,ins.,prop.tax		
100% of wages	14235	
Maintenance materials		
5% of total invest.	4266	6932
Electricity		
for desorption ($)	21100	
for condenser ($)	200	
Refrigerant		
LN2 (1991 dollars)	18016	
CPI 1991-96	1.15	
LN2 (1996 dollars)	20718	
Total operating cost ($/yr)	**74,755**	**77,421**

Table 5.3 Break-even analysis for Scenario II

	YEAR	1	2	3	4	5	6	7	8	9	10	11
Acetone price($/kg)	1 08											
Recovery (kg/yr)	126144											
Revenue($/yr)	136,236								-		-	
Investment($)	138,649											
Depreciation(linear,10yr)		0	13,865	13,865	13,865	13,865	13,865	13,865	13,865	13,865	13,865	13,865
Undepreciated value($)		138,649	124,784	110,919	97,054	83,189	69,324	55,459	41,595	27,730	13,865	0
Operating expenses($)		0	77,421	79,743	82,136	84,600	87,138	89,752	92,445	95,218	98,074	101,017
Interest on undepreciated value(20%)		27,730	24,957	22,184	19,411	16,638	13,865	11,092	8,319	5,546	2,773	0
Interest on half the operating expenses(20%)		0	7,742	7,974	8,214	8,460	8,714	8,975	9,244	9,522	9,807	10,102
Operating profits(loss)		0	58,815	56,492	54,100	51,636	49,098	46,484	43,791	41,018	38,161	35,219
minus interest paid		(27,730)	26,116	26,334	26,475	26,538	26,519	26,416	26,228	25,950	25,581	25,117
minus depreciation		(27,730)	12,251	12,469	12,611	12,673	12,654	12,552	12,363	12,085	11,716	11,252
Losscarried forward($)		0	(33,276)	(25,230)	(15,313)	(3,242)	0	0	0	0	0	0
Profit(loss)before tax($)		(27,730)	(21,025)	(12,760)	(2,702)	9,431	12,654	12,552	12,363	12,085	11,716	11,252
Interest on year-end debt(20%)		(5,546)	(4,205)	(2,552)	(540)	0	0	0	0	0	0	0
Taxable income($)		0	0	0	0	9,431	12,654	12,552	12,363	12,085	11,716	11,252
Taxes(40%)		0	0	0	0	4,150	5,568	5,523	5,440	5,317	5,155	4,951
Income after taxes($)		(33,276)	(25,230)	(15,313)	(3,242)	5,281	7,086	7,029	6,923	6,768	6,561	6,301
Cash flow(add depreciation)		(33,276)	(11,365)	(1,448)	10,622	19,146	20,951	20,894	20,788	20,633	20,426	20,166
Net Present Value at 20% discount rate($)		4,862										

Preliminary Design and Economic Analysis of the Condensation System

Large-scale condenser design can be carried out by first determining the process gas stream characteristics such as TVOC vapor concentration, temperature and gas flow rate. By assuming equilibrium conditions, the desired condenser temperature can be determined from the vapor concentration dependence on temperature at the desired outlet concentration (Wagner equation eq. 3.2). Once the temperature is known, an appropriate refrigerant can be selected (e.g. Table 3.5). Then by modeling the axial concentration profile, the appropriate surface area and condenser length can be determined from the condensing surface required to reach the desired outlet vapor concentration (mass transfer model, Appendix D).

Shell-and-tube condensers range in size from under 1 m^2 to as large as 30,000 m^2 in surface area (Kern, 1950). Kern (1950) provides standard design criteria for the construction of shell-and tube condensers. A common type of condenser is the fixed tube sheet, in which a bundle of inside tubes are encased in an outside shell (Figure 5.1). This type of shell-and-tube condenser will be used for the following analysis, in conjunction with the general design methodology outlined above.

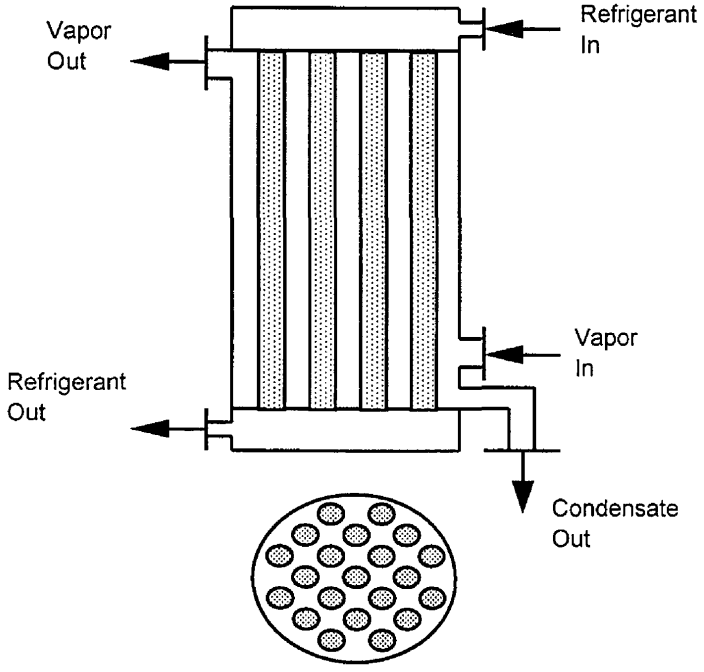

Figure 5.1 Large-scale schematic of a tubesheet shell-and-tube ndirect-contact condenser

The process conditions are the same as given in Table 5.1. Desorption is assumed to decrease the flow rate by an order of magnitude and increase the acetone concentration to the saturation vapor concentration at 294 K (as was shown with the bench-scale system in Section 4). Therefore the condenser inlet stream has the following characteristics:

Inlet vapor concentration to adsorber	=	26% by volume acetone (from Wagner equation)
Carrier gas	=	N_2 gas (approximates air)
Inlet flow rate to adsorber	=	1 m^3/min

Temperature = 294 K
Pressure = 1 atm

To achieve a 99% mass removal efficiency, the outlet acetone concentration must equal 0.24% by volume. The saturation vapor concentration vs. temperature graph shows that the condenser must be cooled to 220 K (Figure 3.3). The refrigerant selected to achieve this condenser temperature is LN_2 (Table 3.5).

Gas stream characteristics are input in the mass transfer/thermodynamic model to determine condensation surface area, mass of LN_2 required and mass of acetone condensed. The results of the model show that a conservative surface area of 20 m^2 is needed to achieve the desired outlet acetone concentration (Figure 5.2). A safety factor of 1.2 is applied to assure that sufficient surface area is available and to account for heat transfer reduction due to condenser fouling (e.g., water vapor). The design surface area required is 24 m^2. Mass flow rate of LN_2 is predicted to be 980 kg/day to condense 890 kg/day of acetone (Table 5.4). Kern (1950) can be used to optimize the geometric configuration to achieve the required 24 m^2 of condensation surface area depending on site specific considerations.

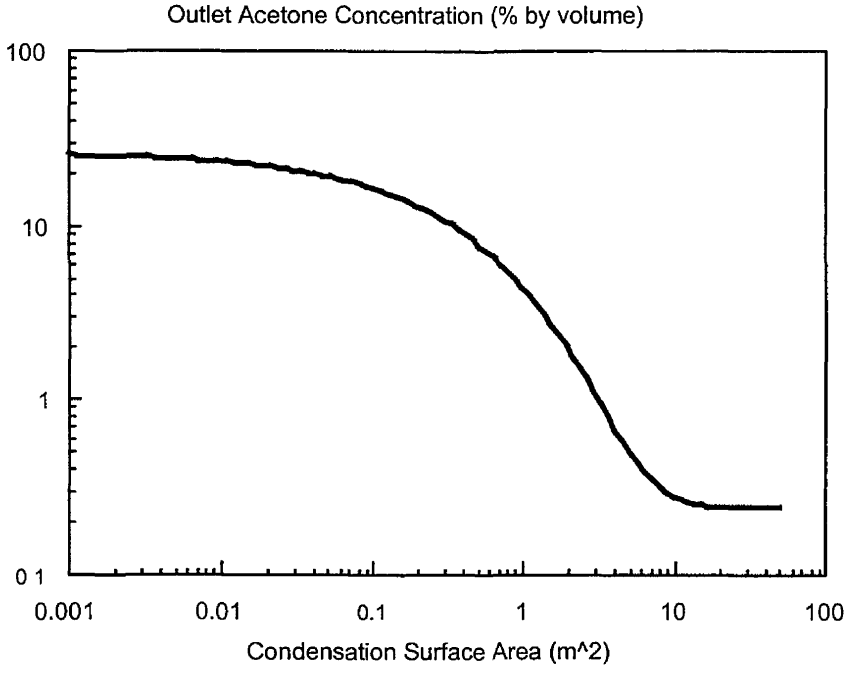

Figure 5.2 Mass transfer/thermodynamic modeled condensation surface area for scale-up condenser design

Table 5.4 Mass transfer/thermodynamic model results for scale-up condenser design.

Required Surface Area (safety factor = 1.2)	24 m^2
Required Mass of LN_2	980 kg/day
Condensed Acetone	890 kg/day

An economic analysis can be conducted based on required condensation surface area. The estimated condenser cost for an 8 ft tube length, 14 BWG fixed tube sheet condenser with 24 m^2 (262 ft^2) of heat transfer surface is approximately $8,000 (Figure 5.3). Other capital costs are also estimated using the USEPA derived cost factors (USEPA[b], 1991). Cost analysis shows that an estimated $73,100 (1996 dollars) capital investment is required for equipment and installation (Table 5.5). Amortized over 10 years at a 10% interest rate, the cost is $11,900/yr (1996 dollars).

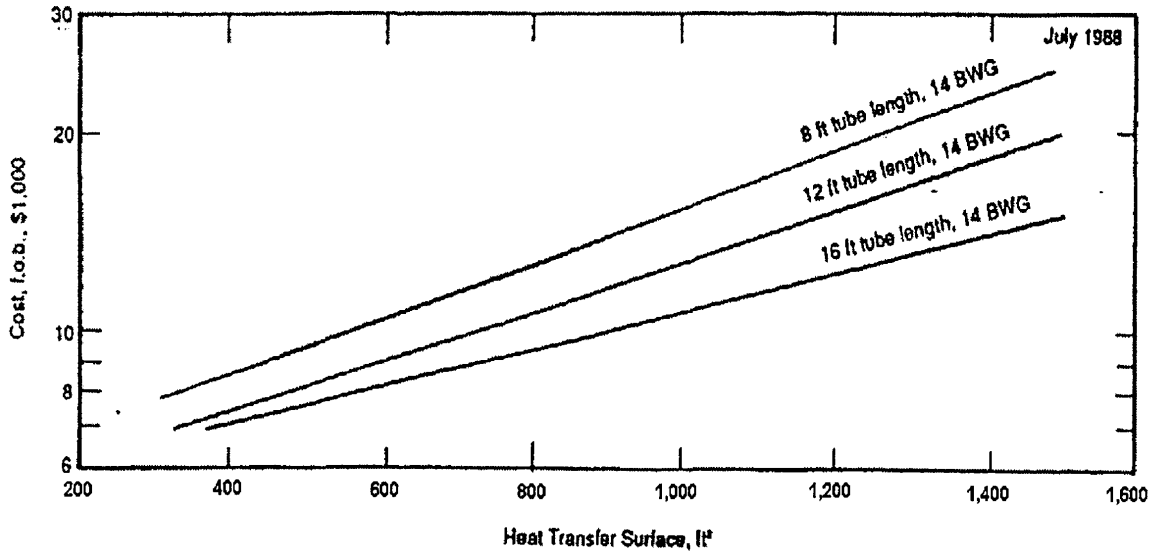

Figure 5.3 Costs for fixed tubesheet condensers. BWG is Birmingham wire gage; 14 BWG is a 0.216 cm tube wall thickness (USEPA, 1991).

Table 5.5 Shell-and-tube capital cost analysis for an 8 ft tube length, 14 BWG fixed tubesheet condenser with 262 ft^2 surface area. Derived cost factors from USEPA[b], 1991. (Carmichael, 1996)

CAPITAL COSTS - 1988 Dollars		
Direct Costs		
Purchased Equipment Costs		
Cost Item	Factor	Cost
Condenser (SA = 325 ft^2)	see Fig. 6.2.3	$8,000
Aux. equip. (duct,fans,etc.)	estimated	$10,000
Capital Equipment Costs	EC=Cond+Aux	$18,000
Instrumentation/Controls*	0.50 EC	$9,000
Sales Tax	0.03 EC	$540
Freight	0.05 EC	$900
Purchased Equip. Cost, PEC	1.58 EC	$28,440
Direct Installation Costs		
Foundation and supports	0.08 PEC	$2,275
Erection and handling	0.14 PEC	$3,982
Electrical	0.08 PEC	$2,275
Piping**	0.05 PEC	$1,422
Insulation	0.10 PEC	$2,844
Painting	0.01 PEC	$284
Direct Installation Cost	0.48 PEC	$13,651
TOTAL DIRECT COSTS, TDC	1.48 PEC	$42,091
Indirect Installation Costs		
Engineering	0.10 PEC	$2,844
Construction	0.05 PEC	$1,422
Contractor fee	0.10 PEC	$2,844
Start-up	0.02 PEC	$569
Performance test	0.01 PEC	$284
Contingencies	0.03 PEC	$853
Total Indirect Cost, IC	1.31 PEC	$37,256
1988 TOTAL CAPITAL COSTS, TTC	1.74 PEC	$49,486
1996 TOTAL CAPITAL COSTS, TTC (@ 5% inflation)		$73,113
Amortized Capital Over 10 yrs @ 10% per annum		$11,899

* EPA suggested factor 0.10 EC;increased to 0.5 EC due to cryogenic controls
** EPA suggested factor 0.02;increased to 0.05 for vacuum jacketed piping

Table 5.6 Shell-and-tube annual cost analysis for an 8 ft tube length, 14 BWG fixed tubesheet condenser with 262 ft^2 surface area. Derived cost factors from USEPA[b], 1991). (Carmichael, 1996)

ANNUAL COSTS				
Direct Costs				
Cost Item		Factor		Cost
Refrigerant Costs - 1991 Dollars				
	LN_2 tank service fee/yr		$1,800	
	Mass LN_2/mass acetone@26%	1.1		
	Mass acetone condensed/yr	126,144 kg/yr		
	Mass LN_2/yr	151,373 kg/yr		
	*1.2 safety factor for loss	181,648 kg/yr		
	LN_2 cost/lb	400,351 lb/yr		
	LN_2 cost/yr	$0.045	$18,016	
	LN_2 cost/yr - 1996 dollars			$26,618
Operating costs - 1996 Dollars				
Direct	Fan Power Electricity	Fp=(1.81e-4)*Q*P*HRS		
		Q (acfm)	360	
		P(inches H2O)	5	
		HRS(hours)	3000	
		Electricity (kWh/hr)	977.4	
		Electricity cost*kWh/hr	$0.059	
		Annual Electricity Cost		$58
	Operating Labor Cost			
		hr/shift	0.5	
		shift (hr)	8	
		Operation time (hr/yr)	6000	
		Labor cost/hr	$13.00	$4,875
		Annual Operating Labor Cost	AOLC	$731
		Supervisory cost	0.15*	$5,625
		Maintenance Labor Cost	AOLC	$5,625
		Maintenance Materials	375 hr/yr* $15	
			1.0* Labor	
	Total Direct Annual Costs			$45,331
Indirect	Overhead		0.6* Labor	
	Administrative		0.02* TTC	
	Property taxes	TTC for 10 yrs @ 10%	0.01* TTC	$6,739
	Insurance		0.01* TTC	
	Capital Recovey			
	Total Indirect Annual Costs			$21,562

The overall recovered acetone credits for the system analyzed in the chapter is $494,400/yr (1996 dollars) resulting in a recovery of $3.92/kg of acetone condensed. Capital costs only attributed approximately $11,900/yr to the overall annual costs. The largest cost factor was expenditures for LN_2 at $26,600/yr. Recovery credits result in an additional income of $561,341/yr.

6. SUMMARY AND CONCLUSION

A novel activated carbon fiber cloth (ACFC) adsorption/electrothermal regeneration/ cryogenic condensation system was developed to separate, concentrate and recover toxic volatile organic compounds (TVOCs) and acetone from industrial flue gas streams. Suitability of this design and soundness of concept was proved by performing evaluation experiments using (MEK) and acetone as sample compounds. The components of the system, adsorber, electrothermal regenerator, and cryogenic condenser were characterized.

ACFC was utilized conveniently in the fixed-bed adsorber. ACFC showed excellent performance due to its high adsorption capacity, high internal and external contact efficiencies, and high adsorption and desorption rates. High adsorption capacity of ACFC was due to its high volume distribution in the optimal pore sizes. Equilibrium capacity of ACFC adsorbent was determined using both the results of breakthough curve (BTC) experiments and gravimetric method. Dubinin-Astakhov (DS) and Dubinin-Radushkevich (DR) isotherms were used to model adsorption capacity of the ACFC. The DA model provided a better regression correlation than the DR model. This is due to the capillary condensation in transitional pores between micro and meso regions. Adsorption dynamics in the ACFC fixed bed resulted in high throughput ratios (TPRs) up to 80% for a packing density of 94.5 mg/cm^3. Increase in packing density to 450 mg/cm^3 increased the TPR to 94%. Adsorption dynamics were modeled to predict the BTCs. The mass transfer rate was second order in the steady state mass transfer zone (MTZ) and at the outlet of the fixed bed. The electrothermal regeneration provided fast desorption rates and efficient energy transfer. The electrothermal regeneration concentrated TVOC vapors up to 63% by volume in less than 5.4 min, without optimization. Supply of a higher initial power resulted in a faster desorption rate and less specific electrical energy use and production of a higher maximum concentration level. Higher carrier gas flow rates resulted in higher desorption rates but produced lower concentration levels. Concentrating the gas stream drastically reduced the amount of the cryogen required to condense the TVOC from the gas stream and enabled the condenser to operate at warmer temperatures while achieving a high recovery efficiency.

The indirect contact shell-and-tube bench-scale cryogenic condenser showed that removal efficiencies of > 98% can be achieved for acetone in N_2 gas streams. Modeling and experimental results also showed that the condenser could operate more efficiently at high TVOC concentrations and low gas flow rates. Carbon adsorption can remove relatively low concentration TVOCs in high flow rate gas streams and desorb at relatively high concentrations and low flow rates. Carbon adsorption/desorption concentrated a 1% by volume gas stream to concentrations as high as 63% by volume and decreased flow rates from 5.0 slpm to 0.5 slpm. Removal efficiencies of the organic compounds by the condenser increased from 70.5% to 98.8% for inlet concentrations between 0.6% and 18.3% by volume.

Trace amounts of high molecular weight compounds were detected in the liquid condensate. However, these compounds accounted for only 1.73% of the acetone condensed.

Two fundamental models were developed to theoretically evaluate TVOC condensation: 1) thermodynamic modeling and 2) mass transfer/thermodynamic modeling. These models were coupled with the Wagner equation to predict the outlet saturation TVOC concentration as a function of condenser temperature. Experimental comparison with modeled results showed that the bench-scale condenser can condense acetone and MEK near the saturation vapor concentration at carrier gas flow rates under approximately 3.0 slpm. At higher flow rates, mass transfer would be limiting, and the mass transfer model could be employed to determine the

condenser TVOC concentration profile. The models developed in this research can provide a method to design a large-scale condenser. The NPV and break-even analyses of the entire ACFC sorption system indicated excellent prospects for economically recovering of acetone.

REFERENCES

American Society of Heating, Refrigeration and Air-Conditioning Engineers, 1983, *ASHRAE Handbook 1983 Equipment Volume*, ASHRAE, Inc., Atlanta, GA.

Avallone, E.A. and T. Baumeister, 1987. *Marks' Standard Handbook for Mechanical Engineers,* McGraw-Hill, Inc. New York, 15-1 to 15-29.

Bansal, R.C., J-B. Donnet, and F. Stockli, 1988, *Active Carbon*, Marcel Dekker, Inc., New York, 1988.

M. Bhandarkar, A.B. Shelekhin, A. G. Dixon, and Y. H. Ma, 1992, Adsorption, permeation, and diffusion of gases in microporous membranes. I. Adsorption of gases on microporous glass membranes, *Journal of Membrane Science*, 75, 221-231.

Buonicore, A.J. and W.T. Davis, eds. 1992, *Air Pollution Manual.* Air and Waste Management Association. New York, NY.

Brunauer, S., P.H. Emmett, and E. Teller, 1938, *J.Amer. Chem. Soc.*, 60,309.

Brunauer, S., L.S. Deming, W.S. Deming, and E. Teller, 1940, *J.Amer. Chem. Soc.*, 62, 1723.

Cal, M.P., 1993, *Adsorption and Experimental Verification of the Adsorption of Volatile Organic Compounds onto Activated Carbon Fibers,* Master's Thesis, University of Illinois at Urbana-Champaign, IL.

Cal, M. P., 1995, *Characterization of gas phase adsorption capacity of untreated and chemically treated activated carbon cloths*, PhD Thesis, University of Illinois at Urbana-Champaign, Illinois.

Carmichael, K. R., 1996, *Cryogenic Recovery of Volatile Organic Compounds for Re-Use*, Master's Thesis, University of Illinois at Urbana-Champaign, IL.

Chilton, T.H. and A.P. Colburn, 1934, Mass Transfer (Absortion) Coefficients, *Ind. Eng. Chem.* 26: 1183-1186.

Colburn, A.P. and O.A. Hougen, 1934, Design of Cooler Condensers for Mixtures of Vapors with Noncondensing Gases, *Ind. Eng. Chem.* 26, 1178-1182.

de Boer, J.H et al., 1966, *J. of Colloid and Interface Sci.*, 21, 415-434.

Donnet, J. B., and R. C. Bansal, 1990, *Carbon Fibers*, 2nd Edn, Marcel Dekker, Inc., New York, NY.

Dubinin, M.M., N.S. Polyakov, and L.I. Kataeva, 1991, *Carbon,* 29, 4/5, 481-488.

Dubinin, M.M., 1989, *Carbon,* 27, 3, 457-467.

Dubinin, M. M.; 1955, Physical Adsorption of Gases and Vapors in Microppores, *Progress in Surface and Membrane Science,* Vol. 9, Academic Press, New York

Dubinin, M. M., 1986, Adsorption Properties and Microporous Structures of Carbonaceous Adsorbents, Carbon, Vol. 25, No. 5, pp. 593-598.

Dubinin, M.M., 1960, *Zhur. Phys. Chem.* 34, 959 ; *Chem Rev.* 60, 235.

Dunn, R.F. and M.M. El-Halwagi, 1994, Optimal Design of Multicomponent VOC Condensation Systems, *J. Haz. Mat.* 38, 187-206.

Dyer, J. A. and K. Mulholland, 1994, Toxic Air Emissions: What is the Full Cost to Your Business, *Environmental Engineering, A special supplement, Chemical Engineering*, Feb., pp. 4-8.

Ermolenko, I. N., I. P. Lyubliner, and N. V. Gulko, 1991, *Chemically Modified Carbon Fibers and Their Applications,* p. 62 & 212.

Foster, K. L., R. G. Fuerman, J. Economy, S. M. Larson, and M. J. Rood, 1992, Adsorption Characteristics of Trace Volatile Organic Compounds in Gas Streams onto Activated Carbon Fibers, *Chem. Mater.,* Vol 4, No. 5.

Fuji, R., 1994, Kynol™ Novoloid Fibers, Nippon Kynol, Inc., Osaka, Japan p. 14

Gilliand, E.R. 1934. *Ind Eng. Chem.* 26, 516-528.

Gregg, S.J., and K.S.W. Sing, 1982, *Adsorption, Surface Area and Porosity, 2nd ed.*, Academic Press, London.

Hayes, J. S. JR. Novoloid Fibers, 1981, *Kirk-Othmer: Encyclopedia of Chemical Technology*, 3rd Edn, Vol 16, 125-138, John Wiley & Sons, Inc., New York, NY.

Holden, K.M., A.S. Wanniarachchi, P.J. Marto, D.H. Boone and J.W. Rose, 1987, The Use of Organic Coatings to Promote Dropwise Condensation of Steam, *Trans. ASME* 109, 768-774.

Incropera, F.P. and D.P. DeWitt, 1990, *Fundamentals of Heat and Mass Transfer*, 3rd ed., John Wiley & Sons, New York, NY.

Jacobs, H.R. and R. Nadig., 1987, Condensation on Coolant Jets and Sheets Including the Effects of Noncondensible Gases, *J. Heat Transfer*, 109, 1013-1020.

Kellenbenz, J. and E. Hahne, 1994, Condensation of Pure Vapours and Binary Vapour Mixtures in Forced Flow, *Int. J. Heat Mass Transfer*, 37 (8), 1269-1276.

Dubinin, M. M.; 1955, Physical Adsorption of Gases and Vapors in Microppores, *Progress in Surface and Membrane Science*, Vol. 9, Academic Press, New York

Dubinin, M. M., 1986, Adsorption Properties and Microporous Structures of Carbonaceous Adsorbents, Carbon, Vol. 25, No. 5, pp. 593-598.

Dubinin, M.M., 1960, *Zhur. Phys. Chem.* 34, 959 ; *Chem Rev.* 60, 235.

Dunn, R.F. and M.M. El-Halwagi, 1994, Optimal Design of Multicomponent VOC Condensation Systems, *J. Haz. Mat.* 38, 187-206.

Dyer, J. A. and K. Mulholland, 1994, Toxic Air Emissions: What is the Full Cost to Your Business, *Environmental Engineering, A special supplement, Chemical Engineering*, Feb., pp. 4-8.

Ermolenko, I. N., I. P. Lyubliner, and N. V. Gulko, 1991, *Chemically Modified Carbon Fibers and Their Applications,* p. 62 & 212.

Foster, K. L., R. G. Fuerman, J. Economy, S. M. Larson, and M. J. Rood, 1992, Adsorption Characteristics of Trace Volatile Organic Compounds in Gas Streams onto Activated Carbon Fibers, *Chem. Mater.,* Vol 4, No. 5.

Fuji, R., 1994, Kynol™ Novoloid Fibers, Nippon Kynol, Inc., Osaka, Japan p. 14

Gilliand, E.R. 1934. *Ind Eng. Chem.* 26, 516-528.

Gregg, S.J., and K.S.W. Sing, 1982, *Adsorption, Surface Area and Porosity, 2nd ed.*, Academic Press, London.

Hayes, J. S. JR. Novoloid Fibers, 1981, *Kirk-Othmer: Encyclopedia of Chemical Technology*, 3rd Edn, Vol 16, 125-138, John Wiley & Sons, Inc., New York, NY.

Holden, K.M., A.S. Wanniarachchi, P.J. Marto, D.H. Boone and J.W. Rose, 1987, The Use of Organic Coatings to Promote Dropwise Condensation of Steam, *Trans. ASME* 109, 768-774.

Incropera, F.P. and D.P. DeWitt, 1990, *Fundamentals of Heat and Mass Transfer*, 3rd ed., John Wiley & Sons, New York, NY.

Jacobs, H.R. and R. Nadig., 1987, Condensation on Coolant Jets and Sheets Including the Effects of Noncondensible Gases, *J. Heat Transfer*, 109, 1013-1020.

Kellenbenz, J. and E. Hahne, 1994, Condensation of Pure Vapours and Binary Vapour Mixtures in Forced Flow, *Int. J. Heat Mass Transfer*, 37 (8), 1269-1276.

Keller, G.E., 1983, Gas Seperation Processes State of the Art, In Industrial Gas Seperation, ACS Symp. Ser. 223, American Chemical Society, Washington, D.C.

Kern, D.Q. 1950. *Process Heat Transfer.* New York, NY: McGraw-Hill.

Langmuir, I.J., 1916, *Amer. Chem. Soc.* 38, 2221.

Lewis, R. G., 1989, *J. Chin. Chem. Soc.* 36, 261-277.

Lide, D. R., Ed., 1993, *Handbook of Chemistry and Physics, 73 ed.*; CRC, Boca Raton.

Lowell, S. and Shields, 1984, *Powder Surface area and Porosity*, Chapman and Hall, London, England.

Majumdar, S., 1993, *Regulatory Requirements for Hazardous Materials*, McGraw-Hill, Inc., New York, USA.

McCabe, L. W., J. C. Smith, and P. Harriott, 1993, *Unit Operations of Chemical Engineering*, 5th Edn, McGraw-Hill, Inc., New York, NY.

McInnes, R.G., *Chemical Engineering Progress*, 1995, *91*, Nov., pp 36-48.

Minkowycz, W.J. and E.M. Sparrow, 1966, Condensation Heat Transfer in the Presence of Noncondensables, Interfacial Resistance, Superheating, Variable Properties and Diffusion, *Int. J. Heat Mass Transfer*, 9, 1125-1144.

Moretti, E. C., and N. Mukhopadhyay, 1993, VOC Control: Current Practices and Future Trends, *Chemical Engineering Progress,* July, pp. 20-26.

Noll, K.E., V.Gounaris, and W-S. Hou, 1992, *Adsorption Technology for Air and Water Pollution Control*, Lewis Publishers, Inc., Chelsea, Michigan.

Nrigau, J.O., Ed., 1992, *Gaseous Pollutants, Characterization and Cycling*, John Wiley & Sons, Inc., New York, 338-339.

Perry, R.H. and D.H. Green., 1984, *Perry's Chemical Engineers Handbook.* 6th ed. McGraw-Hill, New York, NY.

Reid, R.C., J.M. Prausnitz and T.K. Sherwood. 1977. *The Properties of Gases and Liquids.* McGraw-Hill, New York, NY.

Rosenow, W.M., J.P. Hartnett and E.N. Ganic, eds., 1985, *Handbook of Heat Transfer Fundamentals*, 2nd ed., McGraw-Hill, New York NY.

Ruddy, E.N. and L. A. Carrol, 1993, Select the Best VOC Control Strategy, *Chemical Engineering Progress*, July, pp. 28-35.

Ruhl, M. J., Recover VOCs via Adsorption on Activated Carbon, 1993, *Chemical Engineering Progress*, July, pp. 37-41.

Sameshima, G.T. and J.D. Eisenwasser, 1991, Cryogenic Recovery of VOC Emissions, pp 41.1 1-9. 84th Annual Air & Waste Management Association Meeting and Exhibition, Vancouver, British Columbia, June 16-21.

Siddique, M., M.W. Golay and M.S. Kazimi. 1994. Theoretical Modeling of Forced Convection Condensation of Steam in a Vertical Tube in the Presence of a Noncondensable Gas. Nuc. Tech. 106: 202-204.

Sparrow, E.M., W.J. Minkowycz and M. Saddy. 1967. Forced Convection Condensation in the Presence of Noncondensables and Interfacial Resistance. Int. J. Heat Mass Transfer 10: 1829-1834.

Sterling, D. A., *Indoor Air and Human Health*, Proceedings of the 7th Life Sciences Symposium, Knoxville, TN, 1984

Stoeckli, H. F., 1989, Microporous Carbons and their Characterization: The Present State of the Art. Carbon Vol. 28, No. 1, pp. 1-6.

Tancrede, M., R. Wilson, L. Zeise, E.A. Crouch, *Atmospheric Environment,* 21, no. 10, 1987, 2187-2205

Treybal, R.E., 1980, *Mass-Transfer Operations*, 3rd ed., McGraw-Hill, New York, p. 627.

Tubular Exchangers Manufacturers Association. 1978. *Tubular Exchangers Manufacturers Association Standards*. 6th ed. New York, NY: TEMA.

United States Environmental Protection Agency, 1990, Clean Air Act Amendments, USEPA, USA.

United States Environmental Protection Agency[a], 1991, *Toxics in the Community, National and Local Perspectives*, USEPA, USA.

United States Environmental Protection Agency[b], 1991, Control Technologies for Hazardous Air Pollutants, EPA/625/6-91/014, USEPA, USA.

United States Environmental Protection Agency[c], 1991, *Control Technology Guideline Series: Control of Volatile Organic Compound Emissions from Reactor Processes and Distillation*

Operation Processes in the Synthetic Organic Chemical Manufacturing Industry. EPA-450/4-91-031, USEPA, USA.

United States Environmental Protection Agency[a], 1993, National Air Quality and Emissions Trends Report, EPA/454/R-93-03, USEPA, USA.

United States Environmental Protection Agency[b], 1993, Toxics Release Inventory, USEPA, USA.
United States Environmental Protection Agency, 1995, 1993 Toxics Release Inventory, Executive Summary Catalog number PA745595001, USEPA, USA.

Vargaftik, N.B. 1975. *Tables on the Thermophysical Properties of Liquids and Gases.* New York, NY: John Wiley & Sons.

Wilbur, L.C., ed. *1985 Handbook of Energy Systems Engineering.* New York, NY: John Wiley & Sons.

Yang, R. T., 1987, *Gas Separation by Adsorption Processes,* Butterworths Publishers, Stoneham, MA.

Yoon, Y. H., and J. H. Nelson, 1984, Application of gas adsorption kinetics I. A theoretical model for respirator cartridge service life, *American Industrial Hygiene Association Journal,* 45 (8), 509-516.

ACKNOWLEDGMENT

Help of Dr. Subhash Bhagwat, for the economic analysis of the ACFC sorption system, and Linda Schroeder, Helen Mardis and Michael Mulhern during publishing of this report are greatly appreciated.

Appendix A: List of Hazardous Air Pollutants

CAS Number	Chemical Name
75070	Acetaldehyde
60355	Acetamide
75058	Acetonitrile
98862	Acetophenone
53963	2-Acetylaminofluorene
107028	Acrolein
79061	Acrylamide
79107	Acrylic acid
107131	Acrylonitrile
107051	Allyl chloride
92671	4-Aminobiphenyl
62533	Aniline
90040	o-Anisidine
1332214	Asbestos
71432	Benzene (including benzene from gasoline)
92875	Benzidine
98077	Benzotrichloride
100447	Benzyl chloride
92524	Biphenyl
117817	Bis(2-ethylhexyl)phthalate (DEHP)
542881	Bis(chloromethyl)ether
75252	Bromoform
106990	1,3-Butadiene
156627	Calcium cyanamide
133062	Captan
63252	Carbaryl
75150	Carbon disulfide
56235	Carbon tetrachloride
463581	Carbonyl sulfide
120809	Catechol
133904	Chloramben
57749	Chlordane
7782505	Chlorine
79118	Chloroacetic acid
532274	2-Chloroacetophenone
108907	Chlorobenzene
510156	Chlorobenzilate
67663	Chloroform
107302	Chloromethyl methyl ether
126998	Chloroprene
1319773	Cresols/Cresylic acid (isomers and mixture)
95487	o-Cresol
108394	m-Cresol
106445	p-Cresol
98828	Cumene
94757	2,4-D, salts and esters
3547044	DDE
334883	Diazomethane
132649	Dibenzofurans
96128	1,2-Dibromo-3-chloropropane
84742	Dibutylphthalate
106467	1,4-Dichlorobenzene(p)
91941	3,3-Dichlorobenzidene
111444	Dichloroethyl ether (Bis(2-chloroethyl)ether)
542756	1,3-Dichloropropene
62737	Dichlorvos
111422	Diethanolamine
121697	N,N-Diethyl aniline (N,N-Dimethylaniline)
64675	Diethyl sulfate
119904	3,3-Dimethoxybenzidine
60117	Dimethyl aminoazobenzene
119937	3,3¬-Dimethyl benzidine
79447	Dimethyl carbamoyl chloride
68122	Dimethyl formamide
57147	1,1-Dimethyl hydrazine
131113	Dimethyl phthalate
77781	Dimethyl sulfate
534521	4,6-Dinitro-o-cresol, and salts
51285	2,4-Dinitrophenol
121142	2,4-Dinitrotoluene
123911	1,4-Dioxane (1,4-Diethyleneoxide)
122667	1,2-Diphenylhydrazine
106898	Epichlorohydrin (l-Chloro-2,3-epoxypropane)
106887	1,2-Epoxybutane
140885	Ethyl acrylate
100414	Ethyl benzene
51796	Ethyl carbamate (Urethane)
75003	Ethyl chloride (Chloroethane)
106934	Ethylene dibromide (Dibromoethane)
107062	Ethylene dichloride (1,2-Dichloroethane)
107211	Ethylene glycol
151564	Ethylene imine (Aziridine)
75218	Ethylene oxide
96457	Ethylene thiourea
75343	Ethylidene dichloride (1,1-Dichloroethane)
50000	Formaldehyde
76448	Heptachlor
118741	Hexachlorobenzene
87683	Hexachlorobutadiene
77474	Hexachlorocyclopentadiene

CAS Number	Chemical Name
67721	Hexachloroethane
822060	Hexamethylene-1,6-diisocyanate
680319	Hexamethylphosphoramide
110543	Hexane
302012	Hydrazine
7647010	Hydrochloric acid
7664393	Hydrogen fluoride (Hydrofluoric acid)
7783064	Hydrogen sulfide
123319	Hydroquinone
78591	Isophorone
58899	Lindane (all isomers)
108316	Maleic anhydride
67561	Methanol
72435	Methoxychlor
74839	Methyl bromide (Bromomethane)
74873	Methyl chloride (Chloromethane)
71556	Methyl chloroform (1,1,1-Trichloroethane)
78933	Methyl ethyl ketone (2-Butanone)
60344	Methyl hydrazine
74884	Methyl iodide (Iodomethane)
108101	Methyl isobutyl ketone (Hexone)
624839	Methyl isocyanate
80626	Methyl methacrylate
1634044	Methyl tert butyl ether
101144	4,4-Methylene bis(2-chloroaniline)
75092	Methylene chloride (Dichloromethane)
101688	Methylene diphenyl diisocyanate (MDI)
101779	4,4¬-Methylenedianiline
91203	Naphthalene
98953	Nitrobenzene
92933	4-Nitrobiphenyl
100027	4-Nitrophenol
79469	2-Nitropropane
684935	N-Nitroso-N-methylurea
62759	N-Nitrosodimethylamine
59892	N-Nitrosomorpholine
56382	Parathion
82688	Pentachloronitrobenzene (Quintobenzene)
87865	Pentachlorophenol
108952	Phenol
106503	p-Phenylenediamine
75445	Phosgene
7803512	Phosphine
7723140	Phosphorus
85449	Phthalic anhydride
1336363	Polychlorinated biphenyls (Aroclors)
1120714	1,3-Propane sultone
57578	beta-Propiolactone
123386	Propionaldehyde
114261	Propoxur (Baygon)
78875	Propylene dichloride (1,2-Dichloropropane)
75569	Propylene oxide
75558	1,2-Propylenimine (2-Methyl aziridine)
91225	Quinoline
106514	Quinone
100425	Styrene
96093	Styrene oxide
1746016	2,3,7,8-Tetrachlorodibenzo-p-dioxin
79345	1,1,2,2-Tetrachloroethane
127184	Tetrachloroethylene (Perchloroethylene)
7550450	Titanium tetrachloride
108883	Toluene
95807	2,4-Toluene diamine
584849	2,4-Toluene diisocyanate
95534	o-Toluidine
8001352	Toxaphene (chlorinated camphene)
120821	1,2,4-Trichlorobenzene
79005	1,1,2-Trichloroethane
79016	Trichloroethylene
95954	2,4,5-Trichlorophenol
88062	2,4,6-Trichlorophenol
121448	Triethylamine
1582098	Trifluralin
540841	2,2,4-Trimethylpentane
108054	Vinyl acetate
593602	Vinyl bromide
75014	Vinyl chloride
75354	Vinylidene chloride (1,1-Dichloroethylene)
1330207	Xylenes (isomers and mixture)
95476	o-Xylenes
108383	m-Xylenes
10642	p-Xylenes
0	Antimony Compounds
0	Arsenic Compounds (inorganic including arsine)
0	Beryllium Compounds
0	Cadmium Compounds
0	Chromium Compounds
0	Cobalt Compounds
0	Coke Oven Emissions
0	Cyanide Compounds1
0	Glycol ethers2
0	Lead Compounds
0	Manganese Compounds
0	Mercury Compounds
0	Fine mineral fibers3
0	Nickel Compounds
0	Polycylic Organic Matter4
0	Radionuclides (including radon)5
0	Selenium Compounds

APPENDIX B List of Variables

Thermodynamic Model

Variable	Description	Units
CpA	Specific heat of vapor	J/Kg K
CpAN	Specific heat of combined gas--funct. of T	J/Kg K
CpL	Specific heat of condensate	J/Kg K
CpN1	Specific heat of carrier gas in the tube	J/Kg K
EnthN1	Sensible heat change for nitrogen gas T2 to T1`	J/Kg
EnthN2	Sensible heat change for nitrogen gas T3 to T2	J/Kg
EnthL	Sensible heat change of liquid condensate	J/Kg
EnthA	Sensible heat change of vapor	J/Kg
EnthAN	Sensible heat change of vapor and carrier gas T3 to T2	J/Kg
hA	Latent heat of condensation for condensate	J/Kg
hLN	Latent heat of evaporation for carrier gas	J/Kg
J5	Reduced temperature of vapor	------
m1dot	Mass flow rate of vapor and carrier gas at the initial concentration	Kg/s
m2dot	Mass flow rate of vapor and carrier gas at the final concentration	Kg/s
mLdot	Mass flow rate of condensate	Kg/s
mLNdot	Mass flow rate of carrier gas in the tube	Kg/s
MWA	Molecular weight of vapor	g/g-mol
MWN	Molecular weight of carrier gas	g/g-mol
MWT1	Average molecular weight of combined gas at the initial concentration	g/g-mol
MWT2	Average molecular weight of combined gas at the final concentration	g/g-mol
P	Condenser operating pressure	Pa
Q1	Volumetric flow rate of combined gas at the final temperature	m^3/s
Q2	Volumetric flow rate of combined gas at the final temperature	m^3/s
R	Ideal gas constant	Nm/Kkgmol
rho1	Combined bulk gas density in the shell at the initial temperature	Kg/m^3
rho2	Combined bulk gas density in the shell at the final temperature	Kg/m^3
T1	Initial temperature of the refrigerant	K
T2	Final temperature of refrigerant and vapor/carrier gas mixture	K
T3	Initial temperature of the vapor and carrier gas mixture	K
TaveA	Average temperature of bulk gas in the element	K
TaveN1	Average temperature of refrigerant	K

TaveN2	Average temperature of carrier gas	K
xA1	Mole fraction of vapor at the initial temperature	------
xA2	Mole fraction of vapor at the final temperature	------
xAave	Average mole fraction of the vapor	------
xN1	Mole fraction of carrier gas at the initial temperature	------
xN2	Mole fraction of carrier gas at the final temperature	------

List of Variables: Mass Transfer Model

Variable	Description	Units
AAN	Viscosity fitting parameter Chapman-Enskog method--non-polar gas	------
Ak12	Combined gas conductivity fitting parameter Lindsay-Bromley Modification	------
Ak21	Combined gas conductivity fitting parameter Lindsay-Bromley Modification	------
Aouter12	Combined gas viscosity fitting parameter Reichenberg Method w/ Brokaw Approximation	------
Aouter21	Combined gas viscosity fitting parameter Reichenberg Method w/ Brokaw Approximation	------
area1	Heat transfer cylindrical surface area	m^2
area2	Outer tube cylindrical area	m^2
area3	Heat transfer cross-sectional area	m^2
area4	Inner tube cross-sectional area	m^2
area5	Inner tube cylindrical surface area	m^2
Astar	Viscosity atomic bond parameter Reichenberg Method	------
BBN	Gas viscosity fitting parameter Chapman-Enskog method--non-polar gas	------
CCN	Gas viscosity fitting parameter Chapman-Enskog method--non-polar gas	------
CpA	Specific heat of vapor	J/Kg K
CpAN	Specific heat of combined gas--funct. of T	J/Kg K
CpL	Specific heat of condensate	J/Kg K
CpN1	Specific heat of the refrigerant in the tube	J/Kg K
CpN2	Specific heat of carrier gas in the shell	J/Kg K
Cs	Combined gas conductivity parameter Cs = 0.73 for polar gas in mixture Lindsay Bromley Modification	------
DDN	Gas viscosity fitting parameter Chapman-Enskog method--non-polar gas	------
De	Heat transfer effective diameter 4 × Flow area / wetted perimeter	m

deltaAce	Viscosity Stockmayer parameter based on dipole moment--delta>0.1 is considered a polar gas	------
dHvb	Condensate conductivity parameter--molal heat of vaporization at the normal boiling point	------
Dii	Diameter of inside tube	m
Din	Diameter of inside condensation area--i.e. outside tube	m
dipoleAce	Dipole moment of acetone	------
Dout	Diameter of outside condensation area--i.e. inside shell	m
dPlmAC	Log-mean partial pressure difference between bulk vapor and the condensate film from i to i+1	Pa
dSstar	Condensate conductivity--Entropy at normal boiling point	------
dTlmAC	Log-mean temperature difference between the bulk mixture and the condensate film from i to i+1.	K
dTlmALN	Log mean temperature difference between the bulk mixture and the tube side refrigerant from i to i+1	K
dTlmAW	Log mean temperature difference between the bulk mixture and the copper wall from i to i+1	K
dTlmNC	Log mean temperature difference between the condensate film and the tube side refrigerant from i to i+1	K
dTlmNW	Log-mean temperature difference between the wall and the tube side refrigerant from i to i+1	K
dx	Element axial length from i to i+1	m
EEN	Gas viscosity fitting parameter Chapman-Enskog method--non-polar gas	------
Enth1	Latent and sensible heats of vaporization for refrigerant in the tube	W
Enth2	Latent heat of vapor condensation and sensible heats for vapor and gas mixture in shell	W
Enth3	Total heat determined from heat transfer resistance	W
Enth4	Heat transfer from tube side refrigerant to the condenser wall	W
Enth5	Heat transfer from bulk mixture to the condenser wall	W
Enth6	Heat transfer from the bulk mixture to the condensate film	W/m^2
Enth7	Heat transfer from the tube side refrigerant to the condensate film	W/m^2
EnthN1	Sensible heat change for nitrogen gas T2 to T1`	J/Kg
EnthN2	Sensible heat change for nitrogen gas T3 to T2	J/Kg

EnthL	Sensible heat change of liquid condensate	J/Kg
EnthA	Sensible heat change of vapor	J/Kg
EnthAN	Sensible heat change of vapor and carrier gas T3 to T2	J/Kg
epskA	Potential energy constant / Boltzmann's constant for vapor gas--Viscosity determination--Brokaw Approximation--determination of Vb	------
epskN	Potential energy constant / Boltzmann's constant for gas--Viscosity determination--Brokaw Approximation	------
FFN	Gas viscosity fitting parameter Chapman-Enskog method--non-polar gas	------
gamma	Density of condensate fitting parameter based on the reduced temperature	------
Gave	Average mass flow rate of acetone from the bulk mixture into liquid form	Kg/s m^2
GLA	Mass flow rate of liquid refrigerant normalized to flow area	Kg/s m^2
grav	Acceleration due to gravity	m/s^2
h1	Convective heat transfer film coefficient of the gas film mixture	W/m^2 K
h2	Convective film coefficient of the condensate film	W/m^2 K
h3	Convective film coefficient of the tube side refrigerant gas film	W/m^2 K
hA	Latent heat of condensation for vapor	J/Kg
HHkLA	Refrigerant thermal conductivity parameter based on functional groups method of Robbins and Kingrea	
hLAP	Latent heat of condensation for vapor modified by the Jakob Number	J/Kg
hLN	Latent heat of evaporation for the refrigerant	J/Kg
J7	Reduced temperature of vapor	------
JA	Jakob Number	------
Jfactor	Condensate viscosity parameter based on molecular bonds Morris Method	------
kAce	Thermal conductivity of vapor	W/m K
kAceref	Reference temperature for thermal conductivity of the vapor	W/m K
kAN	Combined gas thermal conductivity Wassiljewa Equation w/ Lindsay and Bromley mod.	W/m K
kc	Thermal conductivity of 99.9% pure copper	W/m K
kd	Molecular diffusivity Gilliand Equation	m^2/s
Kg	Mass transfer coefficient	Kg g-mol s m^2 Pa g
kLA	Thermal conductivity of the condensate	W/m K

	Method of Robbins and Kingrea	
kNG	Thermal conductivity of refrigerant gas in tube	W/m K
kNG2	Thermal conductivity of carrier gas in shell	W/m K
kNGref	Thermal conductivity reference for nitrogen gas at 230 K	W/m K
m1dot	Mass flow rate of the vapor and carrier gas at the shell side outlet	Kg/s
m2dot	Mass flow rate of the vapor and carrier gas at the shell side inlet	Kg/s
mLdot	Mass flow rate of condensate	Kg/s
mLNdot	Mass flow rate of liquid refrigerant in the tube	Kg/s
MWA	Molecular weight of acetone	g/g-mol
MWANave	Average molecular weight of combined shell gas	g/g-mol
MWN	Molecular weight of nitrogen	g/g-mol
MWTA1	Average molecular weight of combined gas at the outlet of the shell	g/g-mol
MWTA2	Average molecular weight of combined gas at the inlet of the shell	g/g-mol
mwx12	Combined gas viscosity molecular scaling parameter Brokaw Approximation	------
MWy12	Combined gas viscosity molecular scaling parameter Brokaw Approximation	------
NNkLA	Condensate thermal conductivity parameter based on functional groups Method of Robbins and Kingrea	------
NuA	Atomic volume of acetone for Gilliand Diffusivity Equation	------
NuN	Atomic volume of nitrogen for Gilliand Diffusivity Equation	------
OMEGAvN1	Neufeld empirical equation for computation of Chapman Enskog Non-polar gas viscosity in the tube	------
OMEGAvNO	Neufeld empirical equation for computation of Chapman Enskog Non-polar gas viscosity in the shell	------
OMEGAvNOc	Neufeld empirical equation for computation of Chapman Enskog Non-polar gas viscosity at the gas-condensate interface	------
OMEGAvNw	Neufeld empirical equation for computation of Chapman Enskog Non-polar gas viscosity at the tube side wall	------
omrhoLA	Accentric factor used in determining the density of liquid acetone using the Gunn and Yamada equation	------
P	Condenser operating pressure	Pa
Pa1	Partial pressure of vapor at the outlet of the element	Pa
Pa2	Partial pressure of vapor at the inlet of the element	Pa
Pa2n	Dummy variable to prevent Pa1 from exceeding Pa2 during computational solutions	Pa
Pc	Partial pressure of vapor at the gas-condensate interface	Pa

Pcn	Dummy variable to prevent Pc from exceeding Pa1 during computational solutions	Pa
PHI12	Combined gas viscosity parameter for bulk flow in shell Brokaw Approximation	------
PHI12c	Combined gas viscosity parameter for bulk flow at condensate film--Brokaw Approximation	------
PHI21	Combined gas viscosity parameter for bulk flow in shell Brokaw Approximation	------
PHI21c	Combined gas viscosity parameter for bulk flow at condensate film--Brokaw Approximation	------
PNb	Average bulk nitrogen partial pressure in the element	Pa
PNc	Average carrier gas partial pressure at the gas-condensate interface	Pa
Pngf	Log-mean pressure difference of carrier gas between the bulk and gas-condensate interface	Pa
QAN1	Volumetric flow rate of combined gas at the element outlet	m^3/s
QAN2	Volumetric flow rate of combined gas at the element inlet	m^3/s
R	Ideal gas constant	Nm/Kkgmol
rhoAN1	Combined bulk gas density in the shell at the element outlet	Kg/m^3
rhoAN2	Combined bulk gas density in the shell at the element inlet	Kg/m^3
rhoANave	Combined bulk gas density average in the shell	Kg/m^3
rhoLA	Density of condensate	Kg/m^3
Sace	Sutherland constant for determining combined gas conductivity	------
Sacenit	Sutherland constant for determining combined gas conductivity	------
sigmaN	Stockmeyer potential parameter for determination of carrier gas viscosity	------
Snit	Sutherland constant for determining combined gas conductivity	------
Souter12	Combined gas viscosity parameter for polar--non-polar mixtures Brokaw approximation	------
Souter12c	Combined gas viscosity parameter for polar--non-polar mixtures Brokaw approximation	------
Souter21	Combined gas viscosity parameter for polar--non-polar mixtures Brokaw approximation	------
Souter21c	Combined gas viscosity parameter for polar--non-polar mixtures Brokaw approximation	------
TA1	Temperature of bulk gas in shell at the outlet	K
TA1n	Dummy variable to prevent TA1 from exceeding TA2 in computation	K
TA2	Temperature of bulk gas in shell at the inlet	K
TaveA	Average temperature of bulk gas in the element	K
TaveN1	Average temperature of refrigerant in tube in the element	K

TboilingA	Normal boiling temperature of acetone	K
TboilingN	Normal boiling temperature of nitrogen	K
Tc	Temperature at the gas-condensate interface	K
TN1	Temperature of refrigerant at the tube inlet	K
TN2	Temperature of refrigerant at the tube outlet	K
TrAc	Reduced temperature of vapor at the gas-condensate interface	------
TrAce	Reduced temperature of vapor in the bulk shell flow	------
TrefA	Reference temperature of acetone (373 K)	K
TrefN1	Reference temperature of nitrogen (230 K)	K
TrLA	Reduced temperature of condensate	------
TrLAR	Reduced temperature of reference liquid acetone temperature	------
TstarAc	k T/ epsilon--parameter used in determination of vapor gas viscosity at gas-condensate interface	------
TstarAce	k T/ epsilon--parameter used in determination of vapor gas viscosity in shell side	------
TstarN1	k T/ epsilon--parameter used in determination of carrier gas viscosity in tube side	------
TstarNOc	k T/ epsilon--parameter used in determination of carrier gas viscosity at gas-condensate interface	------
TstarNO	k T/ epsilon--parameter used in determination of carrier gas viscosity in shell side	------
TstarNw	k T/ epsilon--parameter used in determination of carrier gas viscosity in tube side at wall	------
Tw	Temperature of copper tube wall	K
U1	Thermal resistance between bulk tube and bulk shell temperatures	W/m^2 K
U2	Thermal resistance between bulk tube and tube wall temperatures	W/m^2 K
U3	Thermal resistance between bulk shell and tube wall temperatures	W/m^2 K
U4	Thermal resistance between bulk tube and condensate temperatures	W/m^2 K
VboilingA	Normal specific volume of acetone at the boiling point	------
VisAce	Gas viscosity of acetone in the bulk shell side--used in determination of combined gas viscosity	------
VisAcec	Gas viscosity of acetone at the gas-condensate interface--used in determination of combined gas viscosity at the interface	------
VisAN	Combined gas viscosity in the shell	N s/m^2
VisANc	Combined gas viscosity at the gas-condensate interface	N s/m^2
VisLA	Condensate viscosity	N s/m^2
VisLAplus	Reference parameter used in determining liquid acetone viscosity--Morris Method	------
VisNG	Viscosity of refrigerant in the tube	N s/m^2

VisNGO	Gas viscosity of carrier gas in the shell used in determining combined gas viscosity	------
VisNGOc	Viscosity of carrier gas at the gas-condensate interface	------
VisNGw	Viscosity of carrier gas at the tube side wall	N s/m^2
Vro	Liquid acetone density parameter relating reduced temperatures	------
VrrhoLA	Liquid acetone density parameter relating reduced temperatures	------
xA1	Mole fraction of vapor in the shell side gas outlet	------
xA2	Mole fraction of vapor in the shell side gas inlet	------
xAave	Average mole fraction of vapor in the element	------
xAc	Mole fraction of vapor at the gas-condensate interface	------
xN1	Mole fraction of carrier gas in the shell side gas outlet	------
xN2	Mole fraction of carrier gas in the shell side gas inlet	------
xNave	Average mole fraction of carrier gas in the element	------
xNc	Mole fraction of carrier gas at the gas-condensate interface	------

APPENDIX C Thermodynamic Model

```
{mass balance}
mLdot=rho1*xA1*Q1-rho2*xA2*Q2

{Wagner Equation}
xA2=(exp(((-7.45514*J5)+(1.202*(J5^1.5))+(-2.43926*(J5^3))+(-3.3559*(J5^6)))/(
T2/508.1))*47)
J5=1-(T2/508.1)

{Thermodynamic Balance}
mLNdot*hLN+mLNdot*EnthN1=mLdot*hA+mLdot*EnthL+(rho1*Q1)*EnthAN*(T3-T2)

{Correlations}
rho1=P*MWT1/(R*T3)
rho2=P*MWT2/(R*T2)
Q2=(m2dot/rho2)
MWT1=xA1*MWA+xN1*MWN
MWT2=xA2*MWA+xN2*MWN
xA1+xN1=1
xA2+xN2=1
m2dot=m1dot-mLdot
m1dot=rho1*Q1

{Specific Heats}
CpN1=(31.2+-0.0136 * (TaveN1)+0.0000268 * (TaveN1)^2+ -0.0000000117 *
(TaveN1)^3)     *(1/MWN)*(1000) {g-mol/kg-mol}
CpN2=(31.2+-0.0136*(TaveN2)+0.0000268*(TaveN2)^2+-0.0000000117*(TaveN2)^3)
                *(1/MWN)*(1000) {Reid 226}
TaveN1=(T2+T1)/2
TaveN2=(T2+T3)/2
CpL=(2.3388-0.0038942*TaveA+1.1221e-05*(TaveA)^2)*1000 {J/kg K} {correlation
with            experimental data}
CpA=(6.301+0.261*TaveA-0.000125*(TaveA)^2+0.0000000204*(TaveA)^3)*(1/MWA)*(100
0)
TaveA=(T3+T2)/2
CpAN=((xA1+xA2)/2)*CpA+((xN1+xN2)/2)*CpN2

{Enthalpies -- Integrated form of Specific Heats}
EnthN1=(31.2*(T2-T1)+-0.0136/2 * (T2^2-T1^2)^2+0.0000268 /3* (T2^3-T1^3)+
-0.0000000117/4*
                (T2^4-T1^4)) *(1/MWN)*(1000) {g-mol/kg-mol}
EnthN2=(31.2*(T3-T2)+-0.0136/2*(T3^2-T2^2)+0.0000268/3*(T3^3-T2^3)+-0.00000001
17/4*           (T3^4-T2^4)) *(1/MWN)*(1000) {Reid 226}
EnthL=(2.3388*(T3-T2)-0.0038942/2*(T3^2-T2^2)+1.1221e-05/3*(T3^3-T2^3))*1000
                {J/kg K} {correlation with experimental data}
EnthA=(6.301*(T3-T2)+0.261/2*(T3^2-T2^2)-0.000125/3*(T3^3-T2^3)+0.0000000204/4
*               (T3^4-T2^4))*(1/MWA)*(1000)
EnthAN=((xA1+xA2)/2)*EnthA+((xN1+xN2)/2)*EnthN2

{Parameters}
P=101325 {N/m^2}
R=8314 {N m/K kg-mol}
```

```
T3=294 {K}
T1=77 {K}
MWA=58.1 {kg/kg-mol}
MWN=28.02 {kg/kg-mol}
Q1=(.4{Lpm}/(1000*60)) {m^3/sec}
hA=524000*((1-TaveA/508.1)/(1-329.2/508.1))^0.27 {J/Kg}{Reid pg.228}
hLN=199106 {J/Kg}
xA1=0.25
mLNdot=0.00001667 {Kg/sec}
```

APPENDIX D Mass Transfer/Thermodynamic Model

```
{mass balance}
mLdot=Kg*MWA*(dPlmAC)*area1
m1dot=m2dot-mLdot
m2dot=rhoAN2*QAN2

{Wagner Equation}
Pa2=xA2*P
xA1=xA2-(mLdot/m2dot)*(MWTA1/MWA)
Pa1=xA1*P
Pc=((exp(((-7.45514*J7)+(1.202*(J7^1.5))+(-2.43926*(J7^3))+(-3.3559*(J7^6)))/(
Tc/508.1))*47))*                                                    1e5
J7=1-(Tc/508.1)

{Thermodynamic Balance}
mLNdot*hLN+mLNdot*EnthN1=mLdot*hA+mLdot*EnthL+(rhoAN1*QAN1)*EnthAN

{Mass Transfer}
dPlmAC=((Pa2-Pc)-(Pa1-Pc))/ln((Pa2-Pc)/(Pa1-Pc))
Pa2n=Pa2-(1e-10)
xA2n=xA2-(1e-10)
Kg=(h1*((CpAN*VisAN/kAN)^(2/3)))/((CpAN*Pngf*MWANave)*(((VisAN/(rhoANave*kd))^
(2/3))))
Pcn=Pc+(.001)
Kg=(h1*((CpAN*VisAN/kAN)^(2/3)))/((CpAN*Pngf*MWANave)*(((VisAN/(rhoANave*kd))^
(2/3))))
kd=((0.0166*(((TA1+TA2)/2)^(3/2))*((1/MWN+1/MWA)^(1/2)))/((P/101325)*(NuN^(1/3
)+
NuA^(1/3))^(2)){ft^2/hr}*0.0929/3600){m^2/sec}
Pngf=(PNc-PNb)/(ln(PNc/PNb))
PNc=P-Pc
PNb=P-((Pa1+Pa2)/2)
h1=1.86*(kAN/De)*((De*Gave/VisAN)*(CpAN*VisAN/kAN)*(De/dx))^(1/3)*(VisAN/VisAN
c)^(0.14)

{Correlations}
area1=3.14159*De*dx
area2=3.14159*Din*dx
area3=(3.14159*De^2)/4
MWANave=((MWTA1+MWTA2)/2)
rhoANave=((rhoAN1+rhoAN2)/2)
Gave=(rhoAN1*QAN1+rhoAN2*QAN2)/(2*area3)
De=(Dout^2-Din^2)/Din {m}
rhoAN1=P*MWTA1/(R*TA1)
rhoAN2=P*MWTA2/(R*TA2)
QAN1=m1dot/rhoAN1
MWTA1=xA1*MWA+xN1*MWN
MWTA2=xA2*MWA+xN2*MWN
xA1+xN1=1
xA2+xN2=1

{Specific Heats}
```

```
CpN2=(31.2+-0.0136*(TaveN2)+0.0000268*(TaveN2)^2+-0.0000000117*(TaveN2)^3)*(1/
MWN)            *(1000)
TaveN2=(TA1+TA2)/2
CpA=(6.301+0.261*TaveA-0.000125*(TaveA)^2+0.0000000204*(TaveA)^3)*(1/MWA)*(100
0)
TaveA=(TA1+TA2)/2
CpAN=((xA1+xA2)/2)*CpA+((xN1+xN2)/2)*CpN2
CpL=(2.3388-0.0038942*Tc+1.1221e-05*(Tc)^2)*1000 {J/kg K} {correlation with
experimental data}

{Enthalpies -- Integrated form of Specific Heats}
EnthN1=(31.2*(TN2-TN1)+-0.0136/2 * (TN2^2-TN1^2)^2+0.0000268 /3*
(TN2^3-TN1^3)+ -0.0000000117/4*(TN2^4-TN1^4)) *(1/MWN)*(1000) {g-mol/kg-mol}
EnthN2=(31.2*(TA2-TA1)+-0.0136/2*(TA2^2-TA1^2)+0.0000268/3*(TA2^3-TA1^3)+
-0.0000000117/4*(TA2^4-TA1^4)) *(1/MWN)*(1000) {Reid 226}
EnthL=(2.3388*(TA2-TA1)-0.0038942/2*(TA2^2-TA1^2)+1.1221e-05/3*(TA2^3-TA1^3))*
1000 {J/kg K} {correlation with experimental data}
EnthA=(6.301*(TA2-TA1)+0.261/2*(TA2^2-TA1^2)-0.000125/3*(TA2^3-TA1^3)+
               0.0000000204/4*(TA2^4-TA1^4))*(1/MWA)*(1000)
EnthAN=((xA1+xA2)/2)*EnthA+((xN1+xN2)/2)*EnthN2

{Viscosities}
{N2 Gas--Chapman-Enskog Method: Non-polar gas}
{Inner Tube}
sigmaN=3.798 {Ang.}
epskN=71.4 {K} {potential energy constant-epsilon/boltzmann's constant}
AAN=1.16145
BBN=0.14874
CCN=0.52487
DDN=0.77320
EEN=2.16178
FFN=2.43787

{Outer Tube}
VisNGO=26.69*(MWN*TaveN2)^(1/2)/(sigmaN^2*OMEGAvNO) {micro Poise}
OMEGAvNO=AAN/(TstarNO^(BBN))+CCN/(exp(DDN*TstarNO))+EEN/(exp(FFN*TstarNO))
TstarNO=TaveN2/epskN

{Outer Tube at Condensate Film}
VisNGOc=26.69*(MWN*Tc)^(1/2)/(sigmaN^2*OMEGAvNOc) {micro Poise}
OMEGAvNOc=AAN/(TstarNOc^(BBN))+CCN/(exp(DDN*TstarNOc))+EEN/(exp(FFN*TstarNOc))
TstarNOc=Tc/epskN

{Acetone Gas Viscosity--Reichenberg Method: Polar Gas}
VisAce=(Astar*(TrAce)/((1+0.36*TrAce*(TrAce-1))^(1/6)))
TrAce=TaveN2/508.1
Astar=MWA^(1/2)*508.1/(30.1) {30.1 from molecular bond structure of
Acetone--see notes}

{Acetone Gas Viscosity at Condensate Film--Reichenberg Method: Polar Gas}
VisAcec=(Astar*(TrAc)/((1+0.36*TrAc*(TrAc-1))^(1/6)))
TrAc=Tc/508.1
```

```
{Combined Gas Viscosity--Brokaw Approximation of PHIij}
VisAN=((xAave*VisAce/(xAave+xNave*PHI12))+(xNave*VisNGO/(xNave+xAave*PHI21)))*
1e-7
xAave=(xA1+xA2)/2
xNave=(xN1+xN2)/2
PHI12=(VisAce/VisNGO)^(1/2)*Souter12*Aouter12
Aouter12=mwx12*MWy12^(-1/2)*(1+((MWy12-MWy12^(0.45)))/(2*(1+MWy12)+((1+MWy12^(
0.45))*mwx12^(-1/2)/(1+mwx12))))
mwx12=(4/((1+MWy12^(-1))*(1+MWy12)))^(0.25)
MWy12=MWA/MWN
PHI21=(VisNGO/VisAce)^(1/2)*Souter21*Aouter21
Souter21=Souter12
Aouter21=(MWN/MWA)^(-0.37)          {since 0.4 < (MWN/MWA) < 1.33}
Souter12=(1+(TstarAce*TstarNO)^(1/2))/(((1+TstarAce+deltaAce^2/4)^(1/2))*((1+T
starNO)^(1/2)))
TstarAce=TaveA/epskA
epskA=560.2 {K}
deltaAce=(1.94e03*dipoleAce^2)/(VboilingA*TboilingA)
dipoleAce=2.9 {debyes}
VboilingA=82.6 {cm^3/g-mol}
TboilingA=329.4 {K}
TboilingN=77.4 {K}

{Combined Gas Viscosity at Condensate Film--Brokaw Approximation of PHIij}
VisANc=((xAc*VisAcec/(xAc+xNc*PHI12c))+(xNc*VisNGOc/(xNc+xAc*PHI21c)))*1e-7
xAc=(Pc/P)
xNc=(1-Pc/P)
PHI12c=(VisAcec/VisNGOc)^(1/2)*Souter12c*Aouter12
PHI21c=(VisNGOc/VisAcec)^(1/2)*Souter21c*Aouter21
Souter21c=Souter12c
Souter12c=(1+(TstarAc*TstarNc)^(1/2))/(((1+TstarAc+deltaAce^2/4)^(1/2))*((1+Ts
tarNc)^(1/2)))
TstarAc=Tc/epskA
TstarNc=Tc/epskN

{Conductivity of Acetone Gas}
kAce=(TaveA/TrefA)^(1.786)*kAceref
TrefA=373 {K}
kAceref=17.3e-3 {W/m K}

{Conductivity of Gas Mixture--Wassiljewa Eq. modified with the Lindsay and
Bromley Modification}
kAN=(xAave*kAce/(xAave+Ak12*xNave))+(xNave*kNG2/(xNave+Ak21*xAave))
Ak12=(1/4)*(1+(VisAce*1e7/(VisNGO*1e7)*((MWN/MWA)^(3/4))*(TaveA+Sace)
                /(TaveA+Snit))^(1/2))^2*(TaveA+Sacenit)/(TaveA+Sace)
Ak21=(1/4)*(1+(VisNGO*1e7/(VisAce*1e7)*((MWA/MWN)^(3/4))*(TaveA+Snit)
                /(TaveA+Sace))^(1/2))^2*(TaveA+Sacenit)/(TaveA+Snit)
Sace=1.5*TboilingA
Snit=1.5*TboilingN
Sacenit=Cs*((Sace*Snit)^(1/2))
Cs=0.73  {If one of the gases is very polar,  otherwise-->Cs=1.0}

{Parameters}
```

```
{dx=.1}
Dout=0.0191 {m}
Din=0.0127 {m}
P=101325 {N/m^2}
R=8314 {N m/K kg-mol}
TA2=294.1 {K}
TA1=200 {K}
T1=77 {K}
MWA=58.1 {kg/kg-mol}
MWN=28.02 {kg/kg-mol}
```

```
NuN=2*15.6 {2*N}
NuA=3*14.8+6*3.7+7.4 {3*C+6*H+O}
QAN2=(1{Lpm}/(1000*60)) {m^3/sec}
xA2=0.8
kNG2=1.8e-2
hA=524000*((1-Tc/508.1)/(1-329.2/508.1))^0.27 {J/Kg}{Reid pg.228}
hLN=199106 {J/Kg}
mLNdot=0.00001667 {Kg/sec}
```

Illinois
Department of
Natural Resources